Big Earth Data in Support of
the Sustainable Development Goals

2 ZERO HUNGER

6 CLEAN WATER AND SANITATION

11 SUSTAINABLE CITIES AND COMMUNITIES

13 CLIMATE ACTION

14 LIFE BELOW WATER

15 LIFE ON LAND

Chinese Academy of Sciences

September 2020

Big Earth Data in Support of
the Sustainable Development Goals

CONTENTS

Foreword

The Sustainable Development Goals (SDGs), at the core of *Transforming our world: the 2030 Agenda for Sustainable Development* adopted by the 193 Member States of the United Nations in September 2015, represent commitment to address the tri-dimensional social, economic and environmental issues mankind faces, in the most comprehensive way in human history, with the aim of achieving sustainability.

China is fully committed to the 2030 Agenda for Sustainable Development. As progress has been made across the board, there have been "early harvests" of multiple SDGs. The goal to end extreme poverty will be achieved within this year, for example. China is also fully engaged in international cooperation in SDGs, sharing knowledge and experience with and offering assistance, as much as we can, to other developing countries.

The important role science and technology can play, already widely recognized, is reaffirmed as vital to SDG transformations as well as global development and change in the *Global Sustainable Development Report 2019.* The Chinese Academy of Sciences (CAS), as a member of the global scientific community, has worked vigorously, through science-policy-society interface, to provide solutions and support, domestically and internationally, to address the new demands and challenges that humanity must address before the lofty Sustainable Development Goals can be achieved.

SDGs are gigantic, complex and diverse systems with dynamic interactions amongst themselves. Fundamental to their implementation are effective monitoring and evaluation, where many difficulties remain. The Global Indicator Framework for the Sustainable Development Goals was adopted in 2017 by the United Nations as voluntary and nonbinding. This Framework, however, has to be further refined. With only ten years between now and 2030, the prospect of achieving the SDGs is not bright, not to mention the outbreak of COVID-19, that has brought unprecedented challenge to this effort.

The CAS Big Earth Data Science Engineering Program (CASEarth) has studied, since 2018, six SDGs: SDG 2 (Zero Hunger), SDG 6 (Clean Water and Sanitation), SDG 11 (Sustainable Cities and Communities), SDG13 (Climate Action), SDG 14 (Life below Water) and SDG 15 (Life on Land), especially focusing on those indicators where data and methods can be improved. CASEarth issues annual reports, *Big Earth Data in Support of the Sustainable Development Goals,* and leads CAS efforts to support the implementation of the SDGs.

The 2020 report discusses data integration, indicator development and sustainability evaluation concerning the six SDGs through 26 case studies. Each case presents data products, methods and models and how they can support policy-making, through five parts—the background, data used in the case, methodology, results and analysis, and outlook, showcasing the value and prospects of applying Big Earth Data-enabled technologies and methods to the evaluation of SDGs.

In the *Sustainable Development Goals Report 2019*, United Nations Secretary-General António Guterres called for deeper, faster, and more ambitious responses to achieve the social and economic transformations required for the implementation of SDGs. The report laid special emphasis on better use of data, a digital transformation while harnessing science, technology and innovation, and more intelligent solutions. Technologies, especially data, will therefore have to play a more important role in achieving SDGs.

The United Nations "Technology Facilitation Mechanism" (TFM) is fully consistent with China's strategy of driving development with innovation. China and many other developing countries face major challenges and pressure as we pursue SDGs with limited capacity for data collection and processing, and for monitoring and evaluation of SDG indicators, where Big Earth Data has a unique role to play.

2020 marks the 75th anniversary of the United Nations and the start of the Decade of Action to deliver the Sustainable Development Goals by 2030. China will continue to work with other countries to advance the 2030 Agenda and contribute to achieving the SDGs as scheduled. Chinese scientists wish to present this report as part of China's contribution and remain committed to collaboration and sharing with the rest of the world. Finally, I would like to express my respect and appreciation for the CASEarth team of scientists led by Academician Guo Huadong for the effort they have made toward SDGs in the spirit of science and innovation.

Bai Chunli
President, Chinese Academy of Sciences
Head of Leadership Group of CASEarth

Preface

Almost five years after the adoption of *Transforming our world: the 2030 Agenda for Sustainable Development* by the United Nations, the lack of data on indicators is still holding back progress in the scientific evaluation of global implementation of the Sustainable Development Goals (SDGs). The coronavirus pandemic since early 2020 has made the challenges countries face on their way toward the SDGs all the more daunting.

To support global SDG implementation, the United Nations launched the "Technology Facilitation Mechanism", encompassing three parts—the Interagency Task Team, including the 10-Member Group, the collaborative Multi-stakeholder Forum and an online platform. One of the most important and pressing issues now is to achieve breakthroughs in data and methodology for the monitoring of SDG indicators.

Big Earth Data enables macroscopic, dynamic and objective monitoring, by making it possible to integrate and analyze data on the land, sea, atmosphere and human activities to give a holistic understanding of a vast region. This technology can support policy-making by providing information, at a large scale with cyclical changes, on multiple SDG indicators closely related to the Earth's surface, environment and resources.

Our goal is to convert Big Earth Data to information relevant to SDGs, construct and integrate such data to support SDG indicators, study the connections and coupling between SDGs and then serve as a tool for SDG-related policy-making. This year, we selected six SDGs to study, based on the advantages of Big Earth Data and features of SDG indicators.

Big Earth Data can contribute to the evaluation of the six SDGs in three ways: by providing data products, new evaluation methodologies and models, and case studies to monitor progress and inform policy-making.

In this 2020 report, 26 typical cases at local, national, regional and global scales are presented to showcase the studies on and monitoring results of 18 SDG targets, including 24 data products, 13 methodologies and 19 results that are of value to policy-making. The cases cover the topics of tracking the progress of land degradation neutrality, biodiversity conservation, urban sustainability assessment, spatial distribution of vegetated wetlands, offshore ecosystem health assessment in China, and global forest cover. They all point to the great value of Big Earth Data and related technologies and methodologies as new analytical tools with which we will be able to have deeper understanding of and make better policies on the SDGs and related issues.

This report could not have been completed without the leadership and support from the Chinese Academy of Sciences, the Ministry of Foreign Affairs, the Ministry of Science and Technology, and other ministries. We are grateful for the valuable opinions shared by leaders and experts from the National Development and Reform Commission, the Ministry of Natural Resources, the Ministry of Ecology and Environment, the Ministry of Housing and Urban-Rural Development, the Ministry of Transport, the Ministry of Water Resources, the Ministry of Agriculture and Rural Affairs, the National Health Commission, the Ministry of Emergency Management, the National Bureau of Statistics and the National Forestry and Grassland Administration, Finally, our utmost appreciation goes to every scientist in the team for their hard work.

Guo Huadong
CAS Academician
Chief Scientist of CASEarth
Member of the UN 10-Member Group to support the TFM for SDGs

Executive Summary

Five years after the adoption of the 2030 Agenda for Sustainable Development, the implementation of Sustainable Development Goals (SDGs) is still constrained, to a certain extent, by the lack of data on progress, inadequate statistical methods, the diverse issues concerning SDGs localization, and the multitude of indicators that are both intertwined and mutually restrictive. Big Earth Data, an innovative technology, can serve as a new key to unlocking Earth's secrets and a new engine to drive discoveries. The 2019 report *Big Earth Data in Support of the Sustainable Development Goals* showcased the contributions this technology can make to sustainable development. This year's report focuses on Big Earth Data's contributions to monitoring and evaluating six SDGs—SDG 2 (Zero Hunger), SDG 6 (Clean Water and Sanitation), SDG 11 (Sustainable Cities and Communities), SDG 13 (Climate Action), SDG 14 (Life below Water), and SDG 15 (Life on Land)—through data products, methodologies and models, and policy-making support.

With regard to SDG 2 (Zero Hunger), the 2020 report focuses on Indicator 2.2.1 (Prevalence of stunting among children under 5 years old) and Indicator 2.4.1 (Proportion of agricultural area under productive and sustainable agriculture), closely related to the demand and supply of food. It presents a creative technology that integrates multi-sourced Big Earth Data for producing scientific data and evaluating indicators. Key findings and outcomes include: the creation of a model to estimate yield gap, the conclusion that China realized SDG 2.2 in 2017 in terms of the rate of under-five stunting, and the conclusion that national grain output will meet the consumption estimates for 2030 if yield potential of wheat and rice can be achieved in their biggest production areas. It recommends for policy makers the key areas for further reduction in the rate of under-five stunting, a land and water resources distribution plan for increasing potential grain areas, and key regions for sustainable grain production with reduced use of chemical fertilizers. The report presents Big Earth Data's potential for SDG 2 monitoring and evaluation and its strengths in supporting the achievement of Zero Hunger.

With regard to SDG 6 (Clean Water and Sanitation), the report presents Big Earth Data-enabled methods of monitoring and evaluation of SDG 6.3.2 (Proportion of bodies of water with good ambient water quality), SDG 6.4.2 (Level of Water Stress, LWS), and SDG 6.6.1 (Change in the extent of water-related ecosystems over time), focusing on water resources, water environment and water-related ecosystems, and cases of their application at the local, national and regional levels. Datasets produced include: datasets of 86 Ramsar Sites water body distribution in Asia, Europe, and Africa (2000-2018); water transparency in China's lakes (2000-2019); and mangrove forests and *Spartina alterniflora* in China (2015 and 2018). New method and model include: a method to monitor and evaluate transparency of large lakes and a model for level of water stress assessment with coupling glacier module. It concludes that lake transparency has improved, mangrove forests have recovered, invasion of *Spartina alterniflora* is under control, and the level of water stress has worsened in the Shule River basin in China. These outcomes can inform policy-making in China and the rest of the world on water environment monitoring and management, optimal distribution of water resources and protection of wetlands.

With regard to SDG 11 (Sustainable Cities and Communities), the report presents the monitoring and evaluation of six indicators under SDG 11, including SDG 11.1.1 (informal settlements), SDG 11.2.1 (convenient access to public transport), SDG 11.3.1 (urbanization), SDG 11.5.1/SDG 11.5.2 (urban disasters), and SDG 11.7.1 (open public space), and multiple SDG 11 indicators at the provincial level in China, all enabled by Big Earth Data. The outcomes include production of datasets, such as high-resolution gridded population data by age and gender (2015 and 2018), an impervious surface dataset of 433 Chinese cities with 30 m resolution (1990-2018), and an integrated assessment dataset of multiple indicators of Chinese cities covering public transportation, urbanization, disaster, environment and urban open public space; the creation of deep learning network model to

identify shantytowns and disasters; and the proposal of a new indicator—the ratio of Economic Growth Rate to Land Consumption Rate (EGRLCR), which will expand SDG 11. The report concludes that urban open public space has increased continuously since 2015, population with easy access to public transportation has grown by 16.28%, challenges remain in coordinating urbanization, China has stronger capacity for disaster prevention and reduction, and losses caused by natural disasters have dropped significantly on the whole. The results of monitoring and comprehensive evaluation of SDG 11 indicators at the provincial level in China can be used as a basis for monitoring and making policies on urban inclusion, security, land use and environment and finding a Chinese solution to sustainable urban development in the world.

With regard to SDG 13 (Climate Action), this report focuses on Target 13.1 (Strengthen resilience and adaptive capacity to climate-related hazards and natural disasters in all countries) and Target 13.2 (Integrate climate change measures into national policies, strategies and planning) and presents applications of Big Earth Data in monitoring SDG 13 and assessing progress. The findings and deliverables include: in the area of climate-related hazards and natural disasters, the generation of datasets on the frequency and intensity of extreme high-temperature events and heatwaves in China, bringing to light a marked upward trend in such events since the late 1990s; in the area of climate change response, projections on how climate change would impact crop phenology in China, to provide decision support for response to climate change in the interest of food security by forecasting, with a high degree of probability, a forward shift in the anthesis and maturation of wheat and maize.

With regard to SDG 14 (Life Below Water), this report focuses on Target 14.1 (By 2025, prevent and significantly reduce marine pollution of all kinds, in particular from land-based activities, including marine debris and nutrient pollution) and Target 14.2 (By 2020, sustainably manage and protect marine and coastal ecosystems to avoid significant adverse impacts, including by strengthening their resilience, and take action for their restoration in order to achieve healthy and productive oceans) and presents the following three case studies where the Big Earth Data technology is applied to the dynamic monitoring

and integrated assessment of various parameters at the national (China) and local (typical marine areas) levels with spatiotemporal data fusion and model simulation, among other methodologies: distribution and variation of marine debris and microplastics in China's coastal waters; ecosystem health assessment in typical bays; and changes in the scope of raft culture. The findings reveal: a downward trend in the abundance of floating debris in China's coastal waters from 2015 onward and a continuous trend of improvement in microplastic pollution between 2016 and 2019; a generally stable and sound state of health in the ecosystems of Jiaozhou Bay, Sishili Bay and Daya Bay from 2015 onward; and an increase in the areas of raft culture in marine waters and basically stable areas of offshore ecological conservation in Jiangsu and Fujian provinces between 2017 and 2020.

With regard to SDG 15 (Life on Land), this report focuses on three themes, i.e. forests, land degradation and biodiversity, against four SDG indicators, i.e. 15.1.1 (forest area as a proportion of total land area), 15.1.2 (biodiversity conservation), 15.3.1 (proportion of land that is degraded over total land area) and 15.5.1 (Red List Index), and presents Big Earth Data-enabled SDG indicator evaluation models and methodologies, as well as pilot applications at three levels, namely, global, national (China), and local (typical areas). The findings and deliverables are as follows: a global forest cover map at 30 m spatial resolution for 2019 and a spatial dataset on the state and scope of threats to, and cumulative stress on, China's protected flora and fauna; an integrated spatial-temporal-spectral feature extraction model for forests and a spatial abundance simulation methodology for threatened species; critical conclusions that China's Land Degradation Neutrality (LDN) was on a trajectory of continuous improvement between 2015 and 2018 (contributing close to 1/5 of global LDN) and that marked improvements in soil loss on the Loess Plateau and the aeolian desertification and sandification in northern China have been observed since 2000; the introduction of the three global conditions for category-specific conservation and sustainable use of biodiversity into China; and recommendations on the strategies and solutions needed for ecosystem conservation and restoration in the context of the National Projects for the Conservation and Restoration of Major Ecosystems, thus lending effective support for dynamically monitoring and evaluating SDG 15 .

List of Cases on Big Earth Data for SDGs

Target	Case	Data product	Method	Support to policy-making
2.2	The trend of under-five stunting in China	Dataset on change in prevalence of stunting among children under 5 years of age in China		Presenting variations in regional trends and identifying priority areas
2.4	Potential for sustainable cropland intensification in China	Spatial dataset of the multiple cropping index and its potential		Proposing a pathway to sustainable cropland intensification
2.4	Potential for improvement of the sustainability of crop production in China	Spatial dataset of yield gap and reducible fertilizer of three major staple food crops	A remote sensing-based model for yield potential estimates	Informing policy on potential yield increase and fertilizer reduction
6.3	Spatiotemporal patterns of water transparency in China's lakes	Time series datasets of water transparency in China's lakes (2000-2019)	A new lake water transparency monitoring and evaluation algorithm based on dual-band reflectance	Informing policies on water environmental monitoring and management in China and the rest of the world
6.4	Evaluation of level of water stress in the Shule River basin in arid region, Northwest China		A new evaluation method of the LWS with coupling glacier module	Providing reference for optimal distribution of water resources in GGCAAs
6.6	Spatiotemporal distribution of China's vegetated wetlands	Datasets of China's vegetated wetlands (2015), mangrove forests and *Spartina alterniflora* in China (2015 and 2018)	An HOHC method to map vegetated wetlands, mangrove forests and *Spartina alterniflora*	Informing policy on China's implementation of the Ramsar Convention on Wetlands
6.6	Dynamic change of water body in Ramsar Sites	Datasets on 86 Ramsar Sites water body distribution in Asia, Europe, and Africa (2000-2018)		Informing policy on protection and management of Ramsar Sites
11.1	Estimates of population living in shantytowns as a percentage of main urban district residents in cities in China	Data of shantytown population ratio and vector boundaries in cities in China (2019)	A semantic segmentation and transfer learning method for shantytown estimation	
11.2	Proportion of the population with easy access to public transportation in China	Datasets of population with easy access to public transportation, by age and gender, with 1 km resolution (2015 and 2018)		

Target	Case	Data product	Method	Support to policy-making
11.3	Monitoring and assessing urbanization progress in China	A series of 7 datasets of built-up areas of 433 cities in China (1990–2018)	Proposal of a new indicator—the ratio of economic growth rate to land consumption rate	
11.5	Monitoring of disaster loss reduction and promotion of sustainable development in vulnerable areas in China	Data from monitoring indicators of disaster losses between 2013-2019; Data from monitoring reconstruction and sustainability in quake-hit Yushu		Presenting evidence on large reduction in deaths, people affected, and direct economic loss as a result of disasters in China, effectively promoting sustainable development in disaster-prone areas
	Impact assessment of storm surge inundation in Shenzhen	4 km water depth data of Typhoon Nida in 2016 and Typhoon Mangkhut in 2018		Using digital-twin method to assess the impact of storm-surges of different intensities on population and economy
11.7	Share of open public space area in cities in China	Datasets of share of open public space area in cities in China (2015 and 2018)		
11.2 11.3 11.5 11.6 11.7	Integrated assessment of SDG 11 indicators at the provincial scale in China	Dataset of integrated assessment of multiple indicators of 340 Chinese prefectural-level cities		Supporting sustainability assessment of major cities in China and serving as reference for integrated SDGs assessment in other Chinese regions
13.1	Intensity and frequency of extreme high-temperature events and heatwaves in China	Homogenized temperature series datasets	A combination of non-stationary models and parametric/non-parametric methods	
13.2	Predicting the impacts of climate change on the phenology of China's main crops	Near-term probabilistic forecast datasets for the phenology of China's main crops under climate change scenarios		Informing China's policy on food production in response to climate change
14.1	Analysis of the distribution and variation of marine debris and microplastics in China's coastal waters	Datasets on the distribution of marine debris and microplastics in China's coastal waters		Informing policy-making with the state, by-region distribution and patterns of change of pollution by marine debris and microplastics in China's coastal waters for the prevention and control of marine debris and microplastics in typical areas
14.2	Ecosystem health assessment for typical bays in coastal China	Datasets of ecosystem elements in typical bays, i.e. Jiaozhou Bay, Daya Bay and Sishili Bay	Health assessment based on marine ecosystem structures and service functions	Informing policy-making on how environmental factors in China's typical coastal bays contribute to changes in the key elements of ecosystems, to keep the protection of coastal ecosystems anchored in science
	Monitoring changes in raft culture in China's coastal waters	Datasets from monitoring of raft culture in key coastal provinces of China	Deep learning-enabled AI extraction of marine raft culture data	

Target	Case	Data product	Method	Support to policy-making
15.1	Global/regional forest cover (2019)	Global forest cover map at 30 m spatial resolution for 2019	Machine learning-enabled forest classification on global scale	Informing forest cover status at regional and global scales
	Spatiotemporal distribution of forest types in China's Yangtze River basin	Datasets on distribution of forest types in the Yangtze River basin for 2018 (at 10 m resolution)	A method for time series remotely sensed image synthesis based on multi-rules and an integrated spatial-temporal-spectral framework for forest type feature extraction	
	Applying three global conditions framework to the conservation and sustainable use of biodiversity in China	Datasets on 3Cs for the conservation and sustainable use of biodiversity in China		Localizing the three global conditions and recommending strategies for ecosystem conservation and restoration in the context of the National Projects for the Conservation and Restoration of Major Ecosystems
	China's LDN progress tracking and its contribution to global LDN	Datasets on global land degradation/improvement		Tracking and assessing China's LDN with an objective analysis of China's contribution to global LDN based on the IAEG-SDGs indicator system and globally shared data
15.3	Dynamics between large-scale greening and soil and water conservation on the Loess Plateau and sedimentation of the Yellow River		A model for quantifying the effect of vegetation cover on soil erosion control	Identifying spatial variations in the effectiveness of soil conservation on the Loess Plateau and informing policy-making on soil erosion control
	Processes of aeolian desertification in the semi-arid region and its peripheries in northern China and review of control outcomes	Long time series data on the dynamics of aeolian desertification in semi-arid and surrounding areas of northern China (1975–2015)		Assessing the processes and drivers of aeolian desertification in semi-arid and surrounding areas of northern China over the last four decades, to support desertification control
15.5	China's plant diversity: risks and conservation strategies	Datasets on risk distribution and conservation efforts of China's plant diversity	A method for identifying the threats and stressors to biodiversity, developed and refined	Identifying gaps in China's flora diversity conservation and recommending a combination of proactive conservation strategies and restoration solutions to protect the habitats of species

Introduction

The United Nations Sustainable Development Summit adopted in 2015 the 2030 Agenda, which proposed 17 Sustainable Development Goals (SDGs) covering the economic, social and environmental aspects. These goals represent the direction of national development and international cooperation. In the almost five years since their adoption, the monitoring and evaluation of SDGs implementation have been constrained by the lack of data, varying capacities and the indicators being both intertwined and mutually restrictive. Scientific and technological innovation are solution to this pressing issue. The CAS Big Earth Data Science Engineering Program (CASEarth) has released annually scientific evidence-based monitoring results of six SDGs—SDG 2 (Zero Hunger), SDG 6 (Clean Water and Sanitation), SDG 11 (Sustainable Cities and Communities), SDG 13 (Climate Action), SDG 14 (Life below Water) and SDG 15 (Life on Land)—by drawing on Big Earth Data's strengths in multi-scale and near real-time processing and system integration. This is a concrete contribution to SDGs implementation.

Challenges to SDGs Implementation

The Global Indicator Framework for the Sustainable Development Goals and targets was adopted in 2017 by the United Nations (UN) as a preliminary system for Member States to adopt, on a voluntary basis, for monitoring progress in SDGs implementation. The Framework, subject to regular refinement and updating, faces the following problems.

1) Lack of data. The situation where there were neither evaluation method nor data has improved for all indicators in the past five years. However, for 46% of indicators, there are methods but no data; for those where both are available, the results are measured largely in a statistical way without the support of spatial distribution information. Spatial data that are objective, accurate and at varying scales are necessary for the achievement of SDGs. Specifically, data collected scientifically can be used to assess changes in the natural environment regularly and quantitatively, accurately identify the spatial position of disasters, and predict their future trends, in such cases as extreme high temperatures and heatwaves, higher frequency of fires, ocean acidification, increased eutrophication, continued land degradation, reduced biodiversity, and increased environmental impact on agricultural production.

2) Imbalance in capacities. Developing countries are constrained, by the level of their economic growth and carrying capacity of resources and environment, in their abilities to collect and analyze data, regularly and quantitatively. The lack of data has rendered invisible such serious issues as high ratio of stunting, inadequacy of urban housing and public space, weak disaster resilience, lack of access to safe drinking water, and overuse of forests. With Big Earth Data, we can collect objective data at global, regional and other scales, in a timely, accurate and comprehensive way, and improve their compatibility and comparability, so that "no one is left behind" on data essential to SDGs achievement.

3) Intertwined, but mutually restrictive indicators. SDG indicators are wide-ranging, long-term and intertwined. These diverse, complex indicators at multiple tiers come together to form a coherent, feasible whole. How to create methods and models for objective and effective monitoring and evaluation, based on compatible, quantifiable data, is an urgent issue for which a solution must be found.

Big Earth Data

The United Nations launched the Technology Facilitation Mechanism (TFM) to address the above-mentioned issues and challenges through Science, Technology and Innovation (STI) by pooling the collective wisdom of the scientific community, business community, and stakeholders.

Big Earth Data is big data in the field of Earth science with spatial attributes, especially the massive Earth observation data generated by space technology (Guo *et al.,* 2016). Such data is mainly produced at a large spatial scale by scientific devices, detection equipment, sensors, socio-economic observations, and computer simulation processes. Similar to other types of big data, Big Earth Data is massive, multi-sourced, heterogeneous, multi-temporal, multi-scaled, and non-stationary. But more than just that, it has strong spatiotemporal and physical correlations, and the data generation methods and sources are controllable. Big Earth Data science is interdisciplinary, encompassing natural sciences, social sciences, and engineering. It systematically studies the correlation and coupling of the Earth system based on data analysis. Earth is observed and studied as a whole by simultaneously employing big data, artificial intelligence, and cloud computing, so as to understand the complex interactions and development processes between Earth's natural system and the human social system. Big Earth Data can make an important contribution to the realization of SDGs.

CAS launched the Big Earth Data Science Engineering Program (CASEarth) in 2018, an endeavor to accelerate the transformation from Earth data systems and sharing to Digital Earth. It promotes the sharing of data, knowledge, and experience across the world, and supports scientific discovery, technological innovation, and policy-making. Big Earth Data science is a solution to cross-sectoral, multidisciplinary collaboration (Guo *et al.,* 2020a). It is an innovation under the TFM that can support the achievement of SDGs.

Big Earth Data in Support of SDGs

The CASEarth Big Earth Data system can support the implementation of SDGs by converting Big Earth Data to relevant information, providing policy-making support, constructing and integrating an index system, and studying the relationships and couplings between various SDG targets from the perspective of the Earth system. It can also support the monitoring and evaluation of SDG indicators through data-sharing platforms and cloud infrastructure by providing data, online calculations, and visual presentations. Currently, CASEarth shares a total of 8 PB of data, 3 PB of which is updated annually. It can provide 1 PF of high-performance computing and big data processing in the cloud. The Big Earth Data system's full capabilities, from data-to-information visualization to numerical simulation, can support the dynamic monitoring of and macro-level policy-making for SDGs.

CASEarth studies SDGs from the following four aspects:

1) Construct a Big Earth Data infrastructure for SDGs to provide data products to close the gap of missing data and realize data sharing.

2) Create methodologies and a technical system for achieving SDGs.

3) Provide data for monitoring SDG indicators from Earth science satellites.

4) Issue annual reports on Big Earth Data in Support of SDGs to showcase the latest progress.

This year's report presents 26 typical cases concerning six SDGs and discusses methods and pathways by which Big Earth Data can be used for efficient and accurate assessment of the implementation of SDGs, and as timely, scientific evidence to support policy-making.

SDG 2
Zero Hunger

Background

SDG 2 aims at ending hunger, achieving food security, addressing nutritional needs, and promoting sustainable agriculture. It serves as a foundation for the achievement of SDGs around the world. Global food production has more than doubled compared with that in the mid-20th century (FAO, 2020). Undernourished people as a share of the world's population dropped from 36% in 1969 to 11% in 2018 (United Nations, 2019). The number of hungry people, however, has increased slightly for a few years running (FAO, 2019). At the same time, food production has had a considerably negative impact on the world's ecosystems and environment (West *et al.,* 2014). The global food systems must change.

China has consistently pursued a policy of protecting arable land. Thanks to agro-technology and innovation, food production

has doubled in the past 30 years. China produces enough grain to meet over 95% of its domestic demand. There are, however, also issues to be addressed, such as sharply rising demand for food and the impact of food production on ecosystems and the environment (Zuo *et al.,* 2018).

Based on the macroscale dynamic monitoring that Big Earth Data enables, this report focuses on the rate of under-five stunting and proportion of agricultural area under productive and sustainable agriculture, indicators highly relevant to the supply and demand sides of food security, and presents new evaluation method and data product for progress monitoring. It showcases the potential of Big Earth Data in SDG 2 evaluation and the progress China has made toward zero hunger.
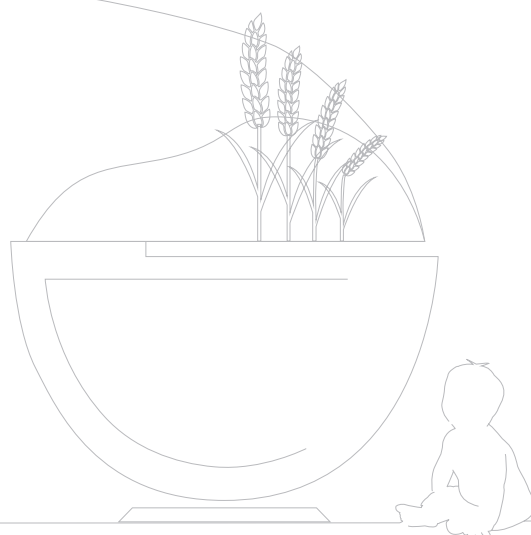
Main Contributions

Focusing on the two indicators, addressing nutritional needs and securing food production, the report proposes a remote sensing-based model for estimating yield potential. The following cases present three data products developed for indicator evaluation and technical support in three aspects to policy-making on maintaining balance in the supply and demand of food (Table 2-1).

Table 2-1 Cases and Their Main Contributions			
Indicator	**Tier**	**Case**	**Contributions**
2.2.1 Prevalence of stunting (height for age <-2 standard deviation from the median of the World Health Organization (WHO) Child Growth Standards) among children under 5 years of age	Tier I	The trend of under-five stunting in China	**Data product:** dataset on change in prevalence of stunting among children under 5 years of age in China **Support to policy-making:** presenting variations in regional trends and identifying priority areas
2.4.1 Proportion of agricultural area under productive and sustainable agriculture	Tier II	Potential for sustainable cropland intensification in China	**Data product:** spatial dataset of the multiple cropping index and its potential **Support to policy-making:** proposing a pathway to sustainable cropland intensification
		Potential for improvement of the sustainability of crop production in China	**Data product:** spatial dataset of yield gap and reducible fertilizer of three major staple food crops **Method:** a remote sensing-based model for yield potential estimates **Support to policy-making:** informing policy on potential yield increase and fertilizer reduction

Case Study

The trend of under-five stunting in China

Target: 2.2 By 2030, end all forms of malnutrition, including achieving, by 2025, the internationally agreed targets on stunting and wasting in children under 5 years of age, and address the nutritional needs of adolescent girls, pregnant and lactating women and older persons.

Highlights

- *China has substantially reduced the prevalence of stunting in children under 5 years of age from 18.8% in 2002 to 4.8% in 2017, which has met the SDG target 2.2 (under 5.9%).*

- *During the monitoring period, the prevalence of stunting among Chinese children under 5 years old decreased from 7.8% to 3.4% in urban areas and decreased from 25.6% to 5.8% in rural areas. The gap between urban and rural areas is narrowing year by year, with a significant decline observed in rural areas.*

Background

Childhood stunting is one of the most important indicators for long-term malnutrition that accounts for nearly 45% of child deaths globally (Black *et al.,* 2013). Improving the nutritional status of children has been recognised as a key component of "Healthy China", a strategic plan for national health in China.

According to the World Health Organization (WHO) Child Growth Standards, this case monitored the spatial pattern and dynamic changes of the under-five stunting rate in China from 2002 to 2017 and provided a more precise and evidence-based nutrition intervention strategy for children.

Data used

◎ Survey data, including data from the Chinese National Nutrition and Health Survey and China Chronic Diseases and Nutrition Surveillance.

◎ Statistical data, including data from the China Statistical Yearbook and Health Statistical Yearbook.

Method

The stunting rate was divided into five grades: <2.5% (very low), 2.5%-9.9% (low), 10.0%-19.9% (medium), 20.0%-29.9% (high), and ≥30.0% (very high) to track the trend of under-five stunting in China, with the definition of stunting as length/height for age <-2 standard deviations from the median of the WHO Child Growth Standards. Meanwhile, the results were presented

by province, urban/rural area, gender (boys/girls), and age group (0-, 1-, 2-, 3-, and 4- years old), and compared with the SDG 2.2 target. Data analysis in different survey years employed data from the sixth census in 2010, with calculation of rates complexly weighted for sampling.

Results and analysis

The prevalence of under-five stunting in China decreased from 18.8% in 2002 to 4.8% in 2017, which achieved the SDG 2.2 target (5.9%). At the provincial level, only 9 provinces were

identified to have a stunting rate of "low" or "very low" in 2002 (Fig. 2-1); by 2017, all 31 provinces were observed with a prevalence of "low" or "very low".
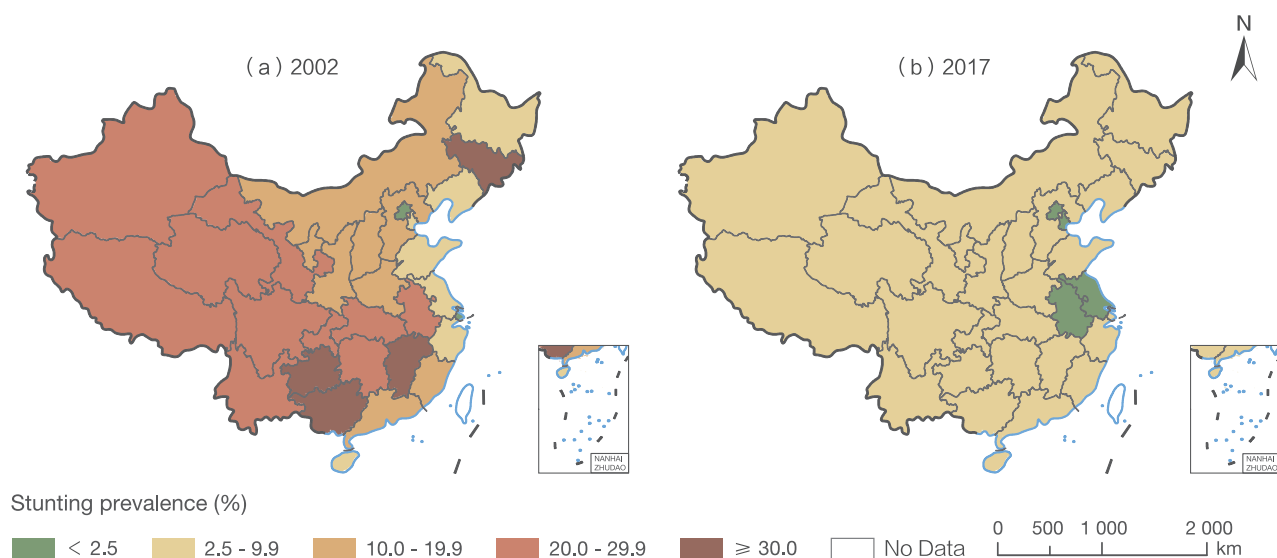
↑ Figure 2-1. Under-five stunting in 2002 (a) and 2017 (b) by province in China
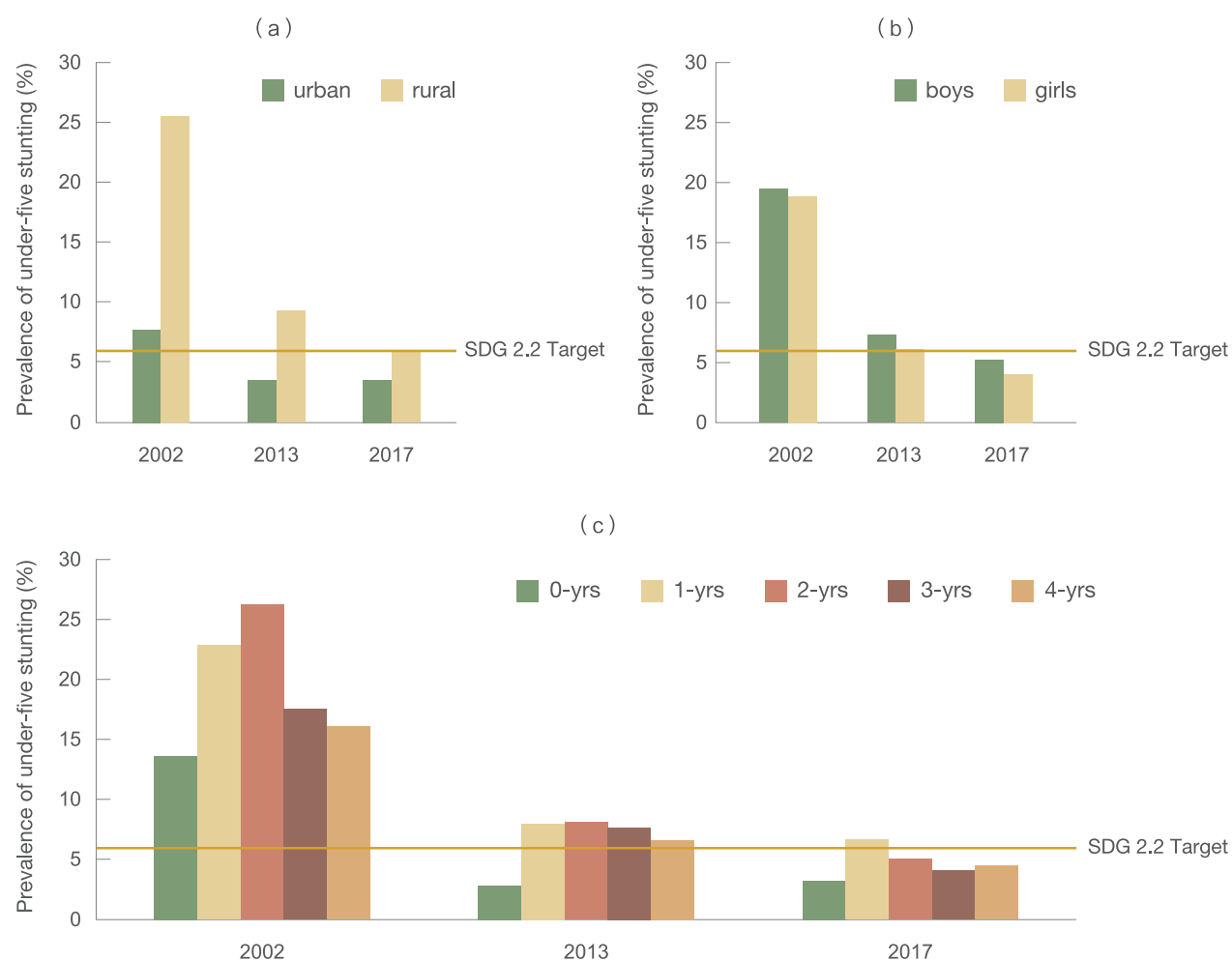
↑ Figure 2-2. Trends of under-five stunting from 2002 to 2017 by urban-rural (a), gender (b), and age group (c) in China

With the continuous implementation of national children's nutrition improvement policies and programs for children under 5 years old in rural and impoverished areas, the nutritional status of children has significantly improved, while urban-rural disparities were also dramatically reduced. During the monitoring period, a significant decline in the under-five stunting rate was observed in all population subgroups, including urban, rural, gender, and age groups (Fig. 2-2). From 2002 to 2017, the ratio of the stunting rate of Chinese children under 5 years old between urban and rural areas decreased from 1:3.3 to 1:1.7, which achieved the SDG 2.2 target. Nevertheless, the disparities among genders and age groups still exist. The stunting rate is slightly higher in boys than girls, and higher in 1-year-old and 2-year-old groups than other age groups.

Outlook

The improvement of children's nutritional status is not only a key focus of "Zero Hunger", but also an important component for promoting and implementing the "Healthy China" strategy. At present, the global food supply system and the progress of improving children's nutritional status have been severely affected by the increasing instability of international politics and global economy, and frequent major disasters such as locust plagues, as well as the global pandemic of COVID-19.

With rapid urbanization, the large-scale population flow from rural to urban areas has also brought uncertainty to children's nutritional status. Paying close attention to international political and economic impacts on the global food supply chain and focusing on children in poor rural areas and migrant children in urban areas are important approaches to ensuring a continuous reduction in the stunting rate among children in China.

Potential for sustainable cropland intensification in China

Target: 2.4 By 2030, ensure sustainable food production systems and implement resilient agricultural practices that increase productivity and production, that help maintain ecosystems, that strengthen capacity for adaptation to climate change, extreme weather, drought, flooding and other disasters and that progressively improve land and soil quality.

Highlights

- *China is able to increase its grain harvest area by about $1.35×10^5$ to $3.63×10^5$ km^2 on existing cropland by increasing multiple cropping index. Under the most realistic scenario, grain production is expected to be increased by 19.6% .*

- *Cropland intensification is largely affected by water constraints: different scenarios affecting the variation of harvest area have given estimations up to 60%. Efficient allocation of resources is of utmost importance to cropland intensification.*

Background

Cropland intensification has great implications for global food security. Although global crop production has been doubled in recent decades by adopting high-yield varieties, yield stagnation has been observed recently in many places around the world, implying that crop yield is close to its potential limit and is difficult to further increase under the current circumstances (Ray *et al.,* 2012). At the same time, it is unlikely to further expand cropland area as it is approaching the "planet boundary" (Henry *et al.,* 2018). Constant human incursions into natural areas for agriculture will come at a hefty price. Consequently, sustainable

cropland intensification by increasing multiple cropping on existing cropland is an alternative to improve global food security.

By using big Earth observation data, this case study presents an assessment of the potential for sustainable cropland intensification in China. It estimates the impact of increasing grain harvest area on existing cropland by increasing the adoption of multiple cropping activities. Moreover, it evaluates the pathways for sustainable intensification by considering water availability as an important environmental constraint.

Data used

◎ Spatial Production Allocation Model global gridded agricultural production dataset.

◎ National Land Cover Dataset, Global synergy cropland cover

data.

◎ Climate Research Unit gridded climate dataset.

◎ Global Agro-Ecological Zones.

Method

Mapping current cropland use intensity. Considering the constraints of climate, soil, and crop suitability, the case study applies a minimum cross information entropy model to allocate crop area, yield, and total production from statistics to spatial grids by 10×10 km resolution. Furthermore, it maps the current cropland use intensity by aggregating harvested areas for grain crops.

Mapping potential cropland use intensity. The case study calculates the potential cropland use intensity according to two parameters: temperature and precipitation. The accumulated temperatures ≥ 3 400 ℃, 4 200 ℃, 5 200 ℃, and 6 200 ℃ are adopted for determining the thermal potential for multiple cropping, and the annual precipitation ≥ 500 mm and 1 200 mm are adopted for determining the water potential for multiple cropping.

Estimating harvested area gap with consideration for water availability. The harvested area gap is determined by dividing the potential cropland use intensity by the current cropland use intensity. Four water allocation scenarios are set to analyse the impact of water constraints on cropland intensification. These scenarios are named *Priority-based allocation* (grid cells with a higher intensity area gap are given the priority to receive water), *Demand-weighted allocation* (using grid level water demand under full intensification as weight), *Equality-based allocation* (irrigation water is equally distributed across grid cells), and *Irrigated area-weighted allocation* (using current irrigated area as weight).

Results and analysis

The current cropland area in China is approximately 1.31×10^6 km^2, of which approximately 1.60×10^6 km^2 harvests grain crops annually. The estimated harvested area gap in China ranges from 1.35×10^5 to 3.63×10^5 km^2, which is comprehensively determined by climate resource potential and water allocation constraints (Fig. 2-3). In the most realistic scenario, the full exploitation of the harvested area gap can bring an extra grain production of approximately 1.17×10^8 t, which equals a 19.6% increase compared to the current national grain production level.

Although the total harvested area in China has been increasing steadily, the estimated harvested area gap first decreased then subsequently increased. The initial decrease was the result of an increase in the actual multiple cropping activities throughout the country, which was larger than the increase in the potential

（a）Priority-based scenario
（3.63×10^5 km^2）

（b）Demand-weighted scenario
（3.37×10^5 km^2）

（c）Equality-based scenario
（1.82×10^5 km^2）

（d）Irrigated area-weighted scenario
（1.35×10^5 km^2）

km^2

No Data 0 5 10 15 20 25 30

0 500 1 000 2 000 km
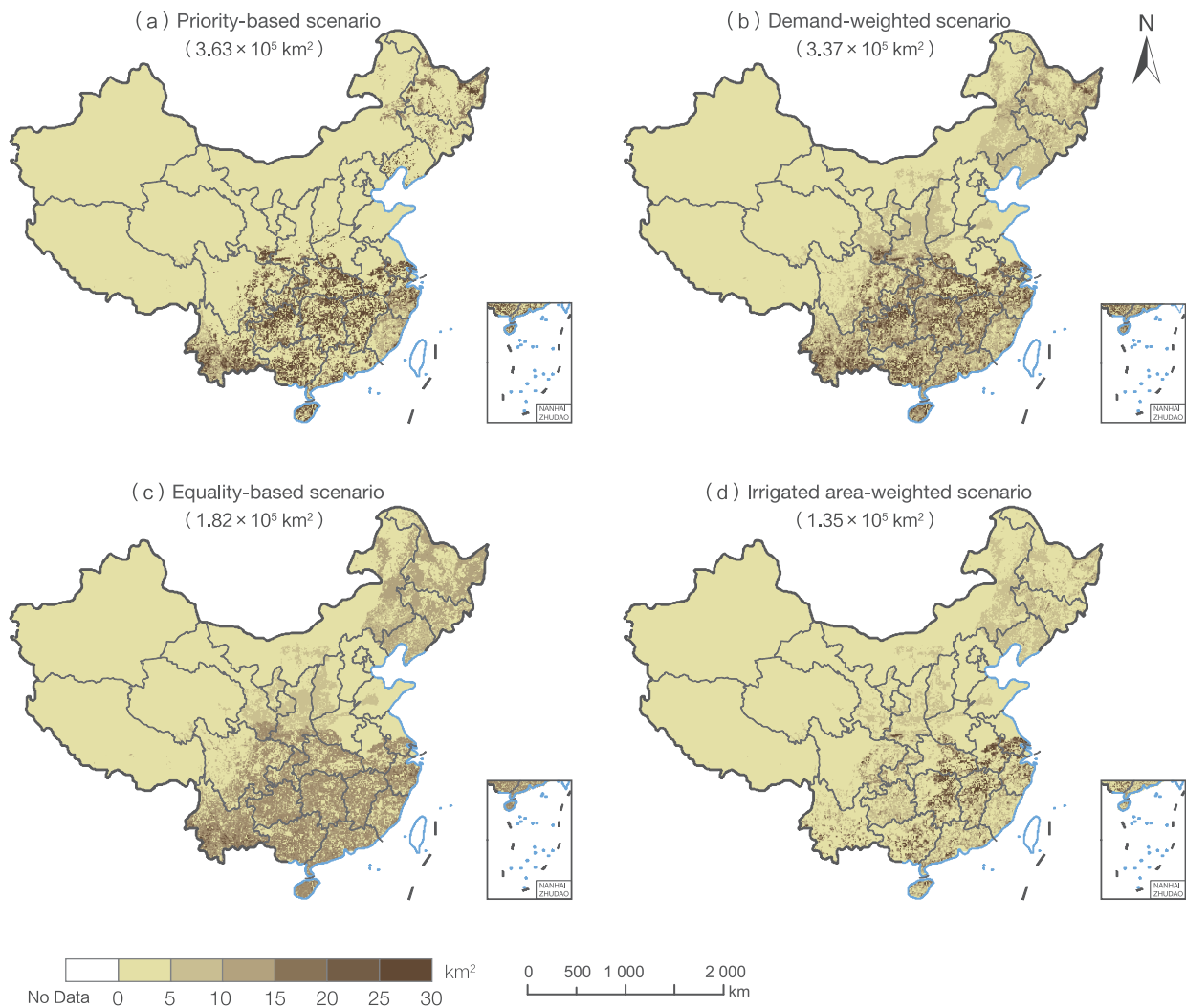
↑ Figure 2-3. Harvest area gap in China regarding different water allocation scenarios

（a）Changes in harvest area gap (1980-1990)　　　（b）Changes in harvest area gap (2000-2010)

N

Land management factors

+

−

Climatic factors

−　　+

0　500　1 000　　　2 000
km

NANHAI
ZHUDAO

NANHAI
ZHUDAO
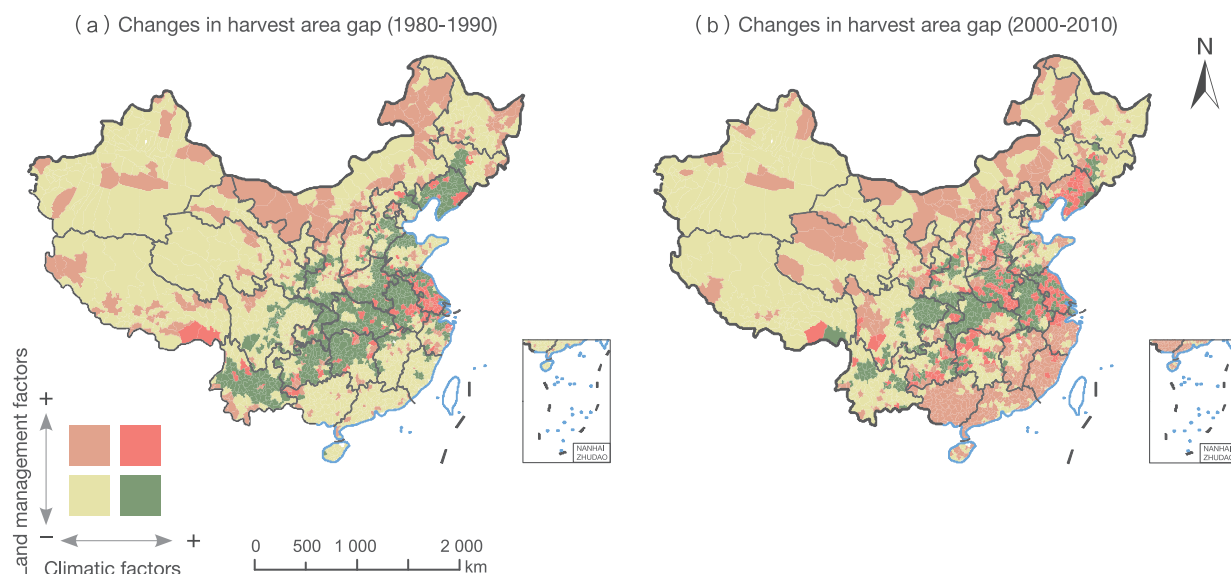
↑ Figure 2-4. Changes in harvest area gap in China and the contributions from climatic and land management factors (Note: no data available for Taiwan province)

multiple cropping as a result of changed climatic factors. The subsequent increase in the harvested area gap is the result of a decrease in actual multiple cropping activities (e.g., land management factors), in combination with a stagnant potential (Fig. 2-4). In some southern regions, both climatic and land management factors have enlarged the harvested area gap, indicating that these areas should be prioritized for cropland intensification.

Outlook

With the target proposed by SDG 2.4, this case study aims to improve the productivity and sustainability of grain production systems in China. Relying on Big Earth Data, it investigates the potential for sustainable cropland intensification and finds that China has great potential to harvest more grain crops on its existing cropland by properly increasing multiple cropping activities. Making full use of this potential, on the one hand, increases crop production to eliminate hunger, and on the other hand, alleviates the environmental pressure caused by the expansion of cropland. However, the complexity of cropland intensification should be fully acknowledged in that it encompasses resource systems, environmental systems, and ecological systems. Resource-saving and environmentally friendly global agricultural production needs to be established for targeting SDG 2.4.

Potential for improvement
of the sustainability of crop production in China

Target: 2.4 By 2030, ensure sustainable food production systems and implement resilient agricultural practices that increase productivity and production, that help maintain ecosystems, that strengthen capacity for adaptation to climate change, extreme weather, drought, flooding and other disasters and that progressively improve land and soil quality.

Highlights

- *A remote sensing-based model was developed to estimate the yield gap (difference between potential and actual yield) of three major staple food crops. It was found that the yield gap of rice and wheat in the agriculture zone with the highest harvest area was 13.3% and 12.5% of the yield in 2015, respectively. Closing the yield gap in the zone can help meet China's forecasted demand for rice and wheat in 2030.*

- *Without loss of food production, the nitrogen and phosphorus fertilizers for the three major staple food crops in China could be reduced by 17% to 19% of the total application. Rational spatial distribution planning for different regions for increasing crop production while reducing excess fertilizer application is critical for effectively improving the sustainability of food production.*

Background

Prompting food production to meet ever increasing human demand while limiting environmental impacts is critical for realizing food security, which is the major concern of SDG 2.4. This case focuses on three indicators referring to sustainable intensification (i.e., land productivity, fertilizer pollution risk, and food security), developing models to estimate the yield gap, reducible fertilizer, and self-sufficiency of three major staple crops (i.e., rice, wheat, and maize) in China. We aim to evaluate the potential for improvement of sustainability of crop production in China.

Data used

◎ China's Agricultural Outlook—forecasted national demand for major crops in 2030.

◎ Remote sensing reflectance, vegetation index, meteorological data, soil data, phenology data, and yield data in major agriculture zones of three major staple food crops from 2010 to 2015.

◎ Dataset on food production, fertilizer application, and water consumption for three major staple food crops in China in 2015.

Method

To quantify the yield potential of crops, a Remote Sensing-Crop Yield Model (RS-CYM) (Wang *et al.,* 2020) was developed to estimate the on-farm yield of the three major grain crops in 2015 over several major agriculture zones in China. Meteorological and environmental factors were then used to divide each agriculture zone into multiple Potential Yield Zones (PYZs), and the yield potential for each PYZ was defined as the 95% quantile of the predicted pixel-level on-farm yield. The yield gap, i.e., the difference between the yield potential and averaged actual yield during the study period, was therefore obtained.

To reduce fertilizer application, input-response models for each crop in different climate zones were developed based on the yield and corresponding nitrogen/phosphate application rate. The types of fertilizer that limited crop yield were determined by

employing the "law of the minimum" (Mueller *et al.,* 2012). The demand for the types of fertilizer other than the limiting one was calculated by an input-response model. As such, the reducible

amount of fertilizer was acquired.

The level of food security was determined by the degree of self-sufficiency, the ratio of total production to total consumption.

Results and analysis

Results show that the yield gap of rice in the Middle-lower Yangtze River Plain (MLYRP), the zone with the largest harvest area of rice in China, was 1.1 t/hm^2 in 2015, accounting for 13.3% of the rice yield potential. Closing the yield gap of rice in the MLYRP could increase the national rice production by 5%, and help to meet the predicted total rice consumption in China in 2030, thus achieving country-level self-sufficiency.

The yield gap of wheat in the North China Plain (NCP), which is

the zone with the largest harvest area of wheat in China, was 0.9 t/hm^2 in 2015, accounting for 12.5% of the wheat yield potential. Such an improvement in yield could increase the wheat production of China by about 8% of the total wheat production in 2015. The potential production over NCP, added with the on-farm production of other regions over China, can fully meet the predicted demand for wheat of the country by 2030, thus achieving country-level self-sufficiency.
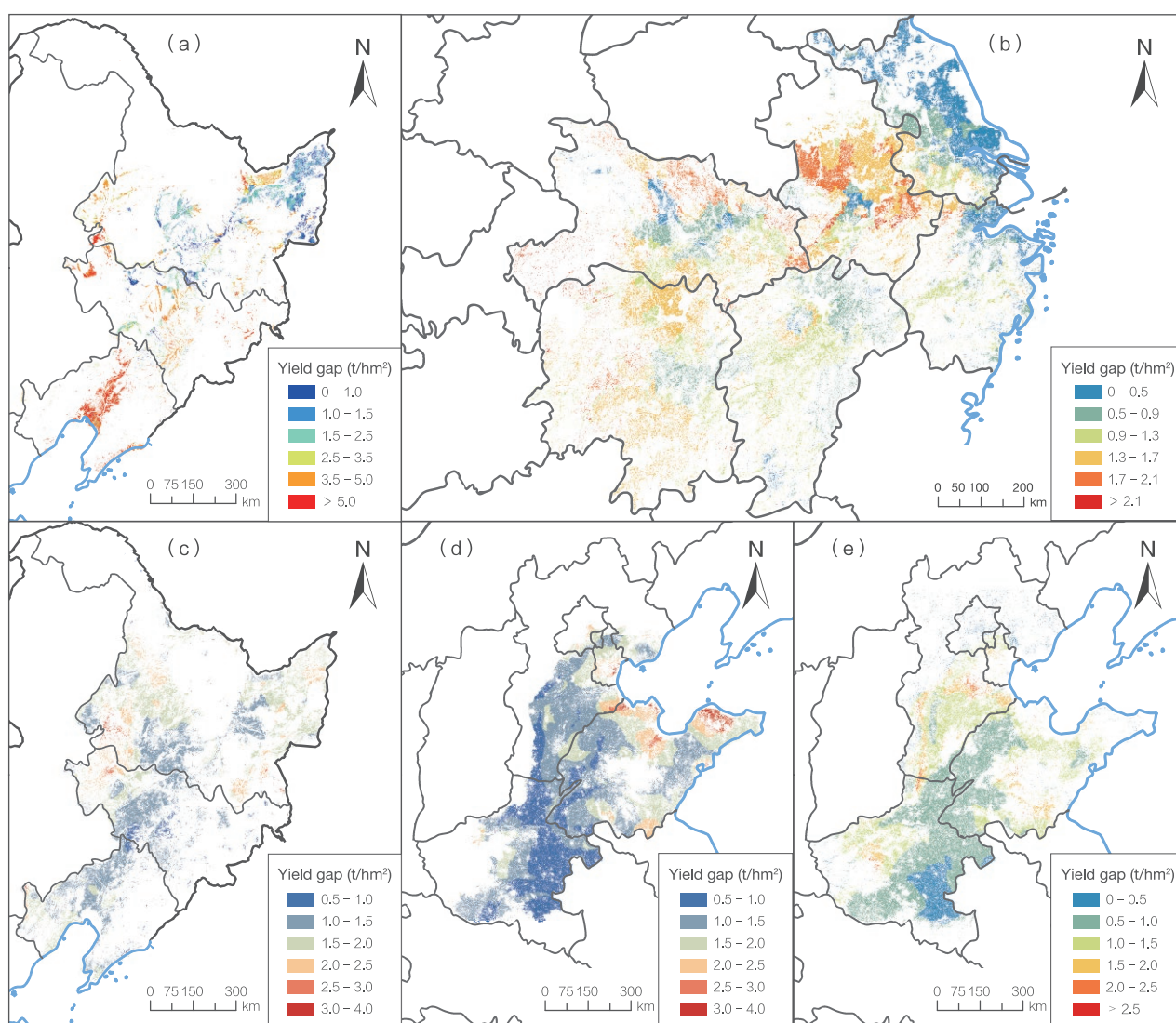
↑ Figure 2-5. Spatial distribution of yield gap for rice in the NECP (a), rice in the MLYRP (b), maize in the NECP (c), maize in the NCP (d), and winter wheat in the NCP (e) in China

The yield gap of maize in the two major agriculture zones, namely, the Northeast Plain (NECP) and NCP, are 1.5 t/hm^2 and 1.3 t/hm^2, accounting for 16.0% and 19.0% of their maize yield potential, respectively. The improvement in production by closing the yield gap in the NECP was about 6% of the national maize production in 2015, while that in the NCP was about 5%. The potential production of maize in the two zones, added with the on-farm production over other regions, can meet 89% of the predicted demand of maize in China by 2030. Therefore, achieving self-sufficiency of maize in China in 2030 requires improvement in the yield across additional regions.
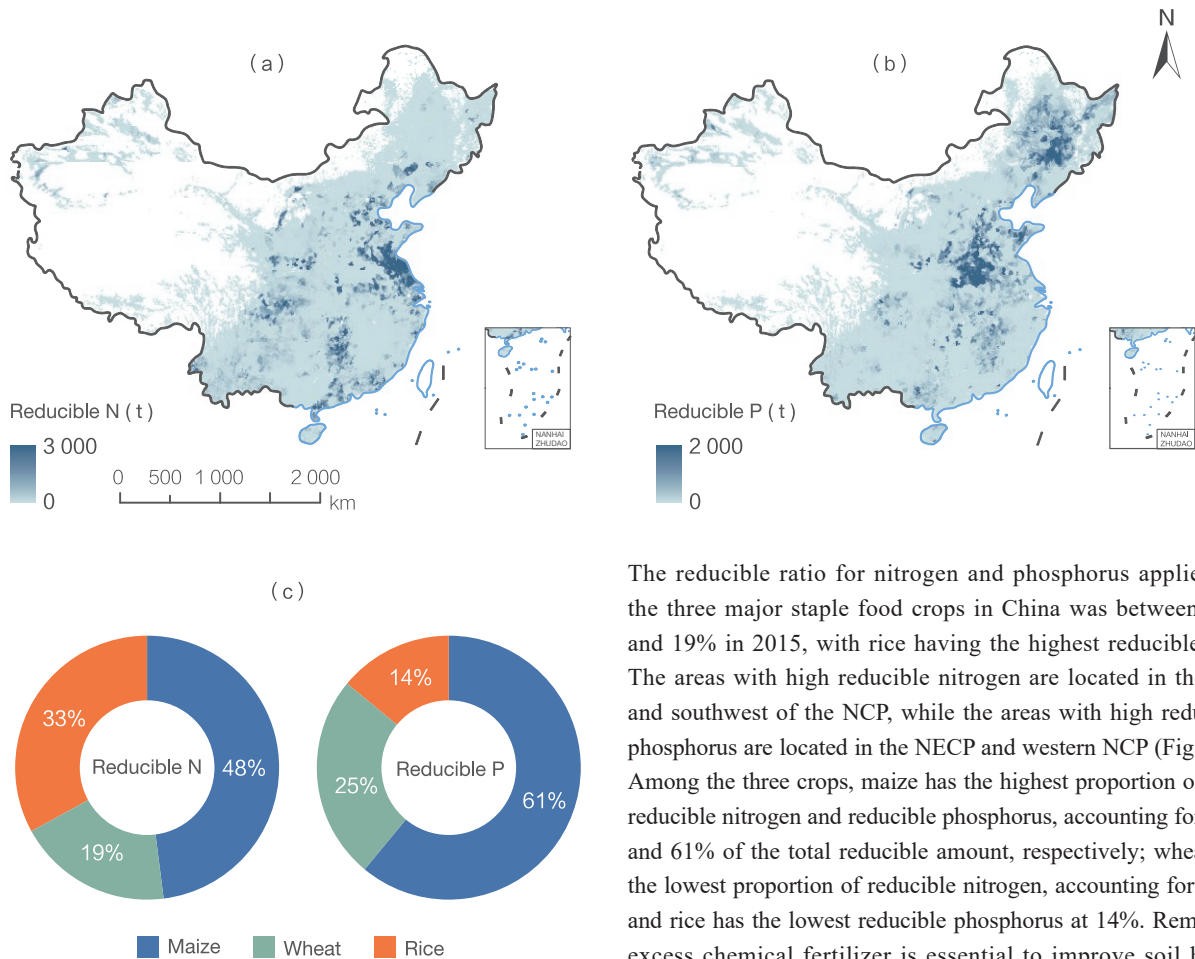
Figure 2-6. Spatial distribution of reducible nitrogen (a) and phosphorus (b) applications for the three major staple food crops and the proportion for different crops (c) (Note: no data available for Taiwan province)

The reducible ratio for nitrogen and phosphorus applied for the three major staple food crops in China was between 17% and 19% in 2015, with rice having the highest reducible rate. The areas with high reducible nitrogen are located in the east and southwest of the NCP, while the areas with high reducible phosphorus are located in the NECP and western NCP (Fig. 2-6). Among the three crops, maize has the highest proportion of both reducible nitrogen and reducible phosphorus, accounting for 48% and 61% of the total reducible amount, respectively; wheat has the lowest proportion of reducible nitrogen, accounting for 19%; and rice has the lowest reducible phosphorus at 14%. Removing excess chemical fertilizer is essential to improve soil health and alleviate agricultural non-point source pollution. Rational planning for different regions for increasing crop production or reducing excess fertilizer application is important for improving food production while reducing environmental impacts, thus helping to achieve sustainable intensification in China.

Outlook

The estimates of yield potential and reducible chemical fertilizer were acquired from two separate models in this case, which highlights difficulties in finding a pathway to increase crop production while removing excess fertilizer simultaneously. We will develop a new model that can couple these two factors in the future to provide useful information for regional optimization and finally deliver a sustainable cropping system to achieve food and ecological security.

Improving the sustainability of crop production faces systemic problems, for which the issues of the reduction of pesticide application and recycling of crop straw, agricultural film, and livestock excrement should be involved. Meanwhile, the achievement of sustainable intensification at the global scale remains uncertain due to climate change. In the future, more factors, including climate change, should be considered in analyses with regard to helping decision makers formulate systematic policies and regulations for a more sustainable cropping system.

Summary

Food systems, adequate to meet the growing need for nutrition by human beings but not at the cost of the supply of any non-agricultural commodities, are fundamental to global sustainable development.

China gives top priority to food security and seeks to boost it through science, technology and innovation. Big Earth Data encompasses data and technologies of multiple disciplines, and can enable macro-level, dynamic monitoring. It can be an effective technical tool for evaluating Goal Zero Hunger from social, economic and environmental perspectives.

Focusing on SDG 2.2.1 and 2.4.1, two indicators reflecting the demand and supply of food respectively, the cases in this section fused data from multiple sources and technologies from different disciplines and developed a remote sensing-based model for yield potential estimates. Through data production and indicator evaluation, they presented the progress China has made in improving the nutritional level of its citizens. Pathways were proposed to achieve sustainable cropland intensification and crop production. Given its great potential, Big Earth Data can offer reliable technical means for the monitoring and evaluation of SDG 2 indicators.

SDG 6
Clean Water and Sanitation

Background

Water sustains life and spurs social and economic development. However, water scarcity, pollution, and degradation are challenges we all face in achieving sustainable development. Now, 840 million people in the world still lack access to safe drinking water; over 40% of the population faces water scarcity; and even in middle-to-high income countries, 20% of waste water is discharged without being treated first (UN-Water, 2018).

To address these challenges, the United Nations proposed SDG 6, i.e. to ensure availability and sustainable management of water and sanitation for all. It includes 8 targets and 11 indicators, ranging from water resources, water environment, and water-related ecosystems to international cooperation. However, given the different levels of social and economic development, varying strengths in monitoring water resources and inconsistent assessment criteria, hard work has to be done before SDG 6 can be monitored and evaluated globally.

China is a typical example of a country suffering from water scarcity. Its fast economic growth has also exerted huge pressure on water-related environment and ecosystems. Thanks to the *Strictest Management of Water Resources* and the *Action Plan for Prevention and Control of Water Pollution*, among a host of measures adopted by the Chinese Government in recent years, there have been marked improvements in water efficiency and ecosystems. A mode of sustainable management of water resources suited for China is taking shape, supported by monitoring and evaluation made possible by Big Earth Data through remote sensing and ground observations.

This report focuses on three aspects: water resources, water environment and water-related ecosystems, and in particular, it zooms in on three indicators: bodies of water with good ambient water quality (SDG 6.3.2), level of water stress (SDG 6.4.2), and water-related ecosystems (SDG 6.6.1). It records the monitoring and evaluation of SDGs done in important wetlands both in and outside of China and the Chinese experience of trying to achieve SDG 6, in an effort to offer modeling, data, and scientific evidence for policy making.
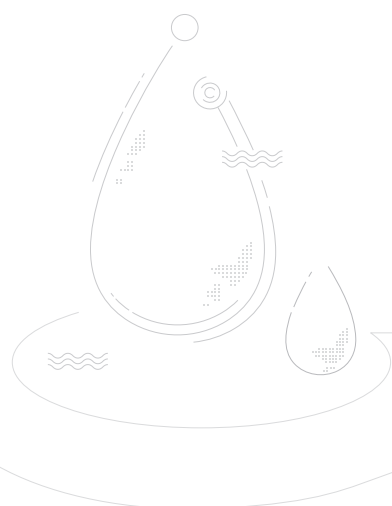
Main Contributions

An algorithm was created to measure water body transparency under SDG 6.3.2, which can be a demonstration, in terms of both methodology and practice, of monitoring water bodies' ambient quality worldwide. Regarding SDG 6.4.2, a new evaluation method was created to assess the level of water stress, useful for water distribution in the global glacier-covered arid areas. Regarding SDG 6.6.1, essential data were shared in support of China's implementation of the Ramsar Convention on Wetlands and global conservation actions (Table 3-1).

Table 3-1 Cases and Their Main Contributions			
Indicator	**Tier**	**Case**	**Contributions**
6.3.2 Proportion of bodies of water with good ambient water quality	Tier II	Spatiotemporal patterns of water transparency in China's lakes	**Data product:** time series datasets of water transparency in China's lakes (2000-2019) **Method:** a new lake water transparency monitoring and evaluation algorithm based on dual-band reflectance **Support to policy-making:** informing policies on water environmental monitoring and management in China and the rest of the world
6.4.2 Level of water stress: freshwater withdrawal as a proportion of available freshwater resources	Tier I	Evaluation of level of water stress in the Shule River basin in arid region, Northwest China	**Method:** a new evaluation method of the LWS with coupling glacier module **Support to policy-making:** providing reference for optimal distribution of water resources in GGCAAs
6.6.1 Change in the extent of water-related ecosystems over time	Tier I	Spatiotemporal distribution of China's vegetated wetlands	**Data product:** datasets of China's vegetated wetlands (2015), mangrove forests and *Spartina alterniflora* in China (2015 and 2018) **Method:** an HOHC method to map vegetated wetlands, mangrove forests and *Spartina alterniflora* **Support to policy-making:** informing policy on China's implementation of the Ramsar Convention on Wetlands
	Tier I	Dynamic change of water body in Ramsar Sites	**Data product:** datasets on 86 Ramsar Sites water body distribution in Asia, Europe, and Africa (2000-2018) **Support to policy-making:** informing policy on protection and management of Ramsar Sites

SDG 6

Case Study

Spatiotemporal patterns of water transparency in China's lakes

Target: 6.3 By 2030, improve water quality by reducing pollution, eliminating dumping and minimizing release of hazardous chemicals and materials, halving the proportion of untreated wastewater and substantially increasing recycling and safe reuse globally.

Highlights

○ During 2000-2019, the water transparency of China's lakes showed a spatial pattern of "high in the west and low in the east". Overall, water clarity was good and showed a positive trend. The proportion of Types I, II, and III water bodies with good clarity increased from 84.11% in 2000 to 92.46% in 2019.

Background

Water transparency (Secchi Disk Depth, SDD) refers to the depth at which a black/white Secchi disk becomes invisible when it sinks vertically into the water and can be used to describe water clarity. In general, the higher the transparency is, the clearer the water. Many studies have shown that satellite-derived water transparency has close relationships with water quality indicators (Chang *et al.,* 2020; Lee and Lee, 2015). To reveal the water clarity in China's lakes at a macro level, this study developed a novel remote sensing algorithm to retrieve the water transparency of large lakes in China (>20 km^2) during 2000-2019, as a useful exploration for the monitoring and evaluation of SDG 6.3.2.

Data used

◎ Land reflectance, land surface temperature, and Normalized Difference Vegetation Index (NDVI) of Moderate Resolution Imaging Spectroradiometer (MODIS) during 2000-2019.

◎ Precipitation data of the Tropical Rainfall Measuring Mission (TRMM) during 2000-2019.

◎ China's Digital Elevation Model (DEM).

◎ Reanalysis products of wind speed during 2000-2019.

◎ Chinese population density per square kilometer in 2010.

Method

This case developed a novel remote sensing algorithm of SDD applicable to the land reflectance of MODIS (MOD09GA):

$$SDD=1\ 699.72 \times e^{-170.92 \times R}, \quad R \leqslant 0.016$$

$$SDD=0.36 \times R^{-1.39}, \quad R > 0.016$$

$$R=(R_{555}+R_{645})/2\pi$$

where R_{555} and R_{645} denote reflectance at two bands of MODIS with central wavelengths of 555 nm and 645 nm respectively; R is an intermediate variable. By applying the algorithm to reflectance during 2000-2019, the daily SDD was remotely retrieved. Then, the annual and climatological mean SDD values for different lakes were further calculated through the arithmetic mean method. For the *in situ* SDD of China's lakes ($N = 2236$), 75% of the synchronous cloudless match-ups were selected randomly for algorithm calibration, and the remaining 25% were used for validation. The results of the new algorithm were comparable to those of reported regional algorithms, indicating the wide applicability of the new algorithm at regional and national scales.

Results and analysis
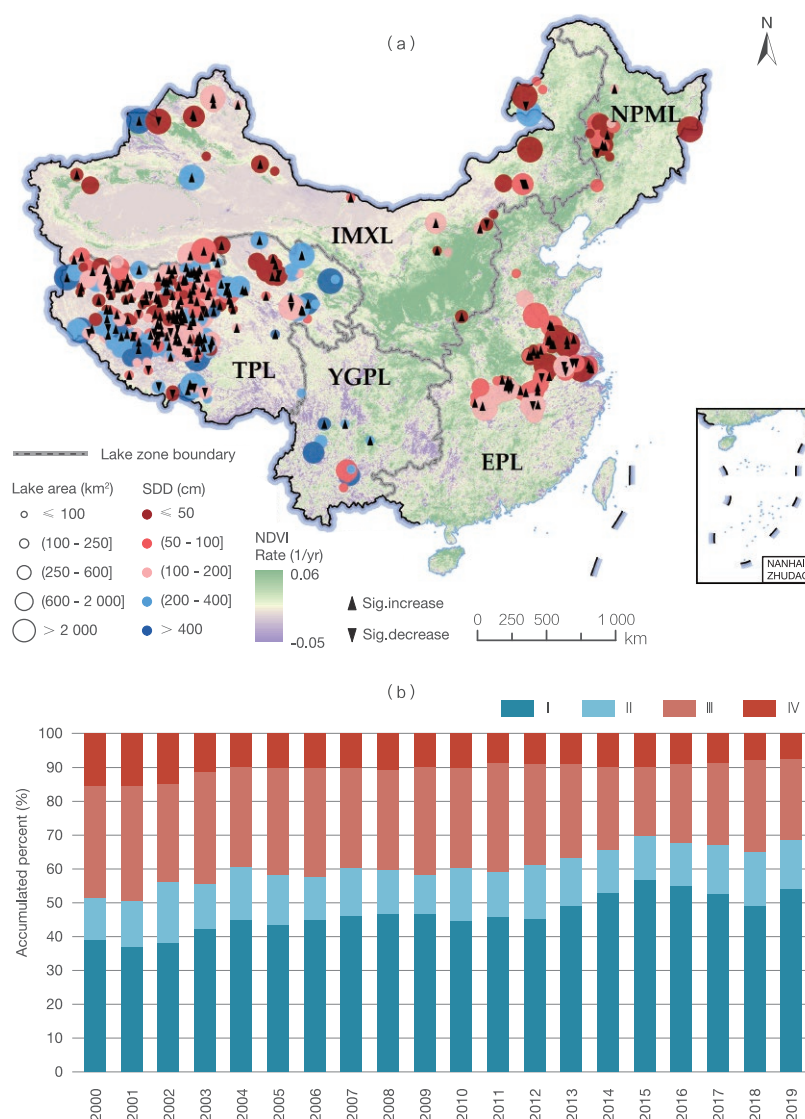
1) Spatiotemporal patterns of SDD in China's lakes

Overall, the SDD of China's lakes showed a geographical pattern of "high in the west and low in the east." The mean SDD of lakes in the three western mountainous lake zones (180.28 ± 171.29 cm) was more than twice that of the two eastern plain lake zones (78.01 ± 40.54 cm) (Fig. 3-1a). The mean SDD values in the Yunnan-Guizhou Plateau Lake (YGPL), Tibetan Plateau Lake (TPL), Inner Mongolia-Xinjiang Lake (IMXL), Eastern Plain Lake (EPL), and Northeast Plain and Mountain Lake (NPML) zones were 404.63 ± 363.98 cm, 182.41 ± 184.29 cm, 139.70 ± 193.96 cm, 92.90 ± 90.09 cm, and 55.05 ± 33.46 cm, respectively (Fig. 3-1). The results showed that the spatial changes in lake SDD were mainly influenced by water depth, which explained 88.81% of the spatial variations. *In situ* showed that water eutrophication also reduced SDD and there was a significant negative power correlation between the measured chlorophyll a and SDD ($N = 1827$, $r = 0.36$, $p < 0.001$).

During 2000-2019, the water clarity of China's lakes improved to a certain extent. For the 412 studied lakes, which accounted for 87.02% of China's total lake areas, 70.15% showed increases in SDD, and 42.72% showed significant increases. Vegetation restoration in the catchment played a major role in increasing lake SDD. Improvement in NDVI contributed 44.95%, 37.87%, 75.66%, 58.12% and 36.34% of the increases in SDD in the IMXL, TPL, YGPL, NPML and EPL zones, respectively. Climate change also showed significant effects on increasing SDD, especially for lakes in the TPL zone. The rising air temperature led to the melting of glaciers and rising lake water levels, which explained 24.98% of the increase in SDD in the TPL zone.

2) Proportions of lakes at different water clarity levels

According to the published standard (Chang *et al.,* 2020; Lee and Lee, 2015), this case set thresholds for different water clarity levels: lakes with annual mean SDD values of ≤ 25, (25, 65], (65, 100] and > 100 (unit: cm) were classified as Types IV, III, II and I, respectively. Most lakes of Type I were located in western China, especially in the TPL zone. For lakes in the two eastern lake zones, most were Type III, and the degradation of water clarity was observed in some of these lakes. From 2000 to 2019, Type I lakes increased significantly from 39.12% to 54.01%; Type II lakes remained stable at approximately 14.21%; Type III

Figure 3-1. The SDD values of China's large lakes during 2000-2019
(a) The mean SDD values; (b) Proportions of lakes with different water clarity levels

The change rate in NDVI was the linear fitting slope during 2000-2019. IMXL: Inner Mongolia-Xinjiang Lake; TPL: Tibetan Plateau Lake; YGPL: Yunnan-Guizhou Plateau Lake; NPML: Northeast Plain and Mountain Lake; EPL: Eastern Plain Lake

lakes decreased significantly from 32.52% to 23.84%; and Type IV lakes also decreased significantly from 15.89% to 7.54%. The combined proportion of lakes with good water clarity (Type I, II or III) increased from 84.11% in 2000 to 92.46% in 2019 (Fig. 3-1), representing an increase of 8.35 percentage points. In general, China's large lakes exhibit good water clarity and are still improving.

Outlook

This case developed a remote sensing algorithm to rapidly map SDD in China's lakes and quantitatively calculated the contributions of different impact factors to the spatiotemporal variations in SDD. Vegetation restoration in the catchment had positive effects on increasing lake SDD during 2000-2019. Overall, the water clarity of large lakes in China is fairly good and still improving, with the proportions of lakes in Types I, II or III up from 84.11% in 2000 to 92.46% in 2019. Based on correlation analyses, this case proposed three measures to improve water clarity of China's lakes: ecological water replenishment, eutrophication control, and vegetation restoration in the catchment.

Evaluation of level of water stress in the Shule River basin in arid region, Northwest China

Target: 6.4 By 2030, substantially increase water-use efficiency across all sectors and ensure sustainable withdrawals and supply of freshwater to address water scarcity and substantially reduce the number of people suffering from water scarcity.

Highlights

● *The average glacier meltwater contribution to the total runoff of the Shule River basin will decrease from the current 23% to 15% by 2030s (RCP 2.6 scenario).*

● *From 2015 to 2020, supply of fresh water resources has been close to the level of demand. Between 2021 and 2030, the level of water stress will increase.*

Background

As a solid body of water, glaciers play an extremely important role in the sustainable water use in the global arid area. The population of the arid areas highly dependent on glacial water resources is nearly 200 million. Against the background of global warming, mountain glaciers across the world have been melting at a faster pace, resulting in weaker capacity for continuous water supply to some arid areas, triggering a chain effect on the downstream ecological-social-economic systems,

such as shortage of water for economic and social purposes, and increase in potential risks of desertification (Allan *et al.,* 2019; Immerzeel *et al.,* 2019).

LWS is the most direct indicator of water resource stress. Currently, however, a module is lacking for glacial runoff LWS, the correct assessment of which is a key to the accurate assessment of the LWS in the Global Glacier-Covered Arid Areas (GGCAAs).
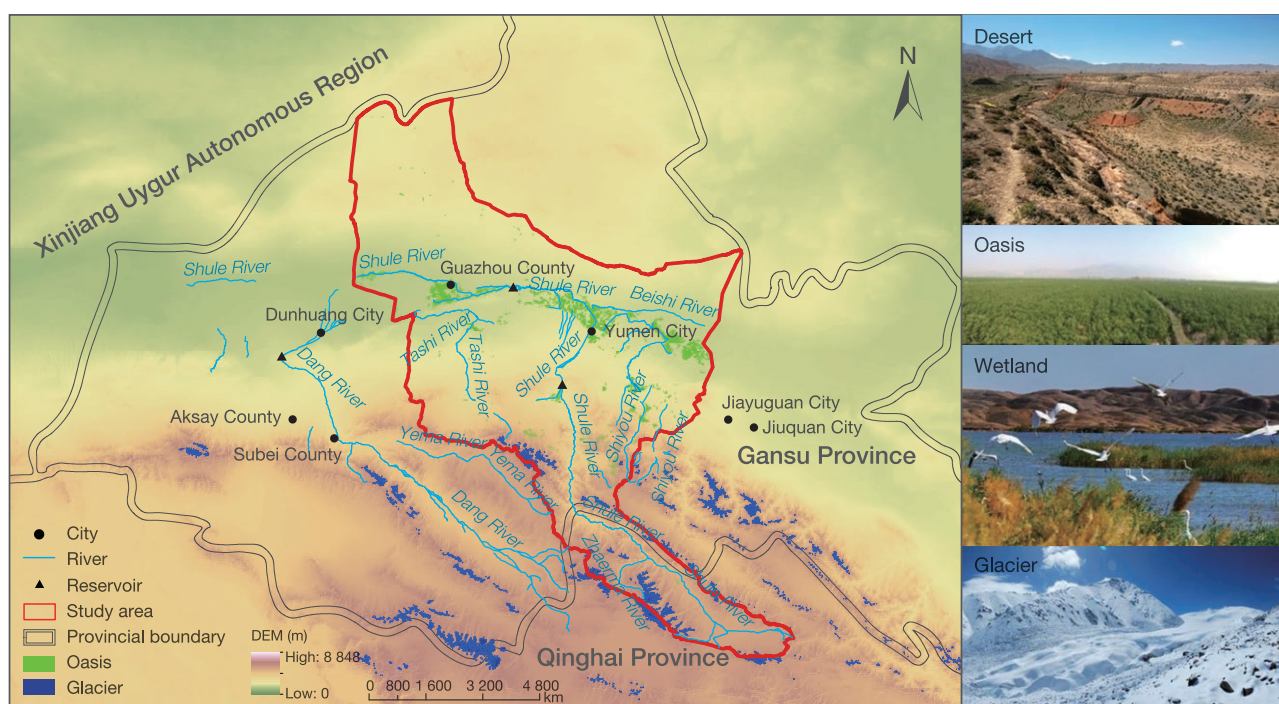
↑ Figure 3-2. Spatial distribution of glaciers, runoffs, and oases in the Shule River basin

The Shule River basin, located in the arid region of northwest China (it straddles Haibei Tibetan Autonomous Prefecture, Qinghai province and Jiuquan city, Gansu province), is a typical example of the GGCAAs (Fig. 3-2). The case calculated and simulated the total runoff, glacial runoff from the upper reaches of the Shule River basin, and basin socio-economic water demand, evaluated the basin's LWS from 2000 to 2030, and put forward policy recommendations on water resources security.

Data used

◎ The First and Second Chinese Glacier Inventory (1970-2004; 2006-2011) .

◎ Runoff data of Changmabao hydrological station from mountainous watershed in the Shule River basin.

◎ Basin Statistical Yearbook, Social and Economic Bulletin and water demand indicators of basin primary, secondary, and tertiary industries during 2000-2018.

Method

The case analyzed the impact of glacial runoff changes on the LWS in the basin under Representative Concentration Pathway (RCP) 2.6 (a sustainable development scenario) and developed a new evaluation method of the LWS with coupling glacier module. The method (as shown below) can be used for the LWS calculation in the GGCAAs.

$$LWS = \frac{D_{se}}{S} = \frac{D_p + D_d + D_{ae}}{R_{total} - D_{ne}}$$

where the LWS is the level of water stress; S is the available fresh water resources; D_{se} is the social and economic water demand, including water needed for production (D_p), domestic consumption (D_d), and artificial ecosystems (D_{ae}) (calculated by the water quota method); R_{total} is the watershed runoff; D_{ne} is ecological baseflow (calculated by the hydrological index method, i.e. the ordinal "90%" observation year out of a list of the average flow of the driest month of each year in descending order). In arid basins, glacial runoff, accounting for a high proportion of the total in dry seasons, is of great significance for maintaining the ecological baseflow of rivers. The Nash efficiency coefficient and R^2 index were selected to evaluate the simulations of upstream runoff in the basin from 1991 to 2013. The results showed fairly good simulation effects, with the Nash efficiency coefficient being 0.89 and R^2 0.89 (Zhang *et al.*, 2019).

Results and analysis

In the context of global warming, the increases in precipitation and glacial meltwater in the upper reach of the Shule River basin lead to an upward trend of the total upstream surface runoff. During the period 2000-2010, the average annual runoff was about $1.04 \times 10^9 \, m^3$, of which the average annual glacial runoff was about $2.64 \times 10^8 \, m^3$. Forecasts indicate that, compared with 2000-2010, the average runoff will increase by 22.8%, while the average glacial runoff will decrease by 11% from 2020 to 2030. The contribution of glacial meltwater to the SLR will be reduced from 23% at present to 15% by 2030s (RCP 2.6 scenario).

During the period 2000-2010, the average annual ecological baseflow in the Shule River basin was $4.20 \times 10^8 \, m^3$, accounting for 40.6% of the average annual surface runoff. During the period from 2020 to 2030, it will decrease to $3.84 \times 10^8 \, m^3$, accounting for 30.2% of the annual average surface runoff. Affected by the reduction of glacial runoff, the ecological baseflow in the Shule River basin has shown a downward trend. The annual available freshwater resources increased generally between 2000-2010, totaling $6.16 \times 10^8 \, m^3$, and will increase by 44.2% to $8.88 \times 10^8 \, m^3$ between 2020-2030 due to increase in precipitation.

From 2000 to 2004, the basin freshwater withdrawal was about $5 \times 10^8 \, m^3$. It increased rapidly to $9.89 \times 10^8 \, m^3$ from 2005 to 2014, due to resettlement and expansion of arable land, with the LWS hovering around 1.45. From 2015 to 2020, under the restriction of water use quota, there has been a basic equilibrium between supply and demand for water resources in the basin. If the current trend continues, during the period 2021-2030, annual freshwater withdrawal will continue to increase, and the LWS will rise (Fig. 3-3). Glacial runoff has contributed to an average reduction of the LWS by 0.71 from 2000 to 2030.
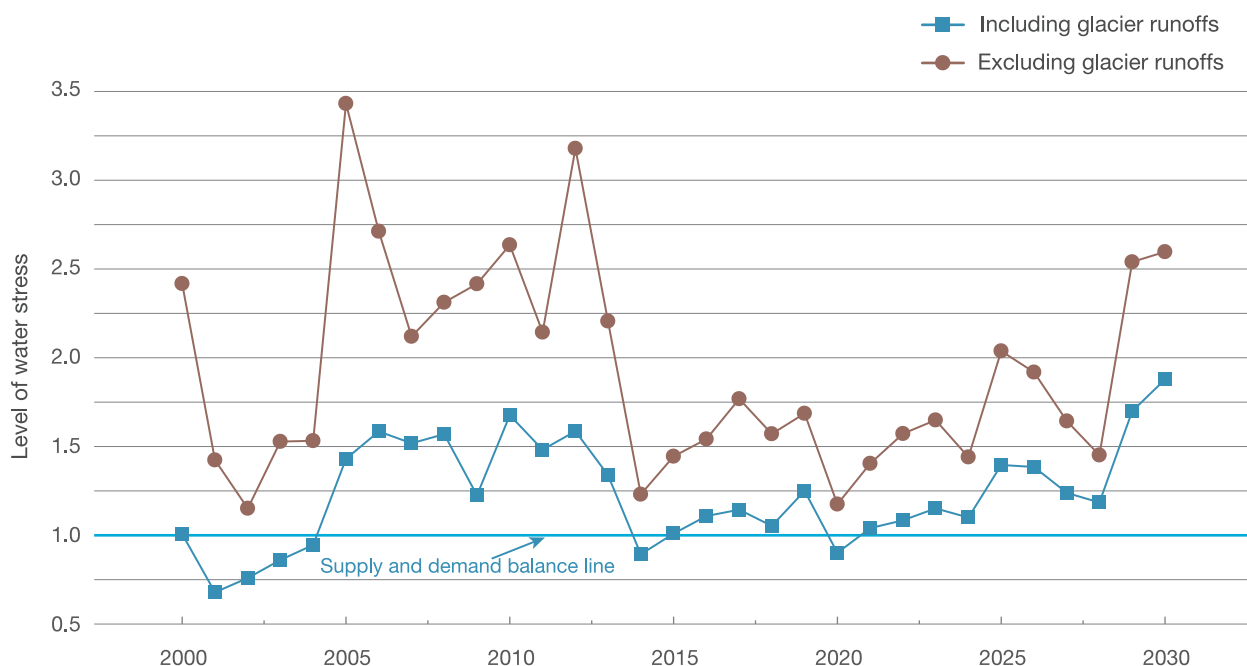
↑ Figure 3-3. The changes of level of water stress in the Shule River basin in arid region of Northwest China

Outlook

Glacial runoff is important to the relief of water stress and sustainable development of eco-economic system in the GGCAAs. Glacial runoff has an obvious regulating effect on surface runoff. In the future, as the glacial meltwater runoff in the Shule River basin continues to decrease, its role in regulating and relieving water stress in the basin will be greatly weakened. In dry years with high temperature and low rainfall and years with large water withdrawals, the LWS in the basin may greatly increase. Higher agricultural irrigation water consumption and lower water use efficiency are the main factors leading to a certain level of water stress in the basin. In the future, strict control over arable land expansion, higher irrigation water use efficiency and developing efficient, water-saving agriculture hold the key to reducing freshwater withdrawal and maintaining the sustainable use of water resources in the GGCAAs.

Spatiotemporal distribution of China's vegetated wetlands

Target: 6.6 By 2020, protect and restore water-related ecosystems, including mountains, forests, wetlands, rivers, aquifers and lakes.

Highlights

- *Analysis of the spatial distribution of China's vegetated wetlands in 2015 and measurement of changes in mangrove forests and Spartina alterniflora in China between 2015 and 2018 showed that the net increase in mangrove forests was 22.11%, and the net decrease in invasive Spartina alterniflora was 2.59%. In China, mangrove forests have been significantly restored and the invasion of Spartina alterniflora was under effective control.*

Background

Wetland is a key component of the life community comprising mountains, rivers, forests, fields, lakes, and grasses. Their protection and management is critical to the Building a Beautiful China Campaign. Analysis of changes in wetlands' spatiotemporal distribution is an important basis for assessing the national achievement of SDG 6.6, and will also provide key data to support the implementation of the Ramsar Convention on Wetlands.

Data used

◎ Landsat-8 Operational Land Imager (OLI) images (2015 and 2018).

◎ DEM, vector data of administrative division, 1:1 000 000 vegetation type map, climatic zones map, global water distribution maps (2015 and 2018).

◎ Massive ground survey samples, governmental statistical and monitoring data.

Method

This case study applied the Hybrid Object-based and Hierarchical Classification (HOHC) approach to map national vegetated wetlands. The work flow includes: first, select remote sensing data of different seasons as data sources by climatic zone and vegetated wetland type; second, classify wetland based on multi-scale segmentation and the hierarchical decision tree method; third, validate or correct classification results based on massive field survey samples (Jia *et al.,* 2018; Mao *et al.,* 2019, 2020). Finally, datasets of China's vegetated wetlands in 2015 and mangrove forests and *Spartina alterniflora* (*S. alterniflora*) in 2015 and 2018 were obtained, with an overall accuracy of classification for the former at 95% and for the latter over 92%.

Results and analysis

1) Spatial patterns of China's vegetated wetlands

Vegetated wetlands in China were estimated to be $1.64 \times 10^5 \, km^2$ in 2015, including inland vegetated wetlands (98%) and coastal vegetated wetlands (2%) (Fig. 3-4). China's vegetated wetlands were observed mainly in Tibet, Qinghai, Inner Mongolia, Heilongjiang, and Xinjiang. They were primarily distributed in areas with annual precipitation between 300 and 600 mm and elevation below 200 or above 3 000 m.

2) Spatiotemporal distribution and areal changes of mangrove forests in China

Mangrove forest is an important part of global biodiversity that must be protected. In recent years, China has been continuously strengthening the protection and restoration of mangrove forests, and has become one of the few countries in the world with net
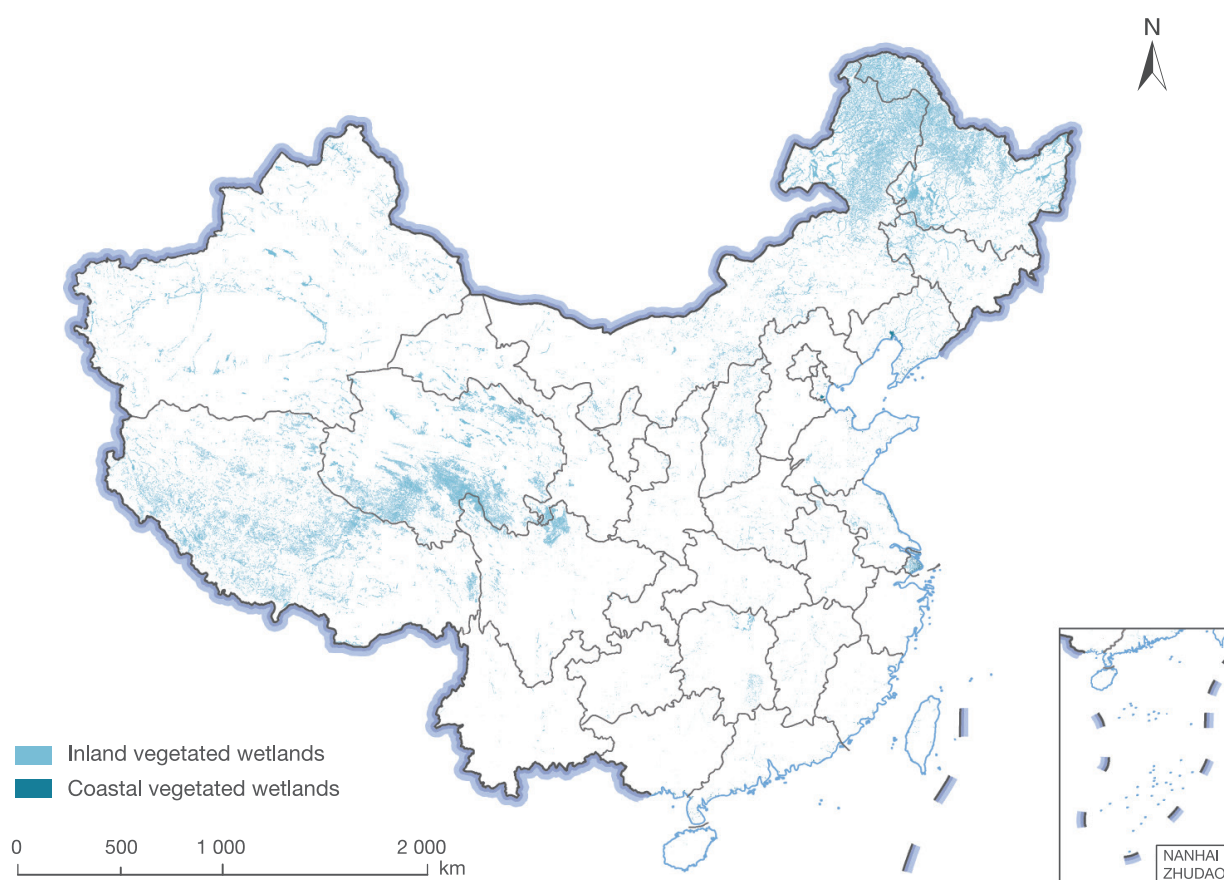
↑ Figure 3-4. The map of vegetated wetlands distribution in 2015

increase in mangrove forest area. In 2018, the Guangdong-Hong Kong-Macao Greater Bay Area had the largest mangrove area, followed by Guangxi and Hainan. The three regions have 95% of the country's total mangrove forest areas. From 2015 to 2018, mangrove areas in China increased from 226.74 km^2 to 276.89 km^2 with a net increase of 22.11 % (Fig. 3-5). The areal extent of mangrove forest increased significantly in Guangxi and Guangdong, increased slightly in Hainan, and decreased slightly in Taiwan province.

3) Spatial distribution and areal changes of *S. alterniflora* in China

The invasive *S. alterniflora* has been regarded as one of the main threats to ecological security along Chinese coasts. In 2018, *S. alterniflora* was primarily observed in four provinces/municipality: Jiangsu, Zhejiang, Shanghai, and Fujian. The largest areas invaded by *S. alterniflora* were in Jiangsu, accounting for one third of the total invaded areas in the country. Such areas decreased from 547.43 km^2 in 2015 to 533.24 km^2 in 2018, with a net decline of 14.19 km^2 (Fig. 3-5). Due to human control and aquacultural expansion, among others, four provinces/municipalities—Zhejiang, Shanghai, Jiangsu, and Tianjin—saw areal declines of *S. alterniflora*, particularly in Zhejiang with the largest area decline of 15.52 km^2. Despite overall areal decline across the country, certain regions still faced a severe invasive trend, for example the Yellow River Delta. No *S. alterniflora* was observed in Taiwan and Hainan provinces.

2018
Spartina alterniflora distribution

Spartina alterniflora

0 75 150   300
|——|——|————————| km

(a) 2015 — 547.43 km²

- 0.78%
- 1.56%
- 0.05%
- 1.43%
- 4.55%
- 13.29%
- 33.61%
- 26.12%
- 18.62%

(b) 2018 — 533.24 km²

- 0.24%
- 2.09%
- 0.62%
- 2.08%
- 6.69%
- 14.52%
- 32.83%
- 23.82%
- 17.11%

NANHAI ZHUDAO

Legend:
- Hebei
- Tianjin
- Shandong
- Jiangsu
- Shanghai
- Zhejiang
- Fujian
- Guangdong
- Guangxi
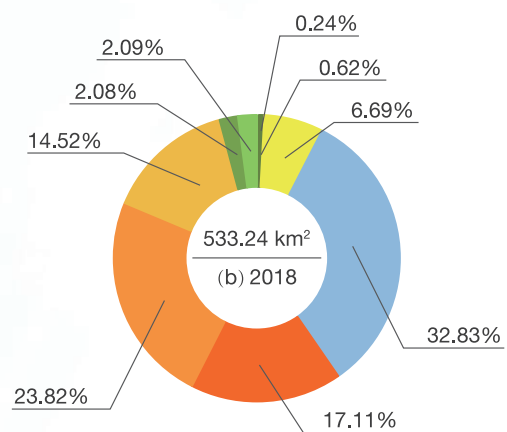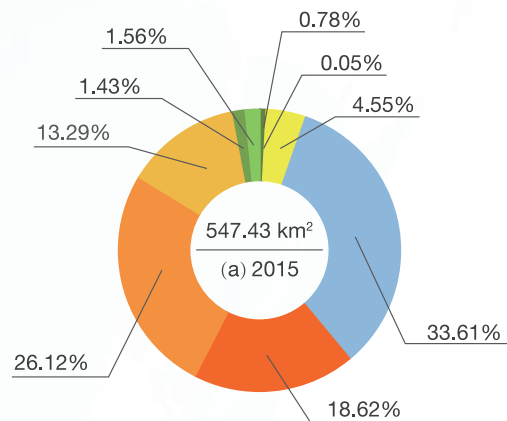
Areal changes of Spartina alterniflora during 2015–2018

- 2015
- 2018

Area (km²): Guangxi, Guangdong, Fujian, Zhejiang, Shanghai, Jiangsu, Shandong, Tianjin, Hebei

2018

Mangrove forest distribution

Zhejiang

Fujian

Guangxi

Guangdong

Taiwan

Hainan

N

■ Mangrove forest

0 50 100 200 km

NANHAI ZHUDAO
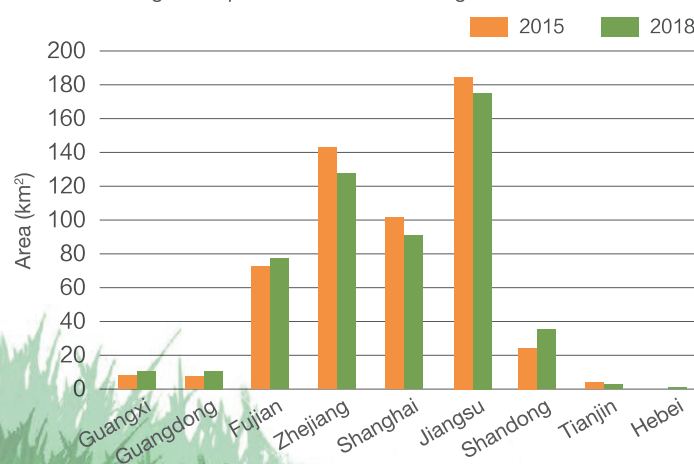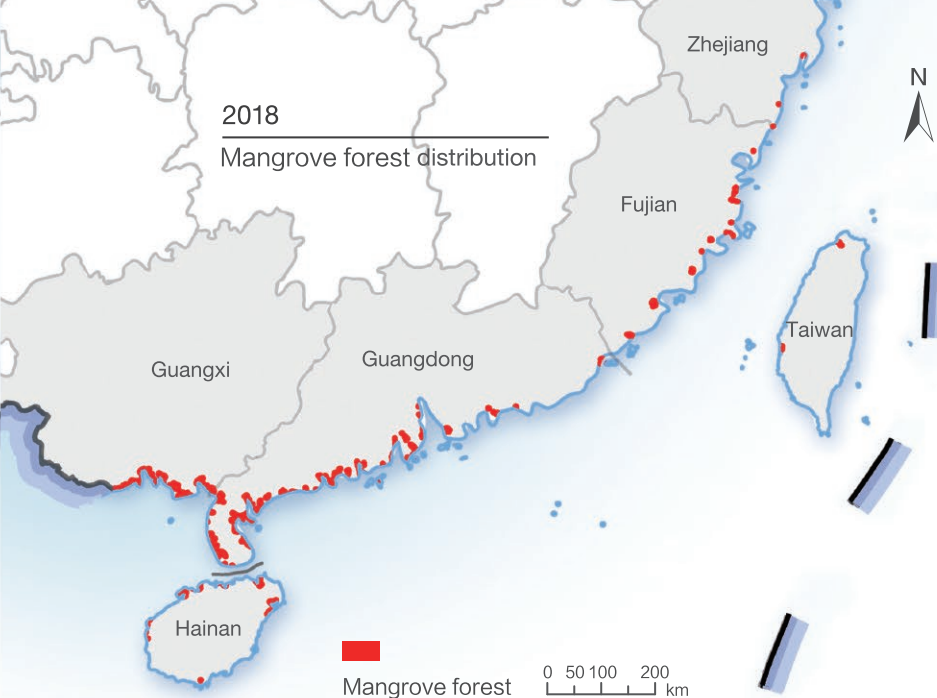
Figure 3-5.

◉ The maps of mangrove forests and *S. alterniflora* distribution in 2015 and 2018. Right maps are mangrove forests and left maps are *S. alterniflora*. (a) 2015; (b) 2018
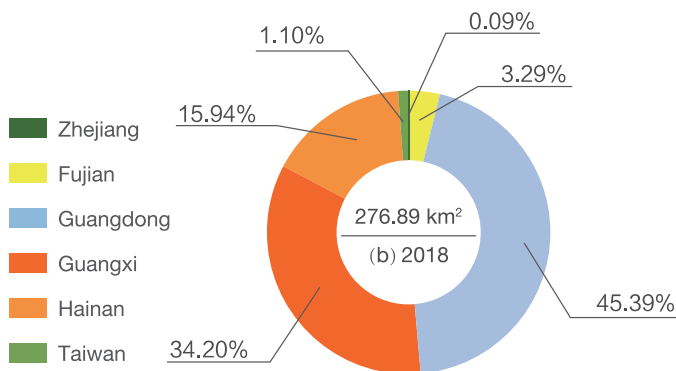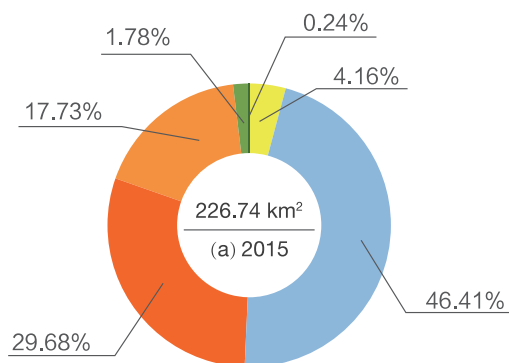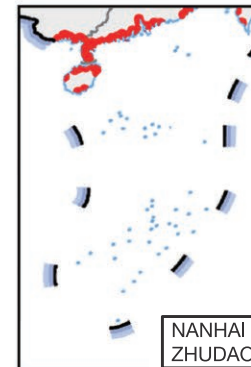
Areal changes of mangrove forest during 2015-2018

■ 2015   ■ 2018

Area (km²)

Guangdong Guangxi Hainan Fujian Taiwan Zhejiang

1.78%   0.24%
17.73%   4.16%
29.68%
46.41%

226.74 km²
(a) 2015

1.10%   0.09%
15.94%   3.29%
34.20%
45.39%

276.89 km²
(b) 2018

■ Zhejiang
■ Fujian
■ Guangdong
■ Guangxi
■ Hainan
■ Taiwan
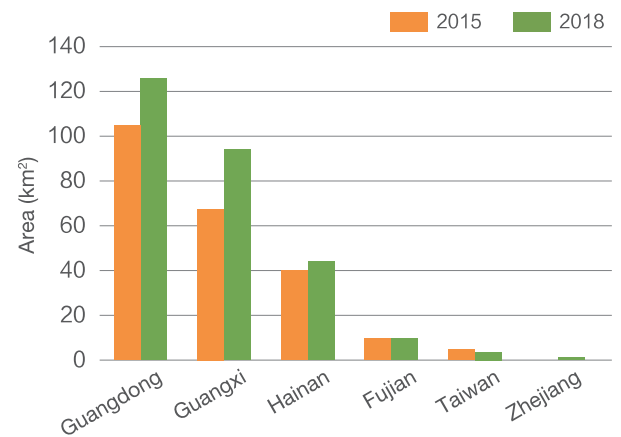
Outlook

This case study developed an HOHC method to map vegetated wetlands in China and applied it to establish datasets of China's vegetated wetlands in 2015 and mangrove forests and *S. alterniflora* in 2015 and 2018 with high mapping accuracy. These datasets can provide an important scientific basis for evaluating SDG 6.6 at the national scale.

This case study finds that: (1) Since 2015, the area of mangrove forests in China has increased markedly, which means a great contribution to the global protection and restoration of mangrove forests; (2) From 2015 to 2018, the area in China invaded by *S. alterniflora* showed a trend of net decrease, reversing the previous upward trend, suggesting that the actions of *S. alterniflora* control in China had produced initial results.

Dynamic change of water body in Ramsar Sites

Target: 6.6 By 2020, protect and restore water-related ecosystems, including mountains, forests, wetlands, rivers, aquifers and lakes.

Highlights

● *Based on the long-term water body dataset with high time resolution, the dynamic changes in water areas in Ramsar Sites were analyzed. The results showed that from 2000 to 2018, 50% of the Ramsar Sites in Asia, Europe, and Africa exhibited a trend of significant change, and most of them (58%) an upward trend.*

Background

The dynamic monitoring of the water bodies in the Ramsar Sites can directly or indirectly reflect the trend of changes and protection effect of the wetland ecosystem (Zheng *et al.,* 2012). At present, there are 171 Contracting Parties to the Ramsar Convention on Wetlands committed to wetland conservation and management. By May 2020, there were 2 391 wetland reserves on the Ramsar Sites List, covering a land area of $2.53{\times}10^{6}\,km^{2}$.

The United Nations Water (UN-Water) has provided datasets

related to SDG 6.6.1, including surface water, mangroves, reservoirs, and wetlands, based on the Global Surface Water Explorer (Pekel *et al.,* 2016) and Global Lakes and Wetlands Database (Lehner and Doll, 2004) developed by the Joint Research Centre of the European Commission (JRC). However, there is no direct and comprehensive monitoring and evaluation of the ecological status of Ramsar Sites. The dynamic change of the water bodies in Ramsar Sites has a direct impact on the ecological environment of such reserves.

Data used

◎ Boundaries of Ramsar Sites in Asia, Africa and Europe (2020).

◎ Global water bodies dynamic datasets from 2000 to 2018, Aerospace Information Research Institute, Chinese Academy of Sciences, with a spatial resolution of 250 meters and temporal

resolution of 8 days (Han and Niu, 2020).

◎ Watershed boundaries data (2000), World Wide Fund for Nature (WWF) .

Method

This case study selected 86 representative inland Ramsar sites and their corresponding 51 basins in Asia, Europe, and Africa. The overall trend of changes in the water bodies and the inter-annual trend of variation within a year was analyzed using the least square linear regression method, and the significance level of the changes was tested through double tail t-test (0.05). According to the time series water body datasets, the water

bodies were further divided into three types: permanent water bodies, seasonal water bodies, and temporary water bodies; their change trends were extracted through wavelet transform and time series decomposition method. Seven typical Ramsar sites of varying degrees of change were further selected for analysis and assessment of water body changes.

Results and analysis

In general, 50% (43/86) of the selected Ramsar Sites showed significant water body changes (Fig. 3-6). Among them, 25

sites showed increase and 18 decrease. In terms of stability (intra-annual variation) of water bodies in Ramsar Sites, the

（a）

N

（b）

Ramsar Site   Basin

● Extremely significant increase

● Significant increase

● No significant change

● Significant decrease

● Extremely significant decrease

0   1 500   3 000   6 000
                              km
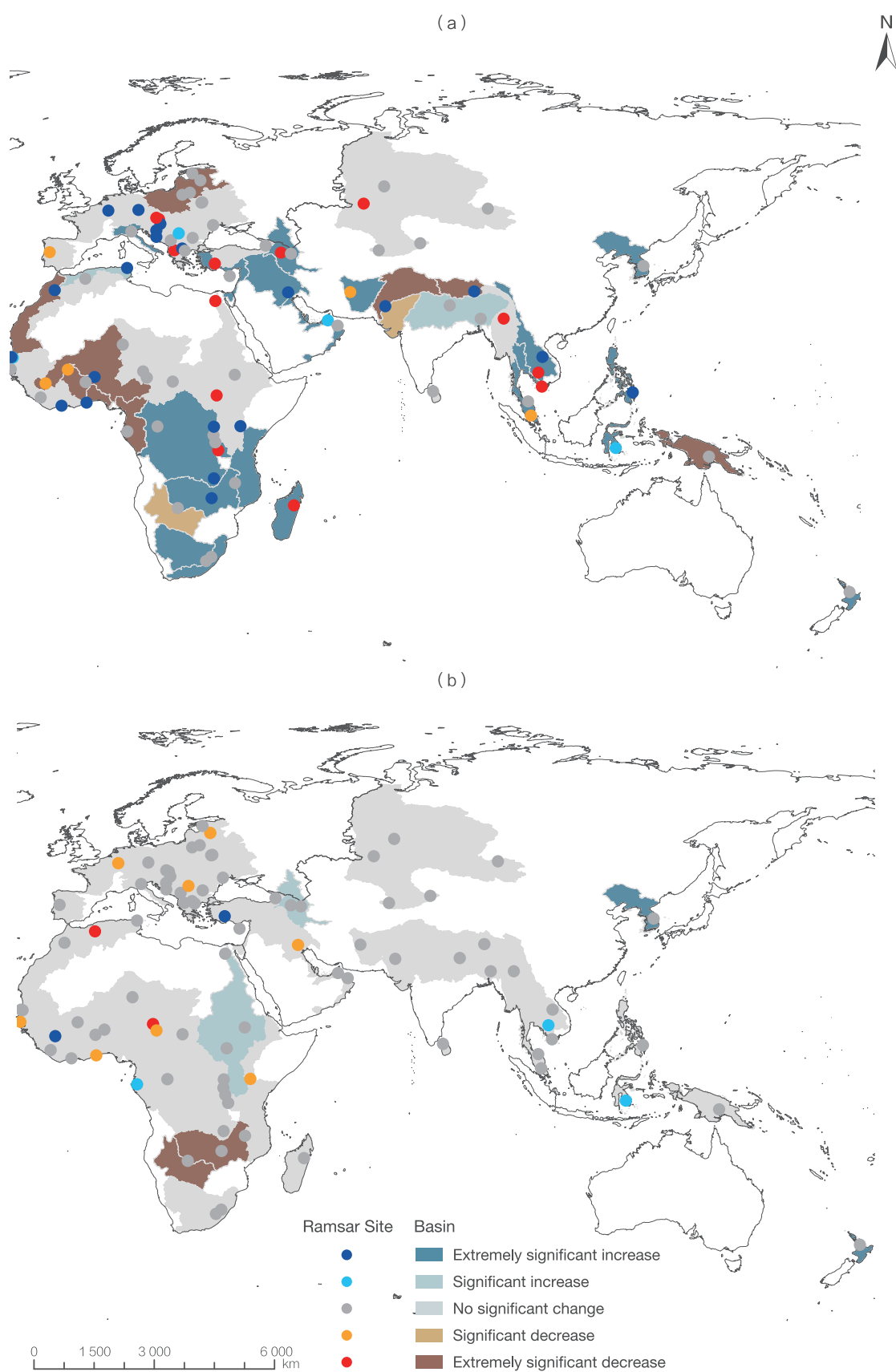
↑ Figure 3-6. The variation trend of the water area of Ramsar Sites and their basins from 2000 to 2018
(a) Interannual variation trend; (b) Seasonal fluctuation characteristics

vast majority (83%) sites remained relatively stable. The water fluctuation level rose in less than 6% (5/68) of the Ramsar Sites, while the level dropped in 12% (10/86).

Different water body types (permanent, seasonal and temporary) of Ramsar Sites showed different change patterns. In the Boeng Chhmar and Lake Burdur reserves, despite increase in temporary water bodies, the total area of water bodies showed a downward trend due to the decrease in permanent water bodies.

Because of the increases in permanent water bodies (2/5) and temporary water bodies (3/5), there was an upward trend in the five Ramsar Sites—Rawa Aopa Watumohai National Park, Central Marshes, Vallée de la Haute-sûre, Keta Lagoon Complex

Ramsar site, and Lake Baringo.

The changes in water bodies in the basins where the Ramsar Sites are located demonstrated different features from those within the Ramsar Sites. For six Ramsar Sites, the water bodies in the basins where they are located exhibited a downward trend, mainly due to the decreases in permanent water bodies in the basins and also related to the changes in seasonal water bodies (basins of Rawa Aopa Watumohai National Park and Keta Lagoon Complex Ramsar) and temporary water bodies (basins of Boeng Chhmar and Lake Baringo). However, the water bodies of the basin of Keta Lagoon Complex Ramsar Site showed a significant upward trend.

Outlook

The case study assessed some Ramsar Sites selected from a multitude of them for the significant changes in their water bodies. In the future, such monitoring can be extended to all Ramsar Sites on a global scale. To achieve SDG 6.6.1, it is necessary to speed up the development of global remote sensing

mapping products of water-related natural ecosystems (Hu *et al*., 2017; Zheng *et al.,* 2015), and research on theories and methods for the monitoring and evaluation of Ramsar Sites and related protected areas.

Summary

This chapter focuses on water resources, water environment and water-related ecosystems. Big Earth Data-enabled models and methods were developed for evaluating transparency of lakes (SDG 6.3.2), water-use efficiency (SDG 6.4.1), LWS (SDG 6.4.2) and water-related ecosystems (SDG 6.6.1), making it possible for multiple SDG 6 indicators to be monitored and evaluated in dynamic, spatial and quantitative ways. Data products, methods and how they can support policy-making on water security were

presented.

Two tasks deserve future attention:

◎ Comprehensive evaluation of the implementation of multiple indicators of SDG 6 in China and the world, such as water resources, water environment and water-related ecosystems.

◎ Coordinated monitoring and evaluation of indicators under Goals 2, 6, 11, 13, and 15.

Nanwenghe Wetland

SDG 11
Sustainable Cities and Communities

Background

Sustainable cities and communities hold the key to achieving all the 17 SDGs. At the current pace, by 2030, 60% of the world's population will be living in cities, and by 2050, the rate will be approaching 70% (United Nations, 2018). Fast urbanization has brought huge challenges on many fronts, such as an increasing number of slum dwellers due to housing shortages, traffic congestion, worsening air pollution and sewage, insufficient fresh water supply, waste disposal problems, and inadequate basic services and infrastructure. Unplanned urban expansion is particularly prone to the impact of climate change and natural disasters.

To address these challenges, the United Nations proposed SDG 11: make cities and human settlements inclusive, safe, resilient and sustainable, encompassing 7 technical targets and 3 policy targets and 15 indicators. However, the availability of data is a problem in the monitoring and evaluation of 13 out of the 15 indicators. SDG 11 is related to at least 11 other SDGs, and about one third of the 230+ SDG indicators can be measured in cities. The course of action for the next 20 years has been charted by the *New Urban Agenda*, adopted at the United Nations Conference on Housing and Sustainable Urban

Development (Habitat III) in October 2016. Under its 13th Five-year Plan, China will advance urbanization by giving more farmer-turned-migrant workers city dwellers' status, improving urban structure and appearance, making cities pleasant and livable, refining the system for housing supply and promoting coordinated development between urban and rural areas. As part of *China's National Climate Change Adaptation Strategy*, the *Action Plan for Urban Adaptation to Climate Change*, issued in February 2016, requires urban planning to be done in a way that improves the management of the urban environment. In December of the same year, the State Council issued the Program of Innovation Demonstration Areas for Implementation of the 2030 Agenda, and so far such demonstration areas have been built in Shenzhen, Taiyuan, Guilin, Chenzhou, Lincang and Chengde to showcase sustainable development.

The report presents Big Earth Data-enabled monitoring and evaluation of informal settlements (SDG 11.1.1), convenient access to public transport (SDG 11.2.1), urbanization (SDG 11.3.1), urban disasters (SDG 11.5.1/SDG 11.5.2), and open public space (SDG 11.7.1) at national and local scales, and integrated SDG 11 assessment at the provincial level in China.

Main Contributions

Cases in this report present studies on monitoring and evaluation of SDG 11 using Big Earth Data to facilitate policy development and actions for enormous challenges as housing shortages, traffic congestion, accelerating urbanization, more human activities in heritage sites, worsening air pollution, inadequate basic urban services and infrastructure (Guo *et al.,* 2020b). Focusing on 6 SDG 11 indicators, China's data products, modeling method and support for policy-making are shared here (Table 4-1).

		Table 4-1 Cases and Their Main Contributions	
Indicator	**Tier**	**Case**	**Contributions**
11.1.1 Proportion of urban population living in slums, informal settlements or inadequate housing	Tier I	Estimates of population living in shantytowns as a percentage of main urban district residents in cities in China	**Data product:** data of shantytown population ratio and vector boundaries in 27 cities in China (2019) **Method:** a semantic segmentation and transfer learning method for shantytown estimation
11.2.1 Proportion of population that has convenient access to public transport, by sex, age and persons with disabilities	Tier II	Proportion of the population with easy access to public transportation in China	**Data product:** datasets of population with easy access to public transportation, by age and gender, with 1 km resolution (2015 and 2018)
11.3.1 Ratio of land consumption rate to population growth rate	Tier II	Monitoring and assessing urbanization progress in China	**Data product:** a series of 7 datasets of built-up areas of 433 cities in China (1990-2018) **Method:** proposal of a new indicator—the ratio of economic growth rate to land consumption rate
11.5.1 Number of deaths, missing persons and directly affected persons attributed to disasters per 100 000 population 11.5.2 Direct economic loss in relation to global GDP, damage to critical infrastructure and number of disruptions to basic services, attributed to disasters	Tier II	Monitoring of disaster loss reduction and promotion of sustainable development in vulnerable areas in China	**Data product:** data from monitoring indicators of disaster losses between 2013-2019; data from monitoring reconstruction and sustainability in quake-hit Yushu **Support to policy-making:** presenting evidence on large reduction in deaths, people affected, and direct economic loss as a result of disasters in China, effectively promoting sustainable development in disaster-prone areas
		Impact assessment of storm surge inundation in Shenzhen	**Data product:** 4 km water depth data of Typhoon Nida in 2016 and Typhoon Mangkhut in 2018 **Support to policy-making:** using digital-twin method to assess the impact of storm-surges of different intensities on population and economy
11.7.1 Average share of the built-up area of cities that is open space for public use for all, by sex, age and persons with disabilities	Tier II	Share of open public space area in cities in China	**Data product:** datasets of share of open public space area in cities in China (2015 and 2018)
Integrated Assessment of SDG 11	Tier I/ Tier II	Integrated assessment of SDG 11 indicators at the provincial scale in China	**Data product:** dataset of integrated assessment of multiple indicators of 340 Chinese prefectural-level cities **Support to policy-making:** supporting sustainability assessment of major cities in China and serving as reference for integrated SDGs assessment in other Chinese regions

11 SUSTAINABLE CITIES AND COMMUNITIES

Case Study

Estimates of population living in shantytowns as a percentage of main urban district residents in cities in China

Target: 11.1 By 2030, ensure access for all to adequate, safe and affordable housing and basic services and upgrade slums.

Highlights

- *The spatial boundaries of shantytowns in the main urban districts of 27 Chinese cities as of 2019 were identified and extracted for the first time by adopting high-resolution satellite images from Gaofen-2 (GF-2) and advanced semantic segmentation models.*

- *Shantytowns in 27 cities covered an area of 124.49 km^2 with a total population of 1.032 million in 2019. There were significant differences between Eastern and Western cities in the ratios of area and population of shantytowns to those of main urban districts. The proportion of Population in Shantytowns (PST) was above 3% in Guangzhou and Haikou, while the percentage of Area of Shantytowns (AST) was higher than 3% in Xi'an, Lanzhou, and Xining. These cities are under great pressure for urgent and orderly shantytown redevelopment.*

Background

Rapid urbanization is accompanied by the increase in shantytown dwellers, inadequate housing, and the excessive burden on urban infrastructure. In 2018, nearly 23.50% of the global urban population lived in shantytowns. COVID-19 in particular has dealt a heavy blow to the public health of more than one billion shantytown dwellers worldwide (Sachs *et al.,* 2020). Improving the living conditions of shantytowns has been widely recognized as one of the primary challenges for sustainable urban development in the coming decades. Based on this, SDG 11.1.1 "proportion of population living in slums or informal settlements" is a key indicator in urban sustainability assessment (United Nations, 2015). There are, however, no explicit definitions or standards for informal settlements, slums and shantytowns in the world (Wurm *et al.,* 2019). The shantytowns in China are hugely different from the slums in Brazil, India, and Africa in terms of infrastructure supply, population density, fire safety standards, and public health conditions. *The Notice on Accelerating the Transformation of Shantytowns (Dangerous and Old Houses)* issued by 7 Chinese government ministries including the Ministry of Housing and Urban-

Rural Development, the National Development and Reform Commission, and the Ministry of Finance defines shantytowns (dangerous and old houses) as areas, situated within the geographical scope of urban planning, where there is a high level of concentration of old, poor, simple-structure homes in great density with building safety concerns, incomplete functions, and inadequate infrastructure. Combining the above definition with the United Nations' standards of informal settlements, and in light of the features observed from the high-resolution satellite images, this study defines shantytowns as continuous areas, situated within the geographical scope of urban planning, where most homes are old, of low building height but in high density, roads are often irregular or dead-end, and necessary facilities are lacking.

Currently, there are no datasets on the area and population of informal settlements in China. To promote sustainable urban development, it is urgently needed to develop a shantytown monitoring and assessment indicators system consistent with SDG 11.1.1 based on Big Earth Data.

Data used

◎ GF-2 panchromatic fusion image (0.8 m) in 2019.

◎ Essential urban land use categories in China (EULUC-China).

◎ World Population (WorldPop) data (100 m) in 2019.

◎ The 6th census data (2010) of China.

Method

In conformity with SDG 11.1.1, a multi-scale shantytown identification scheme based on high-resolution satellite images (GF-2) was developed for the extraction of the spatial boundaries of shantytowns through the Deeplab V3 + semantic segmentation model. First, the proportions of cultivated land, towns, and human settlements were calculated based on EULUC-China vector data, and then the scope of main urban districts were determined (by the threshold of cultivated land being less than 0.01). Meanwhile, sufficient samples were collected through visual selection from GF-2 fusion images of 27 cities. Second, shantytowns in these cities were mapped by adopting semantic segmentation models and transfer learning. Finally, the Populations in Main Urban Districts (PMUD) and shantytowns were estimated by using WorldPop data, and then the Proportion of PST (PPST) was calculated as follows:

$$PPST = \frac{PST}{PMUD} \times 100\%$$

Results and analysis

Shantytowns in the main urban districts of the 27 Chinese cities covered an area of 124.49 km^2 with a total population of 1.032 million in 2019 (Fig. 4-1). There were significant differences among China's four economic regions (East, Central, West, and Northeast China) in the proportions of AST and PST to those of main urban districts. Specifically, East China had the largest shantytown areas of 44.06 km^2 and 578 300 dwellers. West China ranked second, with 42.34 km^2 in area and 228 600 dwellers. The shantytowns in Central China covered an area of 21.48 km^2 with 182 900 dwellers, while those in Northeast China were 16.61 km^2 and had 42 000 people.

The shantytowns existed due to several factors (Fig. 4-2).

↑ Figure 4-1. Difference in AST and PST in 27 major cities of China, 2019

East China

AST: 44.06 km²

PST: 578 300 people

PMUD: 62.75 million people

Central China

AST: 21.48 km²

PST: 182 900 people

PMUD: 18.52 million people

West China

AST: 42.34 km²

PST: 228 600 people

PMUD: 20.81 million people

Northeast China

AST: 16.61 km²

PST: 42 000 people

PMUD: 10.14 million people
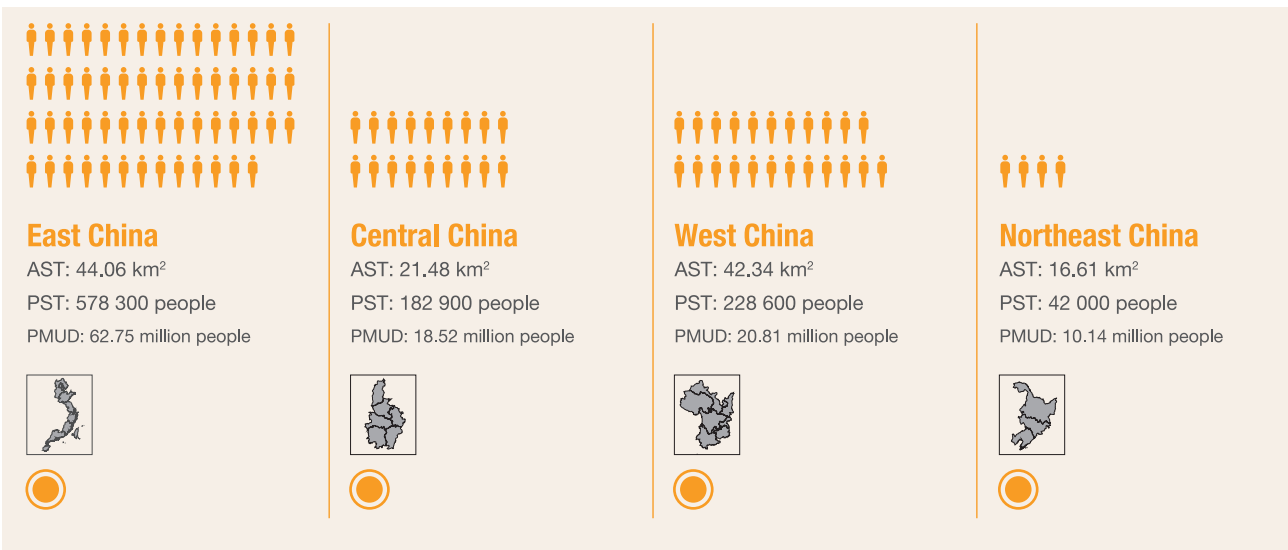
Guangzhou had the largest number of shantytown dwellers (257 600 people) due to the influx of migrant workers and other migrants. In Xi'an, shantytowns scattered around the city, resulting in its AST as large as 19.81 km². Haikou's PST was about 6% due to the weak infrastructure in the old city and unbalanced urban development. In Harbin, which was traditionally an industrial city, the complexity of building types made more difficult the redevelopment of shantytowns, which accounted for about 2.5% of the main urban districts.
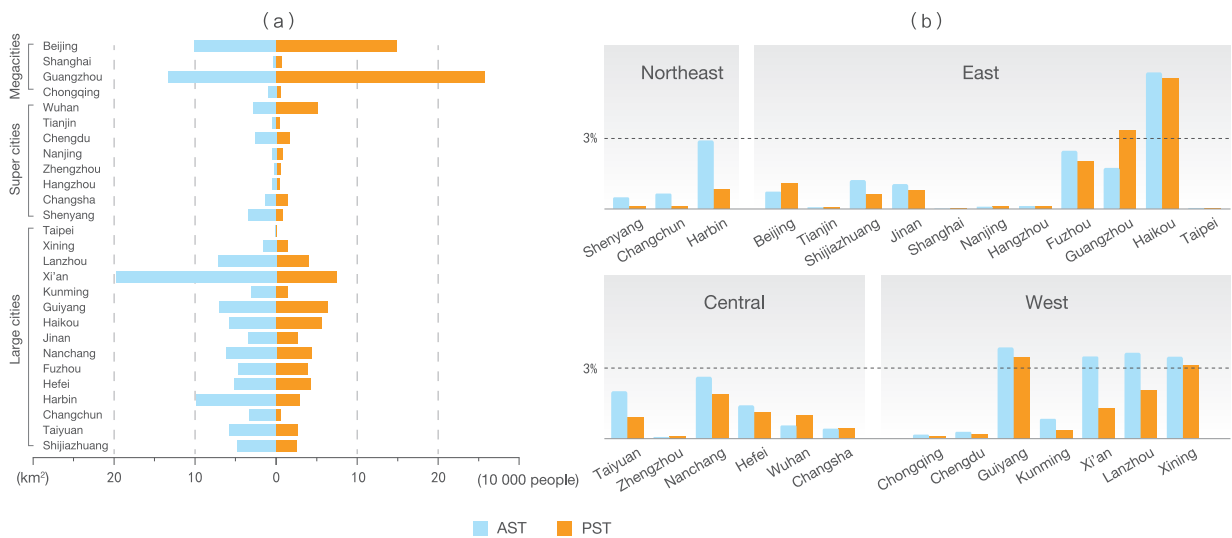
↑ Figure 4-2 The AST and PST (a) and their shares in different regions (b)

Outlook

Based on high-resolution satellite images and population raster data, the AST and PST in 27 cities across the four economic regions in China in 2019 were estimated by adopting semantic segmentation and transfer learning methods. The study produced rapid and accurate estimates, demonstrating a reliable methodology for estimating population living in slums or informal settlements in other countries, in support of achieving SDG 11.1.1.

Proportion of the population
with easy access to public transportation in China

Target: 11.2 By 2030, provide access to safe, affordable, accessible and sustainable transport systems for all, improving road safety, notably by expanding public transport, with special attention to the needs of those in vulnerable situations, women, children, persons with disabilities and older persons.

Highlights

- *High-resolution gridded population distribution data by gender and age group for 2015 and 2018 were produced to address the lack of such data under SDG 11.2.1.*

- *In 2018, the proportion of the population with easy access to public transportation in urban built-up areas was 80.56% on average in China, while the proportions in the eastern coastal region and Sichuan and Chongqing were higher than the rest of the country. Compared with 2015, 80% of Chinese cities saw higher proportions to varying degrees, while about 8% experienced slight declines.*

Background

Public transportation, an irreplaceable part of urban transportation, supports economic activities and life in cities, and is a key factor in achieving most of the SDGs, especially those related to education, food security, health, and the environment (Pojani and Stead, 2015). According to the UN-HABITAT report (2018), the global demand for public transportation generally increased between 2001 and 2014. The greatest increase in public transportation was seen in China, where multiple plans for prioritizing the development of public transportation were implemented vigorously in a top-down approach. However, it is difficult to acquire and quantify complex public transportation networks using traditional analytical methods or to accurately evaluate the degree to which public transportation development matches the pace of urbanization. This is an area where Big Earth Data can be applied (United Nations, 2015; Chen *et al.,* 2019; Deville *et al.,* 2014).

Data used

◎ Public transportation network (e.g., bus and metro networks) data in China, 2015 and 2018.

◎ Land use data with 100 m resolution in China, 2015 and 2018.

◎ 1% national population sample survey data, 2015 and census data, 2010.

◎ Auxiliary data including Visible Infrared Imaging Radiometer Suite Day/Night Band (VIIRS/DNB) night-light remote sensing data, mobile positioning data from Tencent, and Digital Elevation Models (DEMs), 2015 and 2018.

Method

For each administrative unit, the resident population, gender ratio, and proportion of each age group (0-14, 15-64, ≥65 years old) were extracted from the population sample survey and census data. The population was redistributed into the 1 km grid using a spatial downscaling model. Then the grid was superimposed on the rasterized gender ratio and the proportion of each age group to obtain the population distribution by gender and age group.

Next, public transportation stations (e.g., bus and metro stations) with spatial attributes were extracted from China's public

transportation network data, and a 500 m buffer zone was created for each station. This buffer layer was superimposed on the above-mentioned gridded population data to calculate the population within the buffers.

Finally, these layers were first superimposed on the spatial data of urban areas extracted from land-use data and then aggregated from the grid level to the prefectural and provincial levels to calculate the proportion of the population with easy access to public transportation within the built-up area.

Results and analysis

The distribution of SDG 11.2.1 at the provincial level in 2018 is shown in Figure 4-3. The population with easy access to public transportation at the provincial/municipality level was 80.56% on average in 2018, with the proportions in the eastern coastal region and Sichuan and Chongqing generally higher than those in the rest of the country. Chongqing, Beijing, and Shanghai had the highest proportions in China of over 90%, while Tianjin, Sichuan, and eastern provinces Guangdong, Fujian, Zhejiang, and Jiangsu followed closely behind at 85%, and Qinghai and Tibet had the lowest proportions.

In terms of gender, there was little difference across provinces. In terms of age groups, all except Qinghai and Tibet had a relatively balanced distribution with only minor differences. In southern China, including Guizhou, Hunan, and Guangdong provinces, the 15-64 age group was 4-6% higher than other age groups. In the northern and western regions, such as Heilongjiang, Liaoning, Shanxi, Gansu, Hebei, Sichuan, and Yunnan provinces, the proportions in the 15-64 and ≥65 age groups were similar, but that for the 0-14 age group was, on average, 2-4% lower than the other two groups.

The overall proportion of the population with easy access to public transportation

No Data 0.35 0.55 0.65 0.75 0.85 0.95

The proportion of the population with easy access to public transportation by gender and age group

female, 0 - 14   female, 15 - 64   female, ≥ 65
male, 0 - 14   male, 15 - 64   male, ≥ 65
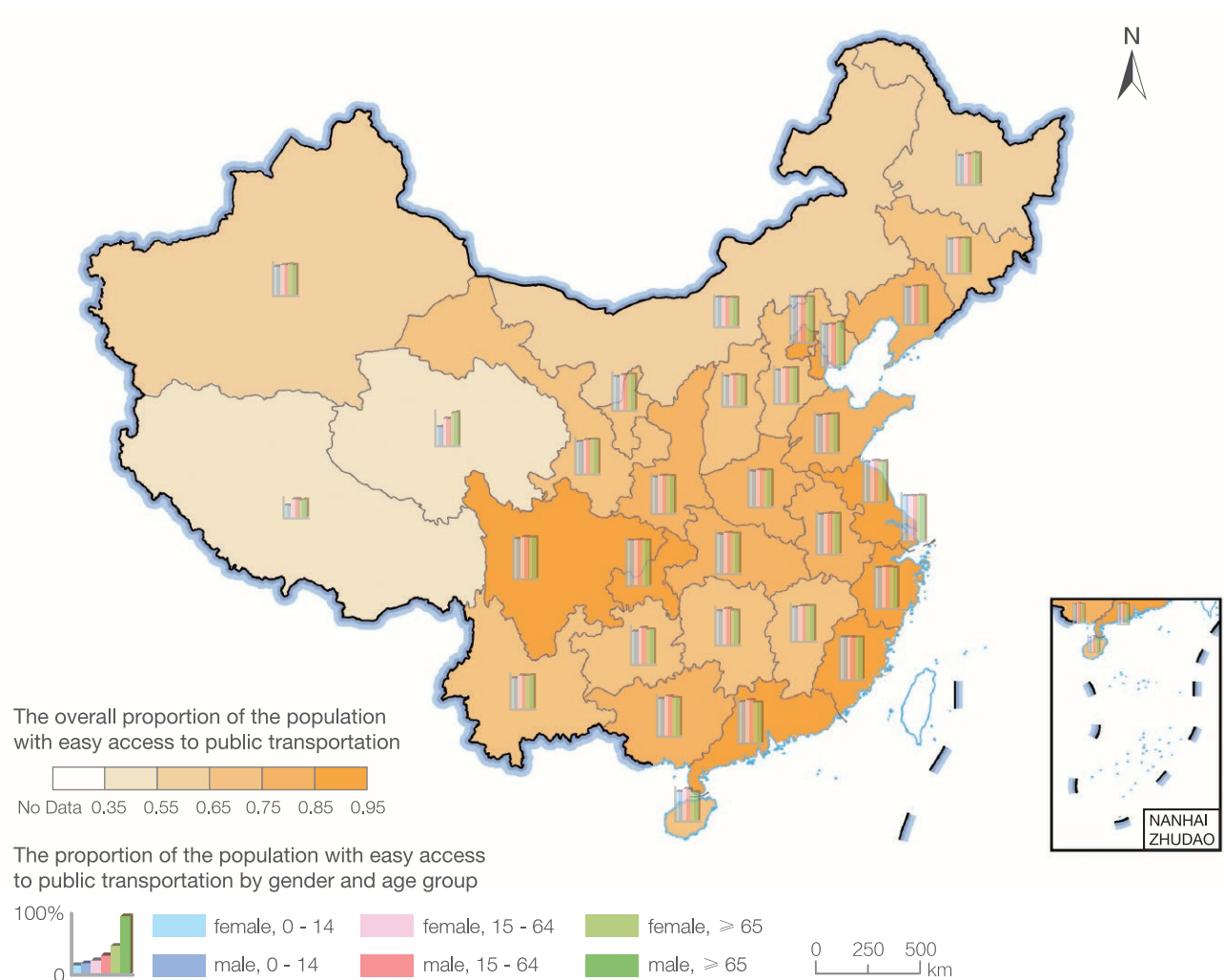
↑ Figure 4-3. SDG11.2.1 at provincial-level by gender and age group

Considering the distribution changes at the prefectural level from 2015 to 2018 (Fig. 4-4), the SDG 11.2.1 indicator increased in about 80% of the cities, with densely-populated cities with weak public transportation infrastructure in the past growing the fastest, and provincial capitals and economically advanced cities growing less because of their existing good public transportation. The indicator dropped slightly in about 8% of the cities where public transportation lagged behind the urban expansion.

Changes in the proportion of the population with easy access to public transportation

-10%   No Data   10%   30%   60%
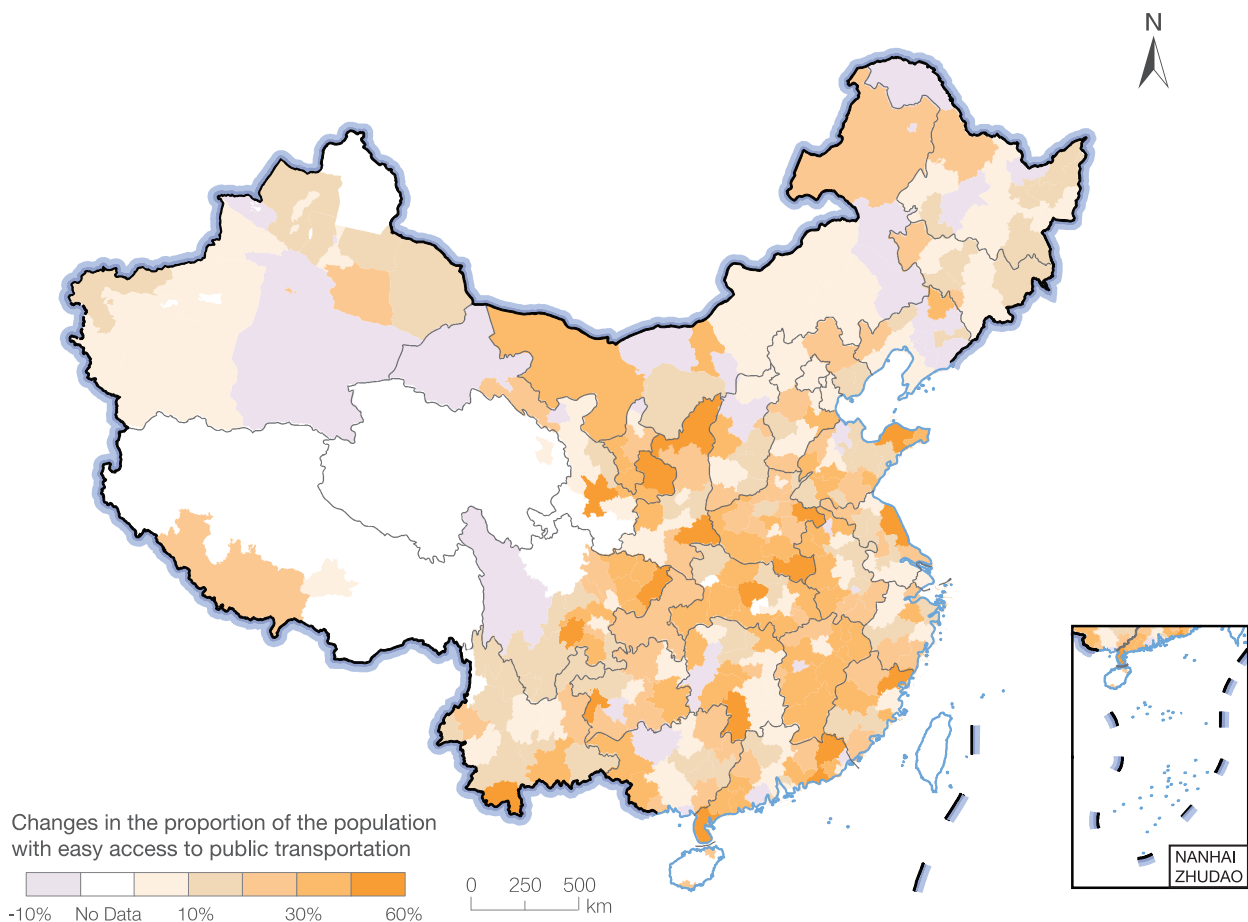
↑ Figure 4-4. Variations of SDG 11.2.1 at prefectural-level from 2015 to 2018

Outlook

This case study used Big Earth Data that included public transportation networks and high-resolution gridded population data to estimate the distribution in China, by gender and age group, of the population with easy access to public transportation, on a grid-scale, in 2015 and 2018. The comparison and detection of variations for indicator SDG 11.2.1 were realized at the prefectural and provincial levels. The methodology this case used is easy to apply with data easy to collect and update, and it can serve as a new approach to national evaluations and international comparisons of SDG 11.2.1.

Monitoring and assessing urbanization progress in China

Target: 11.3 By 2030, enhance inclusive and sustainable urbanization and capacity for participatory, integrated, and sustainable human settlement planning and management in all countries.

Highlights

- *Impervious surface products of 433 Chinese cities with a population over 300 000 from 1990 to 2018 were independently created.*

- *A new indicator—the ratio of Economic Growth Rate to Land Consumption Rate (EGRLCR)— is proposed, as an expansion of SDG 11.3.1, to monitor and evaluate urbanization progress in China tri-dimensionally in terms of land, population, and economic development.*

- *Since 1990, the rise in the ratio of Land Consumption Rate to Population Growth Rate (LCRPGR) had been accompanied by a decline in EGRLCR; the value of LCRPGR rose from 1.33 between 1990 to 1995 to 2.15 between 2010 to 2015; after 2015, the expansion of urban built-up areas has been slowing down, but coordinated development of urbanization still faces challenges.*

Background

SDG 11.3.1—"the ratio of Land Consumption Rate to Population Growth Rate (LCRPGR)" —can be used to quantify the relation between spatial urban expansion and population growth. According to United Nations statistics, between 2000 and 2014, the rate of land consumption in urban areas was 1.28 times that of population growth (UN, 2019). The relation of these two rates is essential to the sustainability of cities. Given that SDG 11.3.1 is classified as a Tier II indicator (methods established but with poor data) and lacks the economic dimension, it cannot measure, in a comprehensive way, the degree of coordination among land, population and economic activities during urbanization. On that account, Big Earth Data can be instrumental in assessing the urbanization progress in China from the environmental, social, and economic perspectives and in improving the accuracy and scientific soundness of the assessments (Guo, 2019).

Data used

◎ Population data of 433 Chinese cities with over 300 000 urban inhabitants from 1990 to 2018 (1990, 1995, 2000, 2005, 2010, 2015 and 2018) retrieved from the 2018 Revision of *World Urbanization Prospects* (UN, 2018).

◎ Global urban impervious surface products with a resolution of 30 m from 1990 to 2010 (1990, 1995, 2000, 2005 and 2010) and with a resolution of 10 m in 2015 and 2018.

◎ Population and Gross Domestic Product (GDP) data derived from the Chinese Urban Statistical Yearbook and China Statistical Yearbook from 1990 to 2018 (1990, 1995, 2000, 2005, 2010, 2015 and 2018).

Method

Following UN terms (UN, 2019), urban impervious surface was converted to built-up area. Based on LCRPGR, a new indicator was proposed—the ratio of Economic Growth Rate to Land Consumption Rate (EGRLCR). The two indicators were computed as follows:

$$LCRPGR = \frac{LCR}{PGR} = \frac{LN(Urb_{t+n}/Urb_t)}{LN(Pop_{t+n}/Pop_t)}$$

$$EGRLCR = \frac{EGR}{LCR} = \frac{LN(GDP_{t+n}/GDP_t)}{LN(Urb_{t+n}/Urb_t)}$$

where Urb$_t$ and Urb$_{t+n}$ are the total areal extent of the land consumed (extent of urban agglomeration area quantified as built-up area) at the initial reference year t, and at the final reference year $t+n$, respectively; Pop$_t$ and Pop$_{t+n}$ are the total population of the specific spatial unit at the initial reference year t, and at the final reference year $t+n$, respectively; GDP$_t$ and GDP$_{t+n}$ are the total amount of GDP of the specific spatial unit at the initial reference year t and at the final reference year $t+n$, respectively;

LN refers to the natural logarithm of the ratio. LCR, PGR and EGR are the land consumption, population and economic growth rates between t and $t+n$, respectively.

The values of LCRPGR and EGRLCR were calculated to measure the level of coordination among land consumption, population and economic growth in 433 cities of different urban sizes and functions and shed light on the spatiotemporal evolution of urbanization in China in the past three decades.
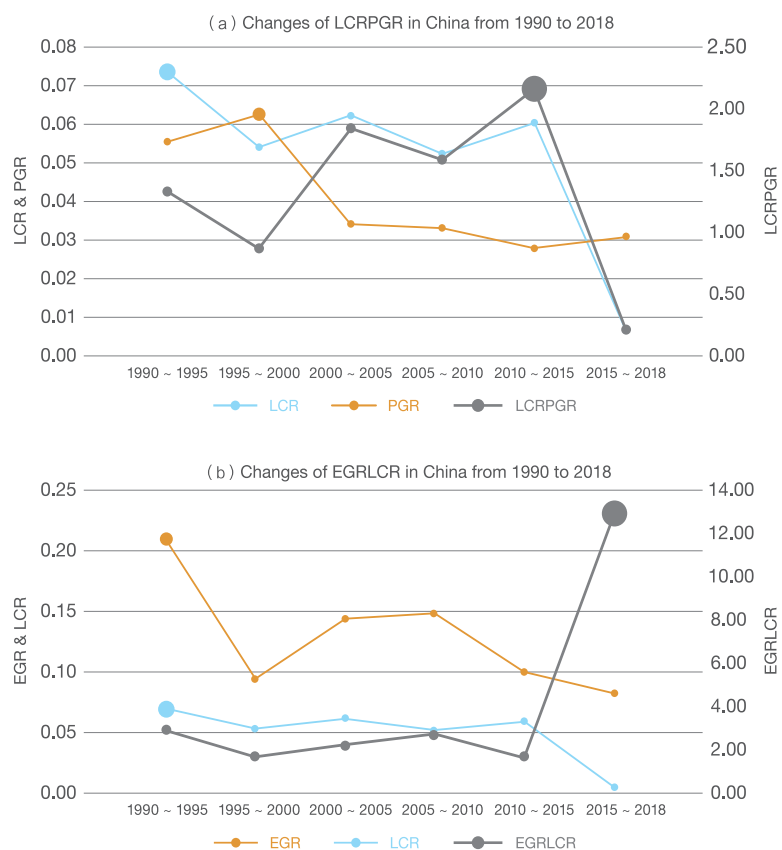
Results and analysis

Figure 4-5 shows the urbanization process in China measured in terms of changes in LCRPGR and EGRLCR of 433 county-level or higher cities. Along with the overwhelming spatial expansion coupled with a continuous slowdown in population and economic growth in urban areas, LCRPGR rose, while EGRLCR declined from 1990 to 2015, suggesting poor coordination among urbanization indicators in China. Thanks to a series of measures implemented by governments at all levels aimed at improving the quality of urbanization, such as the "National New Urbanization Program (2014-2020)", there has been a notable decrease in the areal extent of new urban land since 2015, reversing the trend where LCR had long exceeded PGR, and even been approaching EGR.

The patterns and dynamics of LCRPGR in China over the past several decades are shown in Figure 4-6. The study found that the rapid expansion of urban built-up areas has been effectively controlled since 2015, but the sustainability of urbanization is still under pressure. LCRPGR showed an upward trend in the northeastern and western regions, and remained relatively stable in the central and eastern regions; while it was fairly stable in megacities (with a population above 10 million), it was significantly higher, during multiple time periods, in super-large cities (with a population between 5-10 million) than cities in other categories; for resource-dependent cities, LCRPGR exceeded that of non-resource-dependent cities in most time periods at five-year intervals. These findings suggest that urbanization is more out of balance in super-large cities and resource-dependent cities in the northeastern and western regions and it deserves special attention.

The spatiotemporal evolution in EGRLCR of

Chinese cities shows that the gap between land consumption rate and economic growth rate has been narrowing, but imbalances remain between land consumption, population and economic growth rate. EGRLCR of resource-dependent cities is on a significantly downward trend, while it only fluctuates slightly in the eastern region; in megacities, the indicator is more stable than in cities of other sizes; it is much closer to the national average level in non-resource-dependent cities than in resource-dependent cities. The results indicate that megacities and non-resource-dependent cities in the eastern region have greater advantages in terms of economic resilience and sustainability of urbanization, while other cities face the double pressure of economic transformations and outflow of inhabitants.

(a) Changes of LCRPGR in China from 1990 to 2018

(b) Changes of EGRLCR in China from 1990 to 2018

→ Figure 4-5. Changes in ratio of Land Consumption Rate to Population Growth Rate (LCRPGR) (a) and, in ratio of Economic Growth Rate to Land Consumption Rate (EGRLCR) (b) in China from 1990 to 2018

（a）1990 – 1995

（b）1995 – 2000

N

（c）2000 – 2005

（d）2005 – 2010

（e）2010 – 2015

（f）2015 – 2018

0　500　1 000　　　2 000
km

Urban size

○ Megacity　　○ Super-large city　　○ Large city　　○ Medium city　　· Small city

LCRPGR

● < 0　　● 0 - 1　　● 1 - 2　　● > 2
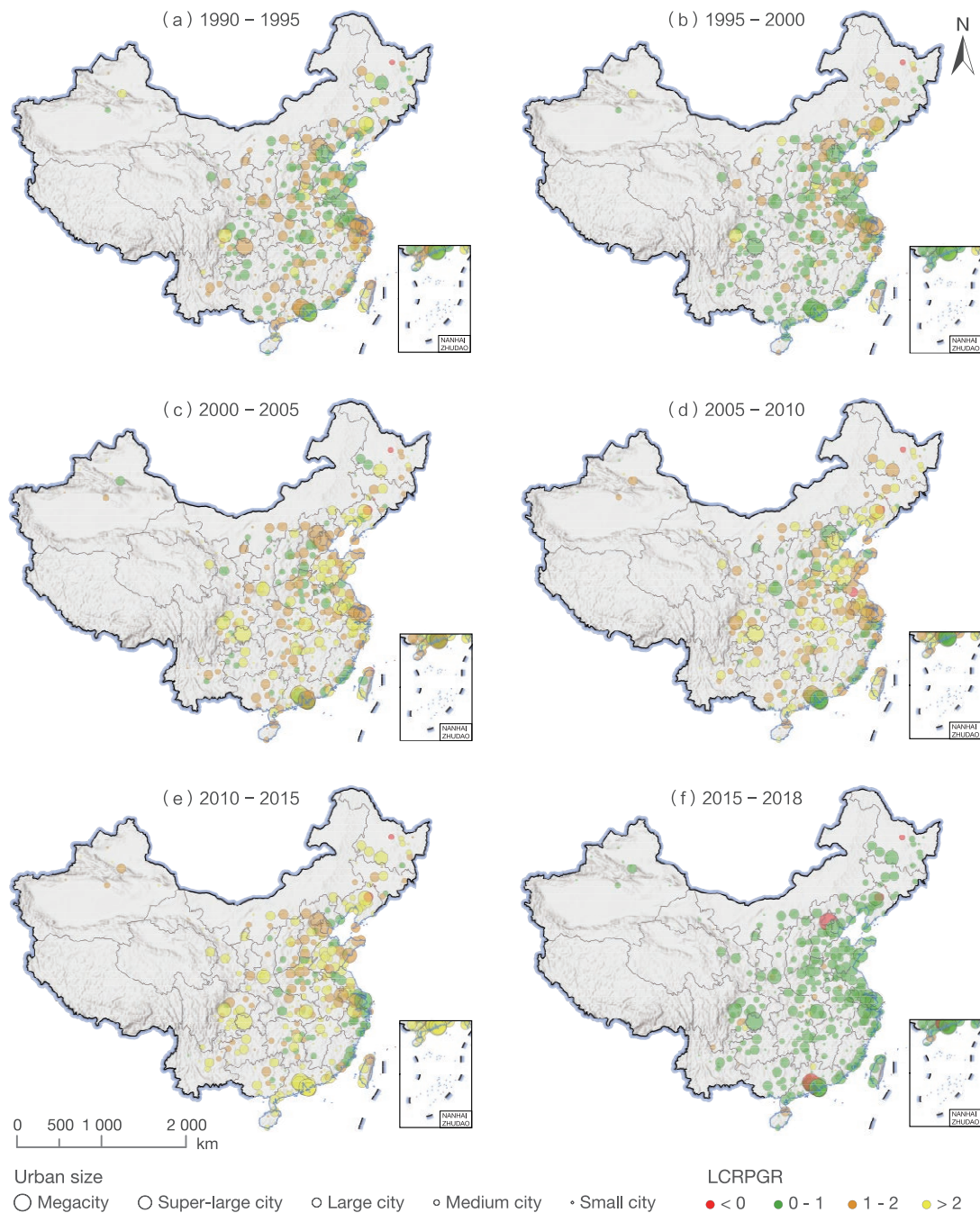
↑ Figure 4-6. Spatiotemporal evolution of land use efficiency of cities in China from 1990 to 2018

Outlook

In this case, multi-sourced remote sensing data were used to map the impervious surfaces of 433 Chinese cities with a population of more than 300 000 from 1990 to 2018, and then produce a comparable dataset on changes in urban built-up areas, needed to calculate LCR. A new indicator was proposed, i.e., the ratio of Economic Growth Rate to Land Consumption Rate (EGRLCR), which coupled with LCRPGR and aided by Earth observations and census data, can evaluate the spatiotemporal evolution of urbanization in China from the economic, social and environmental perspectives. Future work will focus on combining international open data sources and our own global urban impervious surface products to better realize the spatial coupling of population and economic data in urban built-up areas, and improve the quantitative assessment of the coordination of land, population and economic dimensions, so that global level monitoring of urbanization could become possible.

Monitoring of disaster loss reduction and promotion of sustainable development in vulnerable areas in China

Target: 11.5 By 2030, significantly reduce the number of deaths and the number of people affected and substantially decrease the direct economic losses relative to global gross domestic product caused by disasters, including water-related disasters, with a focus on protecting the poor and people in vulnerable situations.

Highlights

● *The losses caused by natural disasters have decreased significantly in China as a whole. Comparing 2013 and 2019, the number of deaths and missing persons per 100 000 population dropped from 0.17 to 0.06, the number of directly affected persons per 100 000 population decreased from 28 739.87 to 9 285.71, and direct economic loss in relation to GDP attributed to disasters dropped from 0.98% to 0.33%.*

Background

In this century, as urbanization and the growth of economy pick up speed, disasters have become a major constraint to sustainable development. Under the United Nations 2030 Agenda for Sustainable Development, substantially reducing losses from disasters, with a focus on protecting the poor and vulnerable groups, is an important indicator for promoting sustainable development, one that has been embraced by the Chinese government, and incorporated into its Plan of National Comprehensive Disaster Prevention and Mitigation (2016-2020). Economically backward regions in western China, especially those that had experienced major disasters, have stepped up efforts of disaster prevention and mitigation, rehabilitation and reconstruction, effectively promoting sustainable development of these disaster-prone regions.

Data used

◎ Multi-sourced remote sensing data from 2009 to 2019: satellite remote sensing data such as Gaofen-1, Gaofen-2 and Beijing-2, as well as airborne remote sensing data.

◎ Statistical and bulletin data from 2009 to 2019, including Chinese statistical yearbooks of regions, counties, cities, population, civil affairs; statistical yearbooks of Qinghai and Gansu; data verified by the Ministry of Emergency Management, the Ministry of Civil Affairs and the Office of the National Disaster Reduction Committee in consultation with other relevant departments on the situation of natural disasters nationwide; China's Flood and Drought Disasters Bulletin; National Geological Disasters Bulletin.

◎ Survey data on the post-disaster reconstruction area of Yushu, 2019.

Method

Statistical and spatial data were used synergistically to finely monitor changes in disaster losses and socioeconomic development from multiple dimensions. Deep learning methods were applied to extract information from imagery on disaster-vulnerable areas, progress of rebuilding projects, distribution of buildings and construction and repair of transportation facilities. Parameter inversion of long time series of satellite remote sensing records was used to monitor in real time the state of the environment.

Results and analysis

1) Dynamic monitoring of changes in China's disaster losses

The overall monitoring of disaster losses, population and economic statistics showed that natural disaster-induced losses decreased significantly (Fig. 4-7). Major reductions were observed in all the indicators as of 2019, compared with those of 2013: the number of disaster-related deaths and missing persons per 100 000 decreased from 0.17 to 0.06 ; the number of directly affected persons per 100 000 population decreased from 28 739.87 to 9 285.71; direct economic loss in relation to GDP attributed to disasters decreased from 0.98% to 0.33%.

（a）Statistics of disaster losses in China

Year	Number of deaths, missing persons attributed to disasters per 100 000 population	Number of directly affected persons attributed to disasters per 100 000 population	Direct economic loss in relation to GDP
2013	0.17	28 739.87	0.98%
2014	0.13	17 595.31	0.53%
2015	0.07	13 858.50	0.39%
2016	0.12	13 778.10	0.68%
2017	0.07	10 101.01	0.37%
2018	0.05	9 332.38	0.29%
2019	0.06	9 285.71	0.33%

（b）Number of deaths and missing persons attributed to disasters per 100 000 population in China
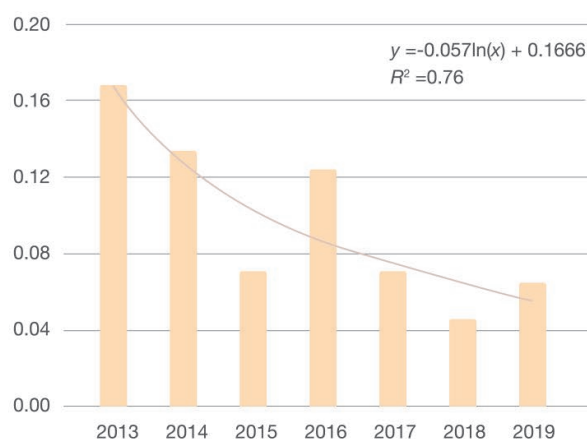
$y = -0.057\ln(x) + 0.1666$
$R^2 = 0.76$

（c）Number of directly affected persons attributed to disasters per 100 000 population in China

$y = 751.63x^2 - 8821.8x + 34925$
$R^2 = 0.94$
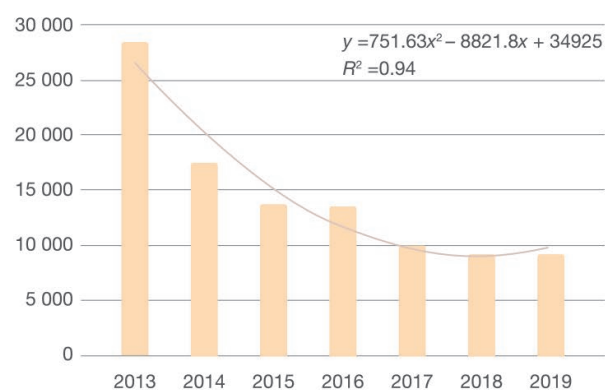
（d）Direct economic loss in relation to GDP attributed to disasters in China

$y = -0.003\ln(x) + 0.0088$
$R^2 = 0.71$
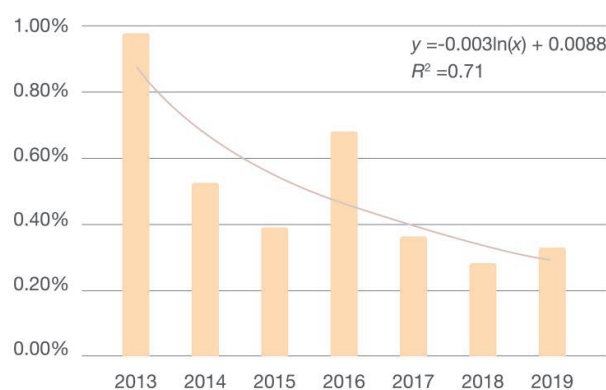
↑ Figure 4-7. Changes in natural disaster losses in China (excluding Hong Kong, Macao and Taiwan province)

2) Monitoring of sustainable development in disaster-vulnerable areas of China

The vast western China, inhabited by many ethnic groups, has a high density of poor population and is prone to disasters. The Yushu earthquake and Zhouqu debris flow in 2010 and the Jiuzhaigou earthquake in 2017 had severe, negative impact on local sustainability. Big Earth Data-enabled monitoring of these disaster-vulnerable areas showed that government projects, such as disaster prevention, engineering interventions, and improving earthquake resistance of residential housing, have effectively promoted sustainable development. Table 4-2 and Figure 4-8 below show the dynamic monitoring of sustainable development in the reconstruction area of quake-hit Yushu.

Table 4-2 Measures to promote sustainable development in disaster-prone areas and their effects in China (using the reconstruction area in quake-hit Yushu as an example)

| Measures to promote sustainable development	Sustainable development status of the reconstruction area after the earthquake in Yushu
1. Strengthening disaster prevention and mitigation works	No major geological disasters or floods occurred by the end of 2019, with the completion of projects to fix 18 mudslide-prone areas and 4 sections of unstable slopes, and to reinforce 11.75 km of the Batang River embankment and 9.65 km of the Zhaxike River embankment.
2. Improving quake-resistance of housing	Earthquake resistance levels were improved for housing of urban residents, farmers and herders. 292 sites of concentrated housing development for farmers and herders had sound infrastructure.
3. Strengthening infrastructure	Gongyu expressway, national highway 214, provincial highways 308 and 309 were completed or reopened to traffic. All prefectures and counties were accessible by secondary asphalt roads.
4. Improving public services capacity	Cultural and religious facilities such as the Yushu Earthquake Site Memorial Hall, Princess Wencheng Temple, and Changu Temple were preserved and protected. Compared with before the disaster, the number of beds in healthcare institutions increased by 3.3 times and beds in social welfare adoption agencies increased by 8.4 times.
5. Conserving ecosystems and the environment	Through afforestation efforts, the ecosystems and environment of the disaster-hit area were rehabilitated, with the average Gross Primary Productivity (GPP) of vegetation up by about 40%.
6. Promoting distinctive local industries	Yak, black barley and other special agro- and animal husbandry industries continued to expand; the cultural tourism industry grew vigorously; poverty was basically eradicated.

(a) Distribution of GPP in post-disaster reconstruction areas, 2011

(b) Distribution of GPP in post-disaster reconstruction areas, 2019

GPP (gC/(m²·a))

| < 50 | 50 - 100 | 100 - 150 | 150 - 200 | 200 - 250 | 250 - 300 | 300 - 350 | 350 - 400 | ≥ 400 |

0 20 40 80 km

(c) Average annual change in GPP in post-disaster reconstruction areas

(d) Average annual change in GPP in each of the seven counties in the reconstruction areas

↑ Figure 4-8. Dynamic monitoring of vegetation recovery in the Yushu post-earthquake reconstruction areas

Outlook

In recent years, China has significantly enhanced its overall capacity of disaster prevention and mitigation in cities and human settlements. Losses caused by natural disasters have dropped sharply. However, the complex disaster-prone environment, coupled with frequent extreme meteorological and hydrological conditions, poses a serious challenge to continued major reduction in disaster-induced losses and the sustainable development of vulnerable areas such as in western China. The way forward is to vigorously promote the integrated application of advanced technologies and sustainable development theories, strengthen research on the dynamics of disasters, and overcome technical bottlenecks in disaster prediction, early warning, monitoring, assessment and management.

Impact assessment of storm surge inundation in Shenzhen

Target: 11.5 By 2030, significantly reduce the number of deaths and the number of people affected and substantially decrease the direct economic losses relative to global gross domestic product caused by disasters, including water-related disasters, with a focus on protecting the poor and people in vulnerable situations.

Highlights

- *Typhoons Nida and Mangkhut that hit Shenzhen in 2016 and 2018, respectively, were simulated and urban floodwater depth data were obtained with an average accuracy of 90.68%.*

- *A storm-surge digital-twin assessment system was established to assess the number of people affected/injured/killed by and direct economic losses from storm surge hazards in Shenzhen.*

- *For Dapeng new district, Bao'an district, Nanshan district, and Futian district, which suffered severe seawater influx, additional flood-control dikes should be built along the coast and be reinforced with sandbags prior to a storm surge.*

Background

Storm surge hazards have become one of the most serious natural disasters, inflicting increasing losses and posing a challenge to social and economic sustainability in Shenzhen and other coastal cities, where there is a great density of both population and economic activities. Currently, three problems hinder the assessment of direct economic losses and the number of people affected: (1) a lack of high-resolution historical data; (2)

an over-reliance on statistical data in traditional methods; and (3) a multitude of influencing factors. A storm-surge digital-twin method, based on Big Earth Data, can quickly evaluate the direct economic losses and people affected in Shenzhen by combining the numerical simulation model and expert empirical model. It can provide vital support for decision-making on targeted disaster prevention.

Data used

◎ The US National Oceanic and Atmospheric Administration's (NOAA) Global Self-consistent, Hierarchical, High-resolution Geography Database (GSHHGD).

◎ The US National Aeronautics and Space Administration's (NASA) 1/8-degree Cross-Calibrated Multi-Platform (CCMP) Wind Vector Analysis Product.

◎ NOAA's 1/60-degree global relief model of Earth's surface that integrates land topography and ocean bathymetry.

◎ Oregon State University's 1/30-degree harmonic constants.

◎ Ten-meter resolution national land classification data in 2018 (Gong *et al.,* 2019).

◎ OpenStreetMap's administrative boundary dataset.

◎ The China Meteorological Administration's typhoon dataset.

◎ WorldPop's 100-meter resolution population count dataset.

◎ The Construction Cost Index and Shenzhen Statistical Yearbook.

◎ Tidal data from the tide-gauge stations in Shekou Port and Yantian Port, Guangdong.

Method

Focusing on SDG 11.5 indicators of direct economic losses, affected people, and deaths, the evaluation method was established as follows. First, the Finite Volume Community Ocean Model (FVCOM), an unstructured-grid based finite-

volume ocean numerical simulation model, was utilized to calculate the depth of floodwater, to overcome the lack of historical data. Second, the economic loss-assessment model, proposed by the National Natural Hazard Comprehensive

Research Group, was utilized to quantitatively estimate the total direct economic losses by evaluating the damage rate and unit value for each affected construction. Finally, the flood risks to people methodology, proposed by the British Hydraulic Research Institute, was adopted to establish the relationships between the people affected and the urban floodwater characteristics, urban characteristics, and population characteristics to quantitatively evaluate deaths and the number of people affected.

Results and analysis

Typhoons Nida and Mangkhut hit Guangdong province on August 2, 2016 and September 16, 2018, respectively. Their storm surges were simulated to calculate the water depths, which were 87.86% and 93.51% accurate, respectively, with an average accuracy rate of 90.68% when compared with the tide level data recorded by the Shekou and Yantian tide gauge stations (113°53′E, 22°28′N and 114°16′E, 22°35′N).

Figure 4-9 shows the simulated direct economic losses from Nida were 367 900 and from Mangkhut 265 million yuan.

According to statistics of the Guangdong Provincial Oceanic and Fishery Department, the direct economic losses from Nida were 360 000 yuan and the statistics of the Guangdong Provincial Department of Natural Resources put the direct economic losses from Mangkhut at 255 million yuan, pointing to a high accuracy of the simulation results.

Figure 4-10 shows the assessment results of the affected population. The simulated results were: for Nida, 18 600 affected, 24 injured, and no death; for Mangkhut, 28 100
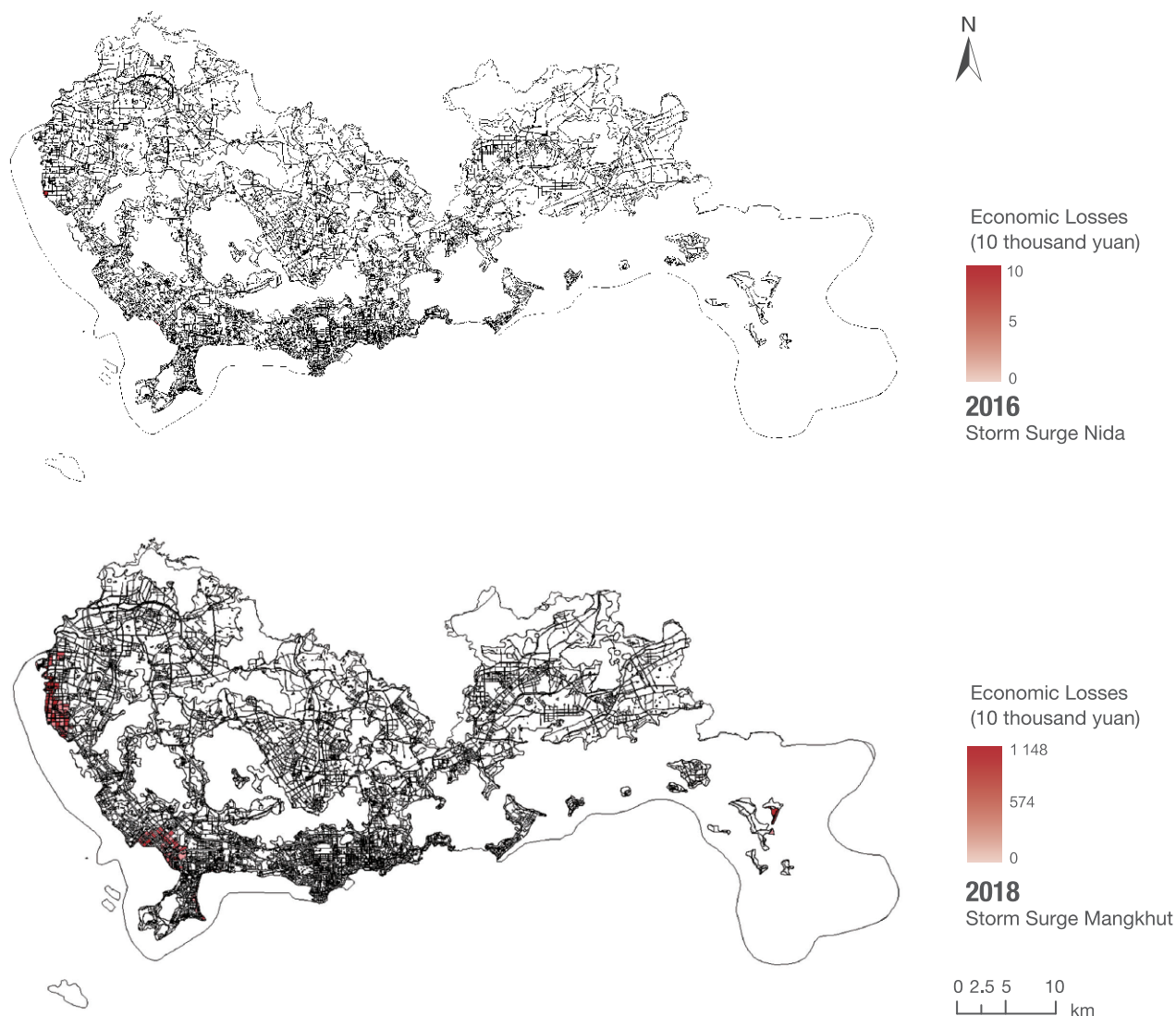
↑ Figure 4-9. The direct economic loss assessments of Nida in 2016 and Mangkhut in 2018 based on the economic loss-assessment model

affected, 41 injured and no death. The statistics published by the Guangdong Provincial Oceanic and Fishery Department showed Nida affected 18 300 people and caused no death in Shenzhen, while the statistics of the Ministry of Emergency Management of China were that Mangkhut caused a total of five deaths in the five provinces of Guangdong, Guangxi, Hainan, Hunan and Guizhou and no death in Shenzhen. The simulated results were accurate.

Most of the direct economic losses and affected people were in Bao'an district, Nanshan district and Futian district, due to their geographical proximity to the sea and flat terrain. Dapeng new district also suffered the influx of seawater, but did not incur too much loss thanks to its mountainous terrain. To reduce future losses, the flood-control dikes should be reinforced and sandbags should be made available in Bao'an, Nanshan and Futian districts.
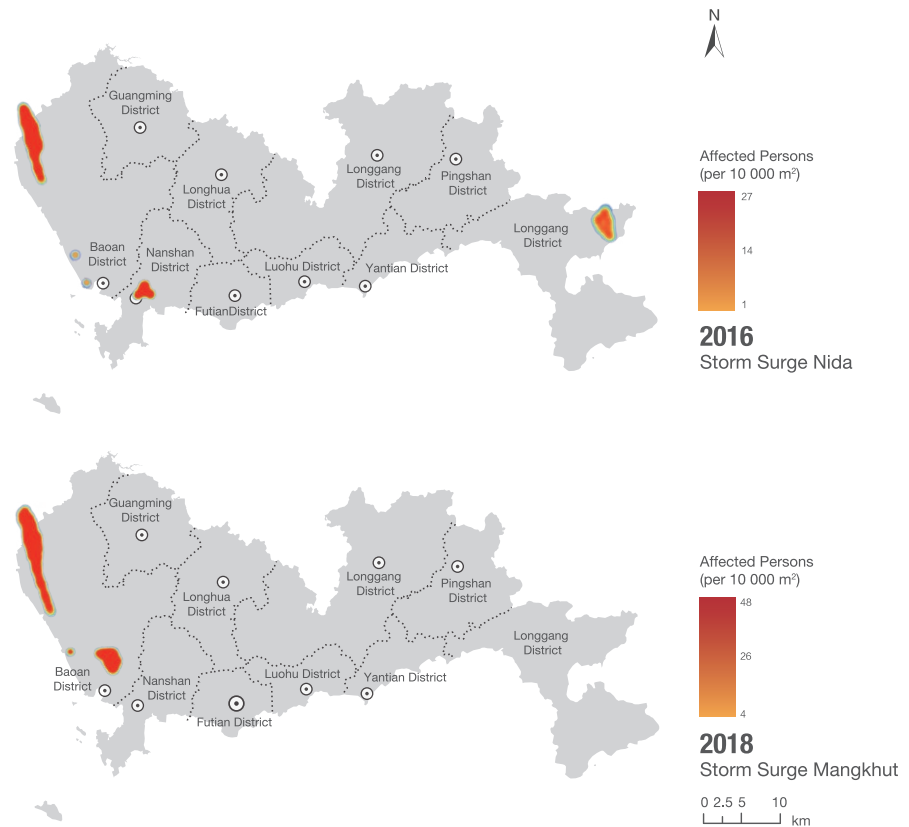
Figure 4-10. The distribution of people affected by Nida in 2016 and Mangkhut in 2018 based on the flood risks to people methodology

Outlook

In light of indicators SDG 11.5.1 and 11.5.2, this case study assessed the direct economic losses, people affected and injured and deaths in Shenzhen caused by storm surge hazards—Nida in 2016 and Mangkhut in 2018, using a storm-surge digital-twin assessment method. The case can provide vital support to decision-making on storm surge hazard prevention in Shenzhen.

For more comprehensive disaster-prevention decision support, future work should: (1) simulate more storm surge hazards that posed a serious threat to Shenzhen; and (2) simulate storm surge hazards of different intensities in Shenzhen and evaluate the direct economic losses and the number of people affected, with the purpose of giving early warning to the disaster-prone areas and informing decision-making.

Share of open public space area in cities in China

Target: 11.7 By 2030, provide universal access to safe, inclusive and accessible, green and public spaces, in particular for women and children, older persons and persons with disabilities.

Highlights

- *The share of open public space area in built-up areas in Chinese provinces (excluding Hong Kong, Macao and Taiwan province) averaged 19.50% in 2018, 1.5 percentage points higher than 17.98% in 2015.*

- *In prefectural-level cities, the share of open public space area in nearly 50 cities exceeded 20%. The share was larger on the southeast side of Hu Line than that on the northwest side. It was larger in the city clusters in the Beijing-Tianjin-Hebei region, Yangtze River Delta, Pearl River Delta, Sichuan basin and central Yunnan than in their surrounding regions.*

Background

The monitoring and evaluation of urban open public space is helpful to promoting urban space transformation, quality upgrading, and sustainable development. The public space as defined in SDG 11.7.1 mainly includes public green space and urban roads. The former can improve people's wellbeing and health, while the latter is a direct indicator of urban prosperity. UN-HABITAT is responsible for SDG11.7 evaluation globally. *The Atlas of Urban Expansion*, that analyzes 95 406 km^2 of built-up areas in selected cities around the world, finds that 59% of them are occupied by urban public spaces, and nearly half are urban roads. According to *China's Progress Report on Implemention of the 2030 Agenda for Sustainable Development (2019)*, by 2018, a total of 56 000 km of greenways had been built, and the urban living environment greatly improved. There is, however, no national monitoring and evaluation result of this indicator. This report adopted the design and method of UN SDGs to evaluate China's progress in SDG 11.7.1 and compared the results of 2015 and 2018.

Data used

◎ SDG 11.7.1 Evaluation Result, 2015 (Guo *et al.,* 2019).

◎ Land cover data for China, 2018.

◎ Navigation vector data of cities in China, 2018.

◎ Statistical yearbook of prefectural-level cities in China.

Method

The "urban land" subcategory was extracted from the land cover data to establish the built-up area, and the public space data (green space, square and roads) was extracted from the navigation vector data. The evaluation process was as follows: (1) Define a Generate Fishnet function, and use the grid transformation method to generate national kilometer grid; (2) Overlay the national grid with the spatial data of green space and square to generate the grid spatial data; (3) Convert highways, provincial roads, county roads, township roads and other urban roads into polygon data by their width, and overlay with the national grid to generate kilometer grid road spatial data; (4) Integrate road data and public green space data at the grid scale and divide by the total urban built-up area to obtain the share of open public space area; (5) Convert the share from the kilometer grid scale to the county, municipal, provincial and national scales through spatial statistical analysis.

Results and analysis

The evaluation of open public space in prefectural-level Chinese cities in 2018 revealed the following. At the municipal scale, the share of open public space in nearly 50 cities exceeded 20%. Beijing, Shenzhen and Xiamen had the largest share, exceeding 30%, with urban roads taking up more than 25%. From the perspective of spatial pattern (Fig. 4-11), the share

of open public space area of cities on the southeast side of the Hu Line was generally larger than that on the northwest side, reflecting significant regional differences. From the perspective of urban agglomerations, the scale of open public space area in the city clusters in the Beijing-Tianjin-Hebei region, Yangtze River Delta, Pearl River Delta, Sichuan basin and central Yunnan was generally larger than in their surrounding regions, demonstrating a clear feature of spatial agglomeration.

The share of open public space in built-up areas in Chinese provinces (excluding Hong Kong, Macao and Taiwan province) averaged 19.50% in 2018, 1.5 percentage points higher than 17.98% in 2015. Guangdong and Beijing had the largest share of 28.60%, while Guangxi had the smallest share of 11.16%. From 2015 to 2018, the share of open public space in all provinces increased slightly except for Beijing, Chongqing, Sichuan, Fujian and Hubei (Fig. 4-12). Both urban built-up areas and open public space mainly including squares, parks and roads increased. The increase in open public space outpaced urbanization, which began to slow down, reflecting the growing attention China pays to the planning and improvement of open public space in urban development.

The share of open public space area increased with the expansion of cities, and the scale of open public space in super-large cities was larger than that in smaller cities. It was also in sync with economic development, being larger in more advanced cities. Level of economic development, living standards, urbanization rate and population size were all factors having a strong influence on the scale of open public space.
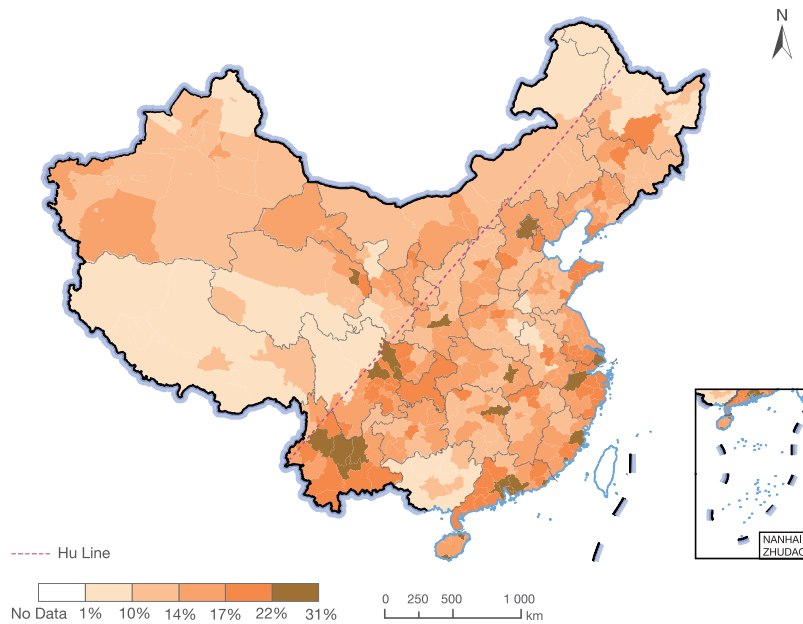
Figure 4-11. Share of open public space area in prefectural-level Chinese cities in 2018

Outlook

This case study evaluated and compared urban open public space, as defined by SDG 11.7, in China in 2015 and 2018 by using navigation and land cover data, and found that the method it adopted to monitor changes in Chinese cities concerning SDG 11.7.1 was easy to apply and data access was not difficult.

This method is a solution to the evaluation of SDG 11.7.1, but it cannot yet be applied to evaluating open public space categorized by gender, age or people with disabilities. Future work needs to be done to address this method's sensitivity to the definition of urban built-up area and data accuracy, and the minor errors in the data of built-up area, extracted from "urban land" subcategory.
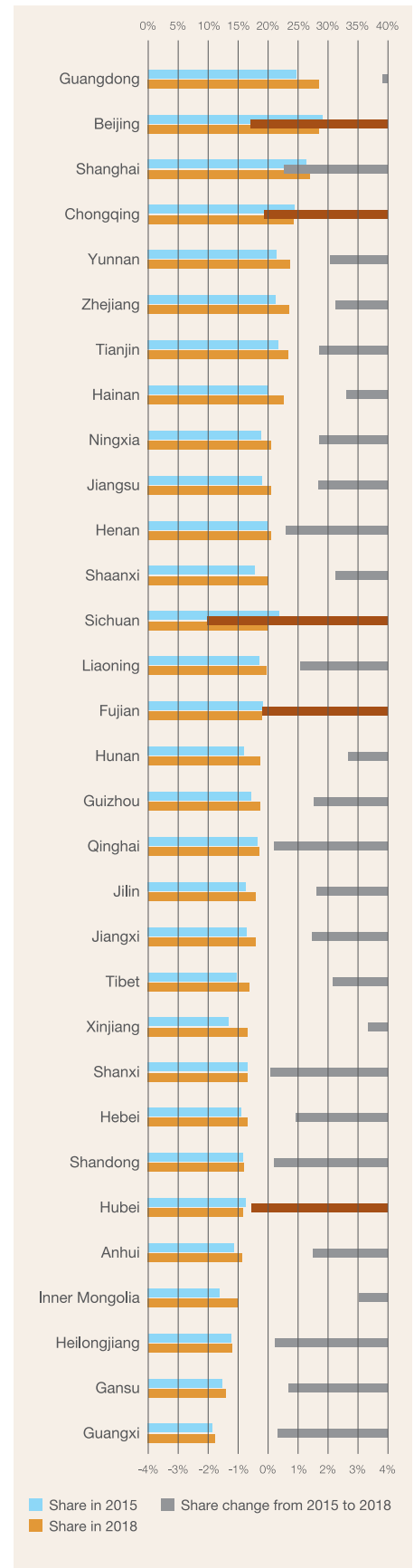
Figure 4-12. Changes in the share of open public space at provincial scale in China

Integrated assessment of SDG 11 indicators at the provincial scale in China

Target: 11.2 By 2030, provide access to safe, affordable, accessible and sustainable transport systems for all, improving road safety, notably by expanding public transport, with special attention to the needs of those in vulnerable situations, women, children, persons with disabilities and older persons.

11.3 By 2030, enhance inclusive and sustainable urbanization and capacity for participatory, integrated and sustainable human settlement planning and management in all countries.

11.5 By 2030, significantly reduce the number of deaths and the number of people affected and substantially decrease the direct economic losses relative to global gross domestic product caused by disasters, including water-related disasters, with a focus on protecting the poor and people in vulnerable situations.

11.6 By 2030, reduce the adverse per capita environmental impact of cities, including by paying special attention to air quality and municipal and other waste management.

11.7 By 2030, provide universal access to safe, inclusive and accessible, green and public spaces, in particular for women and children, older persons and persons with disabilities.

Highlights

○ *The first integrated assessment was undertaken at the provincial scale of the five targets and seven indicators under SDG 11 by utilizing Big Earth Data and national statistical data.*

○ *Compared with 2015, overall sustainability improved in 2018 at the provincial level. The SDG 11 integrated index was higher in the eastern provinces than in the western ones. It increased in 28 provinces but decreased in 3 others. The average value of SDG 11 integrated index increased from 0.58 in 2015 to 0.65 in 2018.*

Background

The Sustainable Development Solutions Network (SDSN) calculated the integrated index of the 17 SDGs for each country in the world using an equal weight method (Sachs *et al.,* 2019). Xu *et al.* (2020) used the same approach to calculate the index for each provincial-level administrative region of China. Based on data availability, this work focused on the five targets and seven indicators under SDG 11 and made integrated assessment of SDG 11 at the provincial-level scale through comparison between 2015 and 2018. Furthermore, for each province, the key targets and indicators were identified, where special attention is required in order for SDGs to be achieved by 2030.

Data used

◎ Public transportation information data of China.

◎ Data product of ratio of land consumption rate to population growth rate.

◎ Hazard data from China's statistical yearbooks.

◎ City statistical yearbooks of China.

◎ Annual average $PM_{2.5.}$

◎ Land use/land cover data.

◎ Gridded population data.

◎ Public spaces in Chinese urban built-up areas.

Method

1) Normalization

In order to eliminate residuals caused by different dimensions, self-variation or extreme values of indicators, it is necessary to standardize the original indicators between 0 and 1 with the following equation:

$$x = \frac{x - \min(x)}{\max(x) - \min(x)}$$

A value of the normalized indicators closer to 0 indicates a worse performance while a value closer to 1 indicates a better performance. To remove the effects of extreme values, data at the bottom 2.5[th] percentile were selected as the lower bound for normalization, which is put forward by Organisation for Economic Co-operation and Development (OECD) and JRC. The selection of the upper bound drew on the method from the *Sustainable Development Report* 2019 (Sachs *et al.,* 2019) and Xu *et al.* (2020).

2) Calculation of the integrated index

The following equation was used to calculate the integrated index according to the method in the 2019 Sustainable Development report (Lafortune *et al.,* 2018):

$$I_i(N_i, N_{ij}, I_{ijk}) = \frac{1}{N_i}\sum_{i=1}^{N_i}\frac{1}{N_{ij}}\sum_{k=1}^{N_{ij}}I_{ijk}$$

where I_i is SDG 11 integrated index of province i; N_i indicates the number of targets of province i; N_{ij} denotes the number of indicators of targets j of province i; N_{ijk} is the value of indicators of targets j of province i.

3) Quantifying the level of achievement of targets

To assess the progress on a particular target at the provincial level, an SDG 11 dashboard was generated, with the indicators divided into four levels (green, yellow, orange and red) (Lafortune *et al.,* 2018). Green is the upper bound of each indicator. The colors yellow, orange and red represent distances to achieving SDG 11. Red denotes the lower bound of each indicator. The upper and lower bounds are the same as for the normalization of the integrated index.

Results and analysis

1) SDG 11 integrated index

Figure 4-13 shows the spatial distribution of SDG 11 integrated index at the provincial scale. In general, the integrated index was higher in the eastern provinces than in the western ones. It went up in 28 provinces and down in 3 provinces in 2018 compared with 2015, with its average value increasing from 0.58 to 0.65. The number of provinces with an integrated index value below 0.6 decreased from 20 to 8, while the number of those above 0.68 increased from 8 to 10.
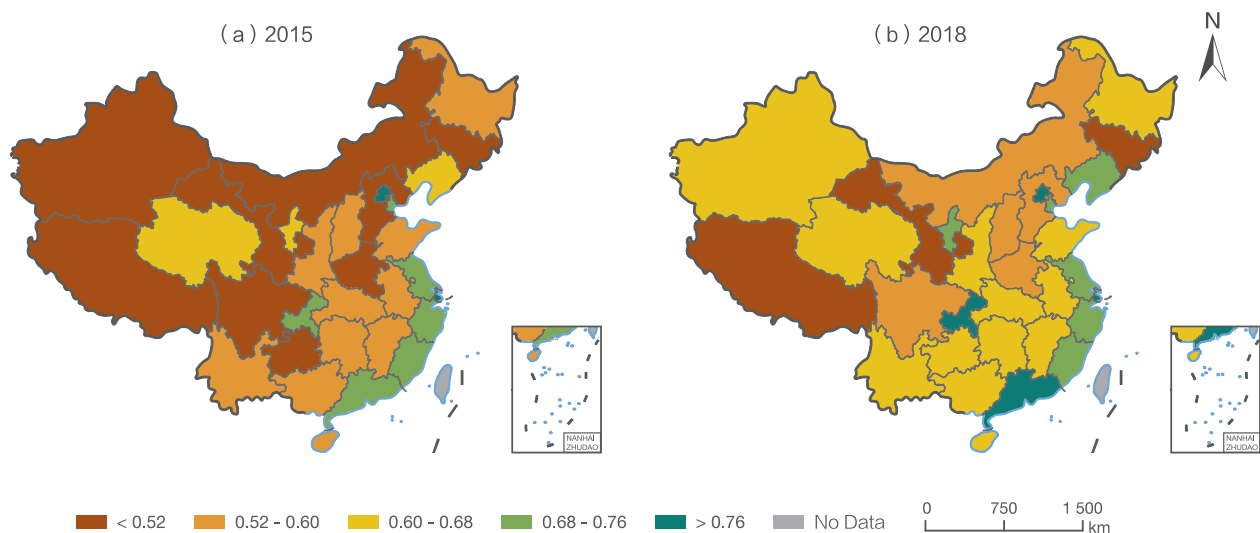
Figure 4-13. The spatial distribution of SDG 11 integrated index at the provincial scale

2) Progress in sustainable development targets

Figure 4-14 shows the SDG 11 dashboard at the provincial scale in China from 2015 to 2018. On the whole, good progress was made in achieving SDG 11.3, while more effort was needed to achieve SDG 11.6. Specifically, eastern provinces were closer to realizing SDG 11.2 and 11.3, while the central and western provinces were still further from realizing SDG 11.5. The provincial governments, while keeping up efforts on targets where good progress is made, should pay more attention to those targets where progress is lacking.

	11.2	11.3	11.5	11.6	11.7
Beijing					
Tianjin					
Hebei					
Shanxi					
Inner Mongolia					
Liaoning					
Jilin					
Heilongjiang					
Shanghai					
Jiangsu					
Zhejiang					
Anhui					
Fujian					
Jiangxi					
Shandong					
Henan					
Hubei					
Hunan					
Guangdong					
Guangxi					
Hainan					
Chongqing					
Sichuan					
Guizhou					
Yunnan					
Tibet					
Shaanxi					
Gansu					
Qinghai					
Ningxia					
Xinjiang					

Distance to SDG realization

very close　close　far　very far

SDG trend from 2015 to 2018

stagnating　increasing　decreasing

↑ Figure 4-14. SDG 11 dashboard

Outlook

In this case, the SDG 11 integrated index was calculated using the method of SDSN in the 2019 Sustainable Development Report, which can serve as a tool for the evaluation of the sustainability of SDG 11. Whether each province performed well or not in achieving SDG 11 is clearly indicated by the value of each indicator and on the dashboard. Indicators and targets under SDG 11 can impact each other, and no indicator should be achieved at the expense of another. Therefore, the interactions between indicators should be studied in the future.

Summary

This chapter focuses on the five technical targets and six of their indicators under SDG 11. A Big Earth Data-enabled method was developed to evaluate multiple SDG 11 indicators in a dynamic, spatially specific, and quantitative way. An integrated assessment was made at the provincial level in China, which can be of value to future dynamic monitoring and integrated evaluation of urban sustainability.

In terms of data products, this chapter created high-resolution gridded population data by gender and age for 2015 and 2018, and independently produced vector dataset of built-up areas of 433 Chinese cities between 1990 and 2018, and datasets of integrated urban assessment, covering shantytowns, public transportation, urbanization, disasters and open public space. All are of great use to evaluating urban sustainability in a comprehensive way.

In terms of methods, the chapter developed an advanced semantic segmentation and transfer learning model to extract data on shantytowns in China, and proposed a new indicator—the ratio of economic growth rate to land consumption rate, which will expand and localize SDG 11.3.1 and enrich the SDG 11 indicator framework system.

The above-mentioned independently produced Big Earth Data and model were applied to monitoring and comprehensive evaluation of SDG 11 indicators in China. The results can be used in policy making and finding a Chinese solution to sustainable urban development.

The following research should be prioritized in future work.

◎ Develop Big Earth Data science, produce high quality evaluation datasets on that basis, and find new methods of monitoring SDG 11 indicators.

◎ Promote SDG 11-related data sharing and technology among developing countries.

◎ Make joint comprehensive evaluations of SDG 11 implementation in typical regions in the world through international cooperation in service of both United Nations goals and China's national strategy.

SDG13

SDG 13
Climate Action

Background

Goal 13 of the UN Sustainable Development Goals (SDG 13) — "Take urgent action to combat climate change and its impacts" (Climate Action) is a call to action to reduce climate change-related hazards and natural disasters, mitigate the impacts of climate change and build greater capacity for climate change response. Far from being a standalone goal, SDG 13 is vital to the attainment of all SDGs.

This report focuses on two targets: 13.1 and 13.2. SDG 13.1 is to "strengthen resilience and adaptive capacity to climate-related hazards and natural disasters in all countries." Climate change is a key driver of disaster losses, according to a report by the United Nations Office for Disaster Risk Reduction (UNDRR), which oversees the implementation of the Sendai Framework for Disaster Risk Reduction, an instrument guiding the implementation of SDG 13.1. The Paris Agreement serves as the basis for the implementation of SDG 13.2 — "Integrate climate change measures into national policies, strategies and planning." Evaluation of their implementation to date has been long on statistics but short on granular analyses and disaggregated data (by disaster type and by scope of impact), along with a dearth of further guidelines and programs for climate change response. Indicators under these two targets, all of which are Tier II, have not caught up with the progress made in monitoring practice aided by Earth observation technology. They need to be updated

as a matter of urgency to also include information on the spatial distribution of climate change-related disasters and climate change impacts. Only then can more targeted responses be elaborated.

As stated in the *2019 Report on China's Policies and Action on Climate Change*, China pursues a proactive national strategy to address climate change, with a series of measures in place including, inter alia, industrial restructuring, energy conservation, emission reduction and afforestation to increase carbon sinks. China's CO_2 emission intensity (volume of emissions per unit of GDP) in 2018 dropped by 45.8% from the 2005 level on a cumulative basis, the equivalent to a 5.26 billion-ton reduction of CO_2 emissions. Given its lasting impacts, climate change is something that humanity has to confront in concert for a long time to come. People are still looking for informed answers to such questions as what climate change impacts are already or will soon be felt in China and elsewhere, and how to reduce impacts and losses from climate change and achieve sustainable development. This report focuses on two targets, namely, SDG 13.1 and SDG 13.2, and presents contributions on three fronts: methodological models that reflect climate change parameters, spatially disaggregated data products and support to policy-making in climate change response.

Main Contributions

Two cases on SDG 13 are presented in this study (Table 5-1), corresponding to two SDG targets on climate-related hazards and natural disasters and climate change response. In terms of data products, datasets on the spatial distribution of heatwaves and a probability ensemble on the phenology of main crops are provided on the basis of past statistics. In terms of methodology, a meteorological data homogenization approach combining non-stationary models and parametric/non-parametric methods is presented. In terms of support to policy-making, pre-emptive response is recommended in view of the projected forward shifts in the anthesis and maturation of wheat and maize that may jeopardize their yields. This report aims to offer a fresh perspective and propose new solutions to help further our understanding of the impact of climate change in all its manifestations and develop mitigation and adaptation strategies in response to a whole range of issues posed by climate change.

Table 5-1 Cases and Their Main Contributions		
Target	**Case**	**Contributions**
13.1 Strengthen resilience and adaptive capacity to climate-related hazards and natural disasters in all countries	Intensity and frequency of extreme high-temperature events and heatwaves in China	**Data product:** homogenized temperature series datasets **Method:** a combination of non-stationary models and parametric/non-parametric methods
13.2 Integrate climate change measures into national policies, strategies and planning	Predicting the impacts of climate change on the phenology of China's main crops	**Data product:** near-term probabilistic forecast datasets for the phenology of China's main crops under climate change scenarios **Support to policy-making:** informing China's policy on food production in response to climate change

Case Study

Intensity and frequency of
extreme high-temperature events and heatwaves in China

Target: 13.1 Strengthen resilience and adaptive capacity to climate-related hazards and natural disasters in all countries.

Highlights

- *The spatiotemporal changes in the intensity and frequency of extreme high-temperature events and heatwaves in China are assessed over the 1990-2018 timeframe, based on homogenized temperature series data from 754 terrestrial weather stations, pointing to significantly increased intensity and frequency of extreme high-temperature events and heatwaves in China since the late 1990s.*

Background

The central aim of the Paris Agreement is "to strengthen the global response to the threat of climate change by keeping a global temperature rise this century well below 2 degrees Celsius above pre-industrial levels and to pursue efforts to limit the temperature increase even further to 1.5 degrees Celsius". Extreme high-temperature events and heatwaves have become some of the predominant climate-related disasters ravaging China in recent decades.

In this study, we introduce the notion of "dynamic reoccurrence periods" to further refine the indicators of extreme high-temperature events and heatwaves and expand the scope of their application. They are particularly serviceable in describing extreme high-temperature events and heatwaves that have occurred in recent years. Characterization of the spatiotemporal evolution of extreme high-temperature events enables an accurate and holistic understanding of the pattern of extreme high-temperature events and heatwaves in China, to provide science-informed support for policy-making under relevant SDGs.

Data used

◎ Daily maximum temperature series data from 754 stations from 1960 to 2018 compiled and published by the Information Center of the China Meteorological Administration, adjusted and homogenized (Li *et al.,* 2015). The baseline period is 1979-2018.

Method

Homogenization of data minimizes the systematic deviations resulting from relocation of stations or changes in observational methods and techniques. The highest values of daily maximum temperatures in the summer half-year (April through September) captured at all stations are used to work out periods and levels of recurrence through Generalized Extreme Values (GEV) fitting. Dynamic reoccurrence periods are computed with a linear model in time using location parameters, from which the annual frequency of "once-in-N-year" extreme high-temperature events is worked out for each station. A "once-in-N-year" extreme high-temperature event is one where the probability of the year's maximum temperature reaching or exceeding a given recurrence threshold under the climatic conditions of the current year is 1/N. Hence the average yearly frequency of extreme high-temperature events at every station across China and in each of the seven regions can be calculated. The intensity of an extreme high-temperature event is expressed as a temperature value (in Celsius) in excess of a given "once-in-N-year" level of recurrence.

Results and analysis

The frequency of "once-in-20-year" extreme high-temperature events in China has markedly increased since the late 1990s (Fig. 5-1). Since 2000, five years, i.e. 2000, 2003, 2010, 2013 and 2017, were marked by an unusually high incidence of extreme high-temperature events and heatwaves. In each of those five years, notable extreme high-temperature events and heatwaves happened in two or three of the seven climatic regions of China, with marked variations in both frequency and intensity from year to year. As a general trend, each region is hit by an unusually high incidence of extreme high-temperature events and heatwaves once every five to ten years. The intensity of extreme high-temperature events and heatwaves in northern regions is relatively higher than that in southern regions.
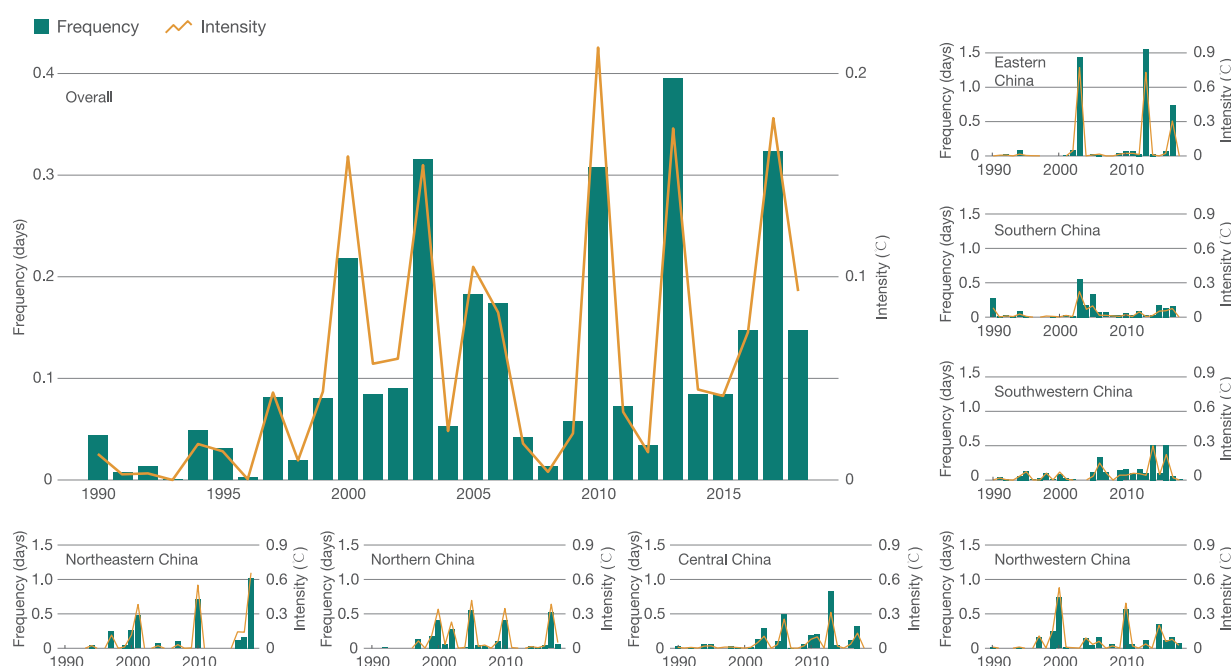
↑ Figure 5-1. The average frequency and intensity of "once-in-20-year" extreme high-temperature events and heatwaves across China and in each region, 1990-2018

Notable extreme high-temperature events and heatwaves have been observed almost every year since 2010 (Fig. 5-2). The most spatially extensive extreme high-temperature events and heatwaves happened in 2010 when more than half of the regions across China recorded extreme high-temperature events. The intensity of extreme high-temperature events and heatwaves peaked in 2013 when dozens of stations in central and eastern China recorded around 10 days of extreme high temperatures. In 2016 and 2017, extreme high-temperature events and heatwaves also affected many parts of China. Worth noting is the high incidence of relatively defined extreme high-temperature events and heatwaves in some high-latitude or high-altitude areas in recent years. A record fifteen-day spell of extreme high temperatures hit a mountainous area in southwestern China in 2014. Similarly, in 2010, 2015 and 2018, eight to ten days of extreme high temperatures were recorded at some high-altitude and high-latitude stations, topping the rest of the country for that year in each case.

● 1 ● 2 ● 3 ● 4 ● 5 ● 6 ● 7 ● 8 ● 9 ● 10 ● 11 ● ≥12
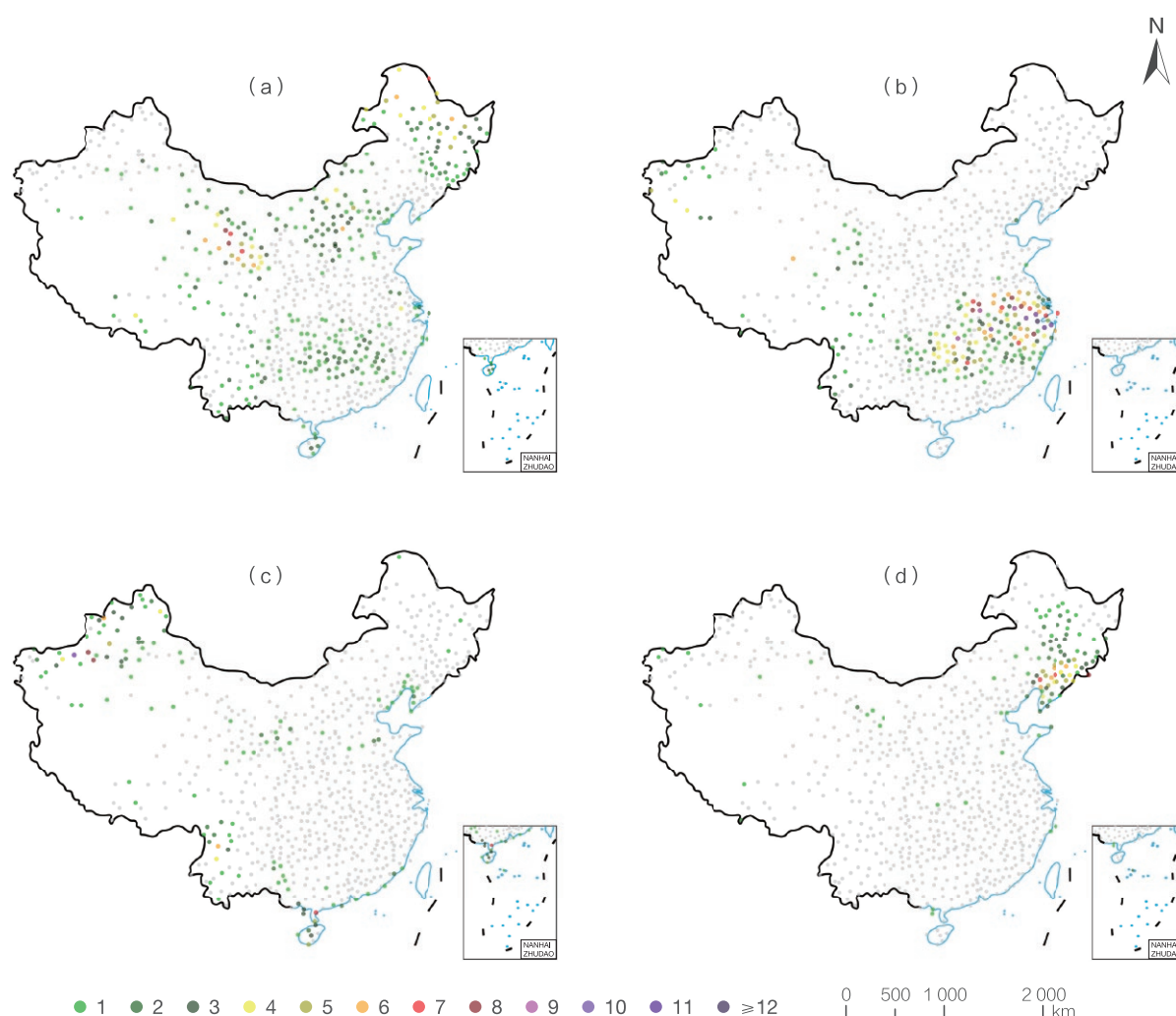
↑ Figure 5-2. The spatial pattern of "once-in-5-year" extreme high-temperature events and heatwaves in 2010 (a); 2013 (b); 2015 (c) and 2018 (d). Grey dots indicate stations with no recorded extremes (Note: no data available for Taiwan province).

Outlook

This study enables a better understanding of extreme high-temperature events and heatwaves through the lens of recurrence periods and levels by modifying the criteria of their definitions. There has been a persistently high incidence of extreme high-temperature events and heatwaves across China in recent years, so much so that they have become routine occurrences – approaching or reaching record high temperatures in approximately one third of regions in China every five years or so since 2000. This trend has been more pronounced in recent years, with extensive or highly intense heatwaves each and every year. It is therefore necessary to better forecast overall climate and weather conditions associated with extreme high-temperature events and build greater capacity for holistic planning to respond to extreme high-temperature events and heatwaves of disastrous proportions in different regions. Furthermore, enhanced monitoring and forecasts are required for relatively defined heatwaves in high-latitude and high-altitude areas. Excessive heat in absolute terms is rare in these areas, hence the tendency to overlook them in the past. Yet, in recent years, relatively defined extreme high-temperature events and heatwaves in these areas have occurred more frequently than in central and eastern parts of China known for a high incidence of classic heatwaves, posing an equally grave threat to local agricultural and forest ecosystems and infrastructure.

Alongside China's rapid socioeconomic development over the recent decades, there has been a huge influx of population into large and medium-sized cities, as well as sea change to land uses. An important question to explore and answer going forward is how to assess, with greater precision, the impacts of extreme high-temperature events and heatwaves on productive activities, daily life, physical health and natural ecosystems by leveraging demographic, land and other Big Earth Data and factoring in the exposures and vulnerabilities of different communities and systems.

Predicting the impacts of climate change on the phenology of China's main crops

Target: 13.2 Integrate climate change measures into national policies, strategies and planning.

Highlights

● *Projections of changed phenology of China's main crops through the 2030s (2011-2040) put the probability of early maturation of wheat and maize at 90.4%-91.2% and 62.9%-64.5% respectively. Without appropriate interventions, climate change will lead to forward shifts in the phenology of these crops and shortened cycles of growth, with negative implications for wheat and maize yields.*

Background

The impact of climate change on food security is a matter of wide concern. Climate change not only leads to altered crop phenology, but also further affects crop yields and threatens socioeconomic stability through its impact on agricultural production and related industries (Liu *et al.,* 2018a). This impact is likely to continue into the future. Therefore, forecasting changes in the phenology of main crops under future scenarios is instrumental in developing appropriate adaptation measures and ensuring regional food security (Liu *et al.,* 2018b). This study presents near-term projections on the spatial distribution of the phenology of China's main crops with a validated crop model, refined by multi-model and multi-scenario probabilistic predictions to reduce the uncertainty in climate change assessments.

Data used

◎ Data on climate change scenarios (RCP 2.6, RCP 4.5 and RCP 8.5) obtained from the Inter-Sectoral Impact Model Intercomparison Project.

◎ Experimental data (crop growth and field management records) and meteorological data (daily minimum temperatures, daily maximum temperatures, total daily precipitation and sunshine hours) captured and provided by the agrometeorological observatories of the China Meteorological Administration for model validations.

◎ Soil data obtained from the China Soil Database and experiments of agrometeorological observatories.

Method

For the purposes of this study, areas where the planting ratio was greater than 0 were selected as study areas and a crop growth model (Decision Support System for Agrotechnology Transfer, DSSAT-Wheat/Maize) was used to predict China's wheat and maize phenology under multiple scenarios (RCP 2.6, RCP 4.5 and RCP 8.5) through the 2030s (2011-2040). The simulation accuracy of the validated DSSAT-Wheat/Maize model is better than 90%. To assess future phenological changes of wheat and maize under the no-adaptation scenario, field management was kept at the same level as in the baseline period. This study aimed to obtain the average values of five atmospheric circulation models by scenario to generate climatic conditions under corresponding climate change scenarios (RCP 2.6, RCP 4.5 and RCP 8.5). Additionally, in order to make the prediction less uncertain, the kernel density estimation method (using Gaussian kernel function) was chosen to estimate the probability density and interval of phenological changes. Furthermore, since the influence of CO_2 concentration was also considered, it was necessary to set the specific value of CO_2 concentration by target period and scenario during the simulation process.
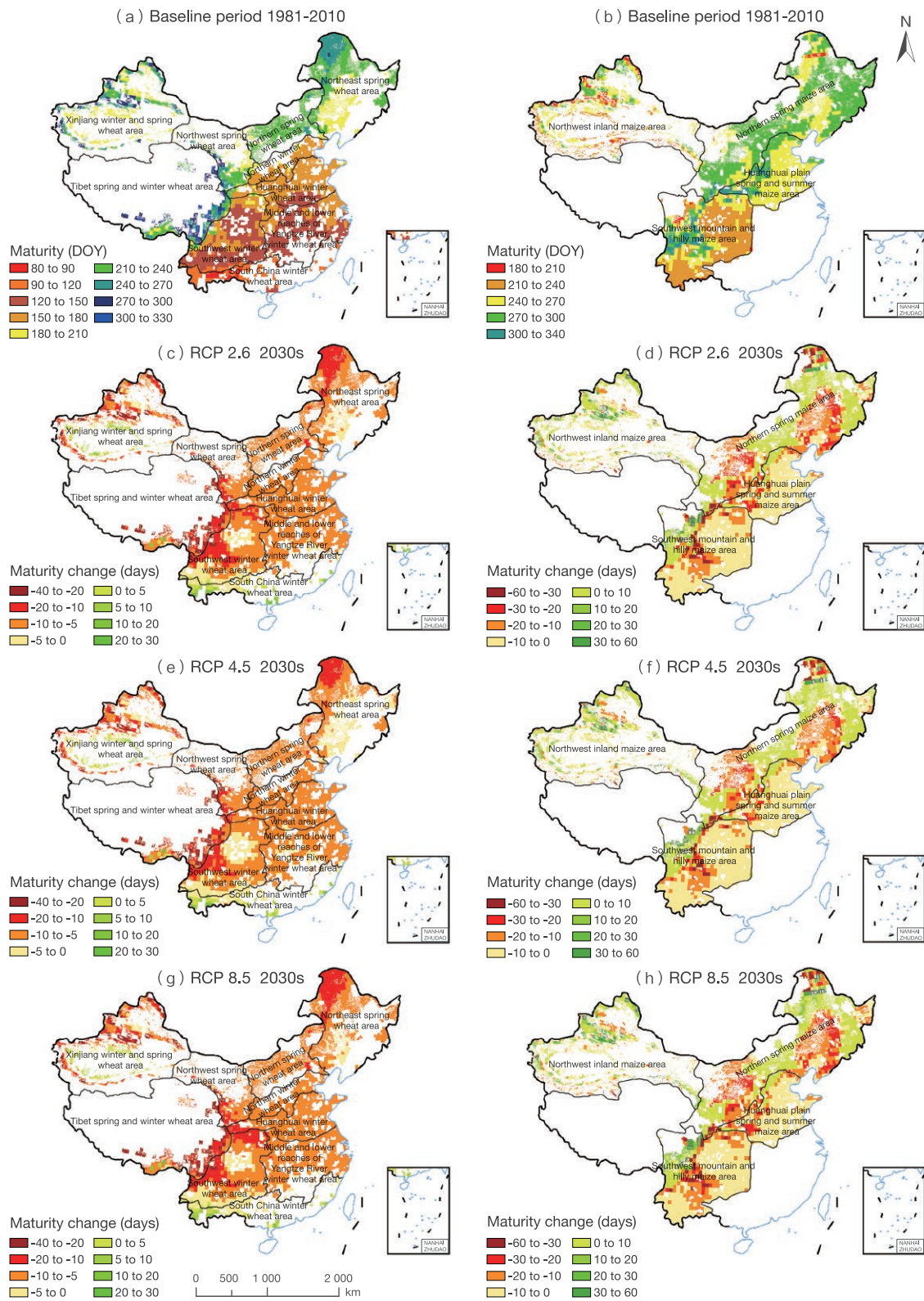
Results and analysis

↑ Figure 5-3. Spatial distribution and changes of wheat (a, c, e, g) and maize (b, d, f, h) maturation in China under climate change scenarios

The spatial distribution of wheat and maize maturation, and changes thereto, in the 2030s are shown in Figure 5-3. Compared to the baseline period of 1981-2010, over 90% of the areas show forward shifts in wheat phenology through the 2030s under all scenarios. The greatest forward shifts in wheat phenology are predicted for those areas in Qinghai and Tibet where spring and winter wheat is grown, while the areas with delayed phenology are concentrated in winter and spring wheat areas of Xinjiang and winter wheat areas of South China. Compared to the baseline period, the flowering period (anthesis) of maize is brought forward under most scenarios, and early anthesis is predicted for 98.0% of the regions under the RCP 2.6 scenario, most notably in the southwest mountainous and hilly maize-growing regions. Unlike anthesis, there are substantial differences in the changes of maize maturation from region to region, with the greatest forward shift in the maturation of maize predicted under the RCP 8.5 scenario. As the latitude decreases, the wheat anthesis and maturation periods change from earlier than the baseline to later than the baseline, which is the most obvious under the RCP 8.5 scenario. In contrast to wheat, delayed anthesis and maturation of maize tend to be concentrated at high latitudes.

In the 2030s, the probabilities of early anthesis and early maturation of wheat are 88.9%-89.1% and 90.4%-91.2% respectively, and the probabilities of early anthesis and maturation of maize are 97.2%-98.0% and 62.9%-64.5% respectively. Under any of the scenarios, the probability of early anthesis of maize is greater than that of wheat, while the probability of early maturation of maize is less than that of wheat. Under the RCP 2.6, RCP 4.5 and RCP 8.5 scenarios, the probabilities of early anthesis for wheat and maize decrease progressively. In the case of RCP 2.6, the probability of early anthesis of maize is as high as 98.0%.

Outlook

Uncertainties abound in the projections of the impacts of climate change. Although uncertainties associated with model output and emission scenarios were factored into the ensemble-based predictions and crop modeling was validated by area to the greatest extent possible, to make the simulation more accurate, a degree of uncertainty remains in the simulation of biophysical processes of the crops.

Future climate change is likely to aggravate the fluctuations in China's wheat and maize production, hence the need to take adaptation measures as a matter of urgency to ensure food security. Improving crop management is an effective way to boosting the resilience and adaptive capacity of agriculture against climate change. Measures such as adjustments to sowing dates, fertilization and irrigation can mitigate the adverse impacts of climate change. Transforming the patterns of photosynthesis of crops through the use of improved crop varieties or breeding new varieties that are more heat tolerant and require more heat is also an important strategy to improve the resilience and adaptive capacity of agriculture.

Summary

This chapter presented case studies in respect to two targets under SDG 13:

◎ In terms of climate change-related hazards and natural disasters, an analysis of the spatial distribution of extreme high-temperature events and heatwaves points to an upward trend in extreme high-temperature events and heatwaves in China since the late 1990s;

◎ In terms of climate change response, an assessment of the possible impact of climate change on the phenology and yields of China's main crops points to the high probability of early anthesis of wheat and maize.

This chapter is an expansion of, and improvement on, spatial information based on the existing indicators under SDG 13. New datasets were generated by using the Big Earth Data platform, to provide information on spatial distribution for SDG 13-mandated response to climate change-related hazards and natural disasters and other impacts of climate change, so that the competent government agencies and institutions can better understand the problems posed by climate change and be better positioned to respond to climate change and minimize climate change-related losses.

SDG14
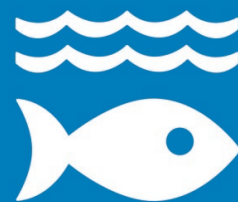
Background

The ocean, which covers 71% of Earth's surface, is one of our planet's three ecosystems, and a balanced marine ecosystem is vital to the survival and sustainable development of humankind. In 2015, the need to "conserve and sustainably use the oceans, seas and marine resources for sustainable development" was written into the 2030 Agenda for Sustainable Development of the United Nations, and has become one of the top priorities on the international agenda. In September 2017, in the margins of the 9th BRICS Summit, a special discussion was held on the "blue economy"; in November 2018, the 1st Global Conference on Sustainable Blue Economy adopted the *Nairobi Statement of Intent on Advancing the Global Sustainable Blue Economy*.

The Chinese Government is strongly committed to the United Nations agenda on the sustainable development of oceans and seas. Since 2015, guided by the national strategic goal — "Accelerate the transformation of China into a maritime power through integrated development of land and seas under unified planning", China's endeavors in the maritime sector have been developing by leaps and bounds, scoring many successes in, inter alia, protecting oceans and seas and promoting economic growth. Such notions as building a "maritime community with a shared future" and "Blue Partnership" are helping to put fairness and reason at the center of the global governance system. However, the sustainable development of oceans and seas in the case of China is not without its fair share of challenges posed by a huge demand for marine resources thanks to high population density in coastal China and the country's rapid economic growth.

The vast marine ecological environment is perpetually in a state of flux. One of the constraints that hampers the objective assessment of SDG targets related to oceans and seas and science-informed policy-making is the lack of monitoring data. Big Earth Data lends itself to macroscale dynamic monitoring and provides an important means of data acquisition for the evaluation of sustainable development of the oceans and seas. This report focuses on two SDG targets, namely, preventing and significantly reducing marine pollution (SDG 14.1) and building resilience against disasters and protecting marine and coastal ecosystems (SDG 14.2). It presents new big data-enabled solutions to provide data and information support for identifying critical issues related to the sustainable development of China's oceans and seas.
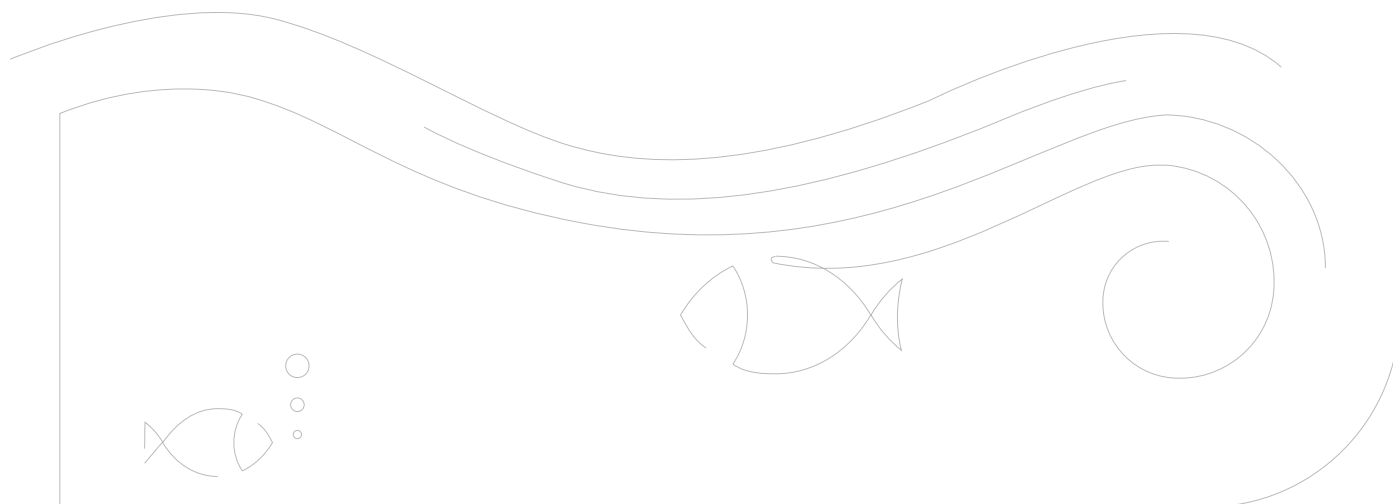
Main Contributions

Under a dual mandate of reducing marine pollution and protecting marine ecosystems, Big Earth Data has been used to monitor and evaluate progress toward the SDG 14 targets in the coastal waters and typical areas of China. Three case studies are presented below to share with the rest of the world China's data products, methodological models, and support to policy-making related to the monitoring of SDG 14 indicators. The names of the cases and their main contributions are shown in Table 6-1.

Table 6-1 Cases and Their Main Contributions		
Target	**Case**	**Contributions**
14.1 By 2025, prevent and significantly reduce marine pollution of all kinds, in particular from land-based activities, including marine debris and nutrient pollution	Analysis of the distribution and variation of marine debris and microplastics in China's coastal waters	**Data product:** datasets on the distribution of marine debris and microplastics in China's coastal waters **Support to policy-making:** informing policy-making with the state, by-region distribution and patterns of change of pollution by marine debris and microplastics in China's coastal waters for the prevention and control of marine debris and microplastics in typical areas
14.2 By 2020, sustainably manage and protect marine and coastal ecosystems to avoid significant adverse impacts, including by strengthening their resilience, and take action for their restoration in order to achieve healthy and productive oceans	Ecosystem health assessment for typical bays in coastal China	**Data product:** datasets of ecosystem elements in typical bays, i.e. Jiaozhou Bay, Daya Bay and Sishili Bay **Method:** health assessment based on marine ecosystem structures and service functions **Support to policy-making:** informing policy-making on how environmental factors in China's typical coastal bays contribute to changes in the key elements of ecosystems, to keep the protection of coastal ecosystems anchored in science
	Monitoring changes in raft culture in China's coastal waters	**Data product:** datasets from monitoring of raft culture in key coastal provinces of China **Method:** deep learning-enabled AI extraction of marine raft culture data

SDG 14

14 LIFE BELOW WATER

Case Study

Analysis of the distribution and variation of marine debris and microplastics in China's coastal waters

Target: 14.1 By 2025, prevent and significantly reduce marine pollution of all kinds, in particular from land-based activities, including marine debris and nutrient pollution.

Highlights

- *An analysis of the distribution and variation of floating debris in 22 typical coastal areas of China showed that the abundance of floating debris in China's coastal waters in 2018 was approximately 25% below the 2010 to 2014 average.*

- *Microplastics shape found in China's coastal waters in 2019 were mainly fibrous, linear, spherical, and fragmented and the distribution of microplastics varied from region to region, with the average abundance of microplastics at low to medium levels.*

Background

In recent years, marine debris and microplastics, being a major cause of environmental woes, have gained greater attention as a major concern to various constituencies. Today, work in this area is moving beyond research to tangible actions of pollution control and joint global endeavors. Reducing plastic debris is one of the key indicators of marine pollution control in the framework of UN 2030 Agenda for Sustainable Development. However, it remains a Tier II indicator to this day because of a dearth of data on this phenomenon at the international level. The competent authorities and research institutions in China have been working hard on monitoring and analysis, delivering a range of outcomes.

Data used

◎ Data on marine microplastics used in this study primarily from monitoring of microplastics in China's coastal waters by the Ministry of Natural Resources and the *Bulletin on the State of China's Marine Ecological Environment 2019* published by the Ministry of Ecology and Environment.

◎ Marine floating debris data primarily from the *Bulletin on the State of China's Marine Ecological Environment 2018* published by the Ministry of Ecology and Environment and relevant papers published in international journals.

Method

This study aims to map the current state of pollution by marine debris and microplastics in China's coastal waters and the distribution of same by region by consolidating the available mapping data, data from marine bulletins and data from academic literature on marine debris and microplastics in the said waters, with an analysis of the trends of variation in respect of these pollutants against historical data.

SDG 14

Results and analysis

1) Distribution and change of floating debris in China's coastal waters

According to the monitoring data, the abundance of floating debris in China's coastal waters has been on a decline since 2015. The abundance of floating debris in 2018 was approximately 25% lower than the average of 3 207 pieces/km^2 recorded for the period 2010-2014 (Zhou *et al.,* 2016).

In 2018, most of the floating debris in China's coastal waters was plastic waste (88.7%), followed by wood (4.4%) (Fig. 6-1). The plastic waste identified was mostly polystyrene foam, plastic bags and plastic bottles.

A study of the distribution of floating debris in 22 typical coastal areas of China identified significant variations in the abundance of floating debris in different areas (Fig. 6-2), the highest abundance found in: Xinghai Bay, Dalian, Liaoning province; Yuetou Bay, Huangcheng, Xiangshan, Zhejiang province; Dacheng Bay, Chaozhou, Guangdong province; and Guanhai Bay, Zhanjiang, Guangdong province.

2) Distribution patterns of microplastics in China's coastal waters

A study of the distribution of microplastics in China's coastal waters in 2019 in terms of shape, color, size and polymer type finds: (a) that most of the microplastics was in the form of fibers, threads, pellets/granules and fragments; (b) that the highest proportion of microplastics found was 1.0-2.0 mm in size; (c) that the microplastics came in eight colors, namely, white, black, red, yellow, blue, green, purple and transparent, with a different mix of colors in each of the sample areas; and (d) that the predominant types of microplastics were Polyethylene Terephthalate (PET), Polystyrene (PS), Polyethylene (PE) and Rayon.

Monitoring of the abundance of microplastics in China's coastal waters in 2019 showed that the abundance of microplastics floating on the surface in the section of the Bohai Sea monitored was 0.82 items/m^3 and in the section of the East China Sea monitored, 0.25 items/m^3, with the average abundance of microplastics at low to medium levels.

Outlook

Reducing marine debris and microplastics pollution is one of the priorities on the agenda of global ocean governance, which requires all countries to work together. The current gaps in the scientific knowledge of marine microplastics pollution make it necessary to better analyze the impacts of marine microplastics on environmental pollution in the future. While pollution by marine debris and microplastics in China's coastal waters has been declining, much remains to be done to tackle marine debris and microplastics in the marine environment with more conclusive solutions. Dynamic monitoring of plastic waste and microplastics in coastal waters should be continued and a database built, along with studies on the distribution of microplastics in the oceanic and polar environments, to provide a scientific basis for the management of marine debris and microplastics at the global level.

Bijia Mountain, Jinzhou

Bingjia, Huludao

Dalu Island, Dandong

Xinghai Bay, Dalian

Tanggu, Tianjin
Dagang, Tianjin

Sishili Bay, Yantai

Dongying Modern Fishery
Demonstration Area

Shilaoren, Qingdao

Taigong Island, Rizhao

Lian Island, Lianyungang

Floating garbage (items/km²)

● 0 - 100

● 100 - 500

● 500 - 1 000

● 1 000 - 2 000

● 2 000 - 5 000

● > 5 000

0   100   200
|————|————| km

Rudongyangkou, Nantong

Zhujiajian, Zhoushan

Huangchengyuetou, Xiangshan

Dongtou, Wenzhou

◉ Distribution of floating debris in
22 typical coastal areas of China

Xiuyu, Putian

Dacheng Bay, Chaozhou

Sanzao Island, Zhuhai

Zhapo, Yangjiang

Qiao Port, Beihai

Guanhai, Zhanjiang

Sanya Bay

Qiao Port, Beihai   Sanzao Island, Zhuhai
Zhapo, Yangjiang
Guanhai, Zhanjiang

Sanya Bay

NANHAI
ZHUDAO

◉ Types of floating debris in
China's coastal waters and their
respective proportions, 2018

88.7%

4.4%

1.1%

1.4%

1.5%

1.7%

0.5%

0.6%

■ Plastics   ■ Wood

■ Paper   ■ Fabric

■ Glass   ■ Rubber

■ Metal   ■ Others
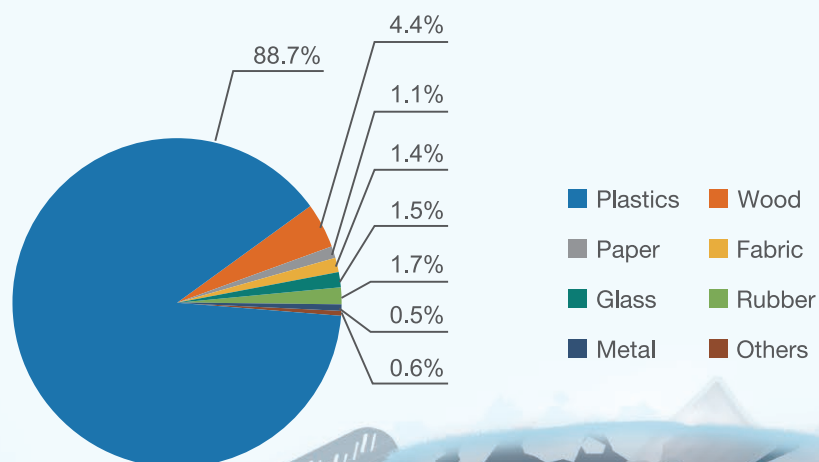
Ecosystem health assessment for typical bays in coastal China

Target: 14.2 By 2020, sustainably manage and protect marine and coastal ecosystems to avoid significant adverse impacts, including by strengthening their resilience, and take action for their restoration in order to achieve healthy and productive oceans.

Highlights

- *The ecosystems of Jiaozhou Bay, Sishili Bay and Daya Bay are in relatively good health at present. For more than a decade from 2007 to 2019, the overall health of the Jiaozhou Bay ecosystem was stable with some upticks, while that of Sishili Bay and Daya Bay remained stable. The health condition of Daya Bay showed slight improvement from 2016 onward.*

Background

Industry, agriculture, aquaculture, tourism and other human activities bring compounding pressures on global coastal ecosystems. According to SDG Target 14.2 of the UN 2030 Agenda for Sustainable Development, it is time to "sustainably manage and protect marine and coastal ecosystems" and "achieve healthy…oceans". Marine ecosystem health assessments, which are instrumental in ocean governance and the development and use of oceans and seas, provide an important scientific basis for the protection of marine ecosystems and environment and ecological management, and help us move forward on a range of issues related to the marine environment and resources protection (Rapport, 1995; Pollard, 1998).

Data used

◎ Datasets on hydrological, chemical, planktonic, benthic, microbiological and other environmental/ecological factors in the typical bays available on the National Ecosystem Research Network of China (CERN) for the period of January 2007 to December 2019.

Method

Linked to Target 14.2, this study aims to refine the methodology of assessment in light of the characteristics of bay ecosystems, analyze the current state and variation trends of different ecosystem elements, and adjust and select parameters against the SDG indicators; conduct machine learning-enabled data mining to introduce additional threshold criteria or improve existing ones for assessment; and develop a report card assessment model in support of policy-making on coastal ecosystem management.

Results and analysis

For the purposes of this study, Sishili Bay, Jiaozhou Bay and Daya Bay were chosen as typical bays, representing different ecological environments and human activities: Sishili Bay is located in the northern part of the Yellow Sea, and the bay itself and its surrounding areas are home to agriculture, industry, aquaculture, port services and so on, with a high incidence of red tides in the bay; Jiaozhou Bay is located in the southern part of the Yellow Sea and is subjected to a range of anthropogenic stressors, including port services, aquaculture and a long bridge arching over the bay; Daya Bay is located in the South China Sea, home to the Daya Bay Nuclear Power Base with six units in operation. Joint health assessments were used to provide scientific information for the protection and management of different marine areas.
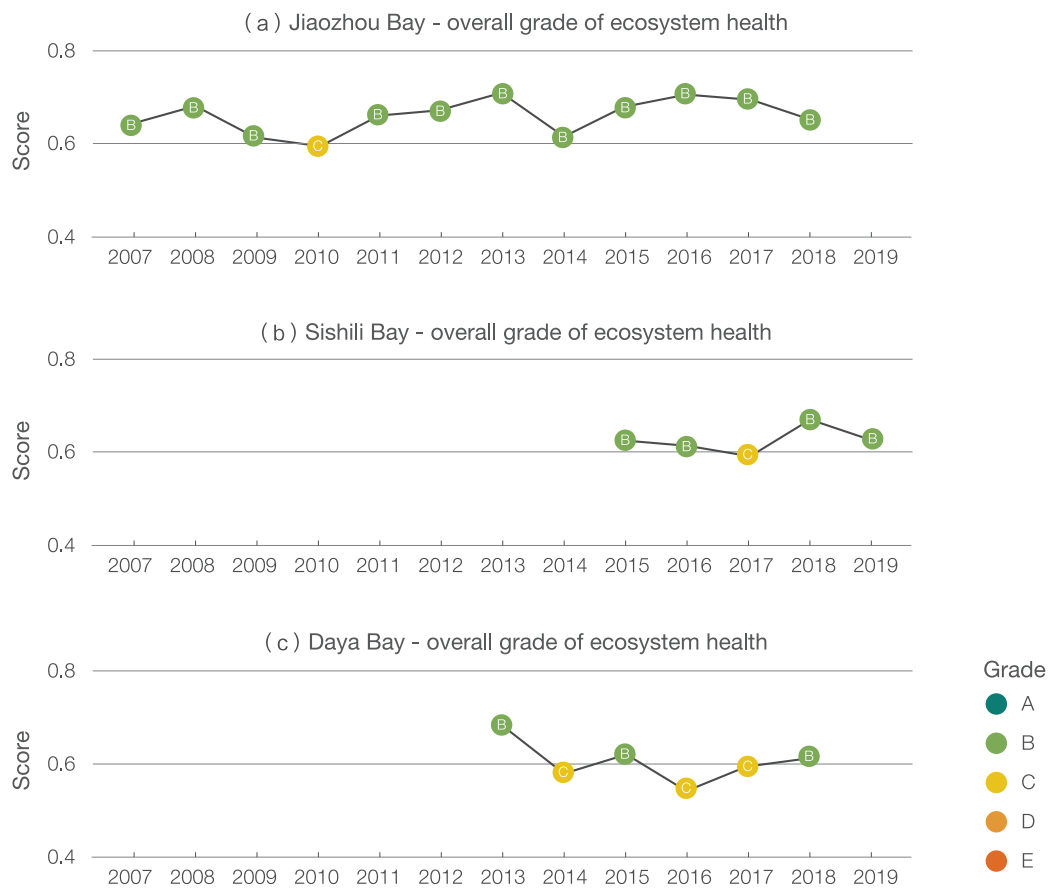
↑ Figure 6-3. Ecosystem health mapping results in selected bays 2007-2019

1) A general mapping of the health of typical bay ecosystems

The findings indicate that the ecosystems in Sishili Bay, Jiaozhou Bay and Daya Bay are in good health at present. From 2007 to 2018, the health of the Jiaozhou Bay ecosystem was stable with moderate improvement. The overall ecosystem health of Sishili Bay from 2015 to 2019 and Daya Bay from 2013 to 2018 was stable. Starting in 2016, there was a moderate improvement in the ecosystem health of Daya Bay. The assessment findings are
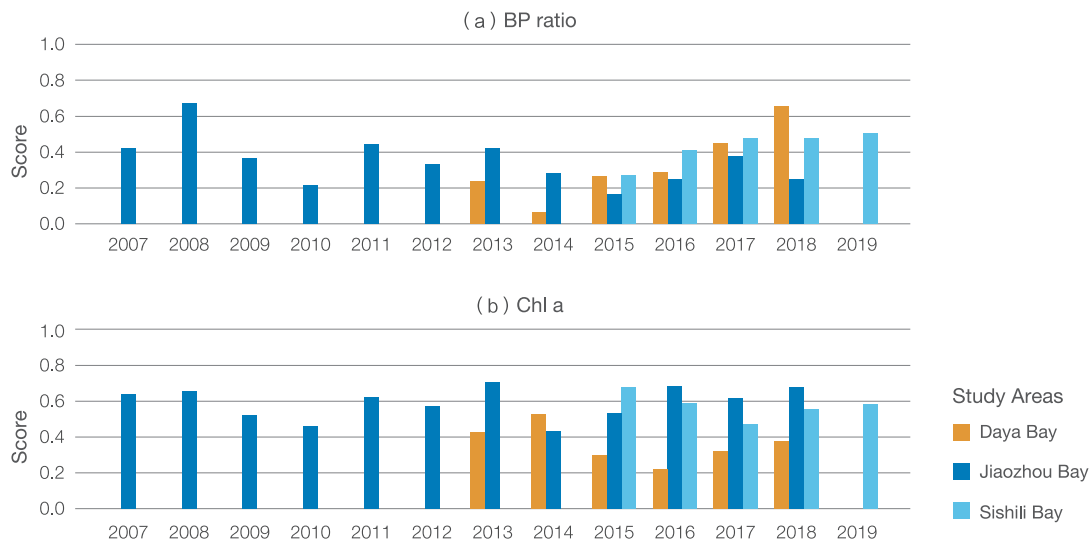
↑ Figure 6-4. Assessment results of key elements of typical bays (Grades and levels as shown in Fig. 6-3)
(a) Bacillariophyta Pyrrophyta ratio (BP ratio); (b) Chlorophyll a (Chl a)

shown in Figure 6-3.

2) Assessment of individual key elements of typical bay ecosystems

The sea surface Chlorophyll a (Chl a) concentration and the ratio between the Bacillariophyta and Pyrrophyta abundance (BP ratio) can respectively represent the primary productivity level and phytoplankton community structure in a given area to some extent and are therefore important indicators of its ecosystem health. We assessed the health of the three typical bays by measuring those two values and the results are as follows: The health of the phytoplankton community structure in Sishili Bay, as indicated by the BP ratio, showed a trend of sustained improvement and its primary productivity remained good and stable. The phytoplankton community structure of Daya Bay improved as from 2014, but its primary productivity was rated the lowest among the three bays, which might be attributable to its nutrient level. Jiaozhou Bay was rated slightly lower than the other two in phytoplankton community structure health while its primary productivity health remained good. See Figure 6-4 for details.

3) An analysis of contribution of environmental factors to changes in key elements of ecosystems

Machine learning was used to study how key environmental factors contributed to the variations in Bacillariophyta abundance in the bays (Fig. 6-5). Higher contribution indicates a greater role in changing Bacillariophyta abundance. The results indicate that the greatest contribution to Bacillariophyta abundance variations came from nutrients in Jiaozhou Bay and Sishili Bay while water temperature was the number one contributing factor to the Bacillariophyta abundance variations in Daya Bay. They are consistent with the characteristics of the three bays studied: In both Jiaozhou Bay and Sishili Bay, the ecological elements were closely correlated with nutrients because of higher concentration of nutrients as a result of significant impacts from human activities such as industry, agriculture and aquaculture. On the other hand, the water temperature variations in Daya Bay contributed the most to changes in Bacillariophyta abundance, probably as a direct consequence of the heated water discharged from the nuclear power plants located around Daya Bay.
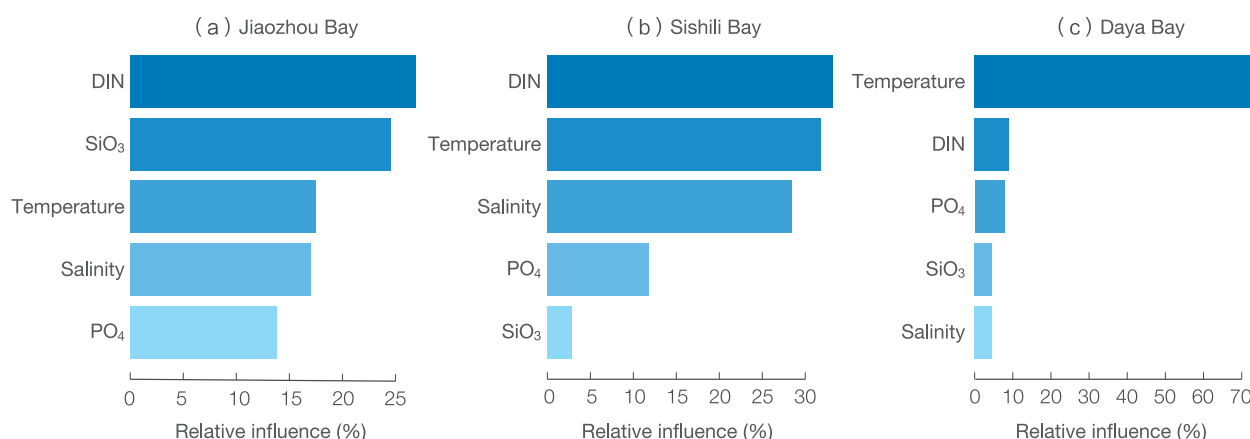
↑ Figure 6-5. Contributions of environmental factors to abundance of Bacillariophyta, a dominant species of phytoplankton
(a) Jiaozhou Bay; (b) Sishili Bay; (c) Daya Bay

Outlook

Using the coastal ecosystem health assessment approach, this study involves a number of assessments jointly conducted in the three typical coastal bays of China, analyzing the current status and variation trends of these coastal ecosystems, comparing their key ecosystem health elements and investigating major contributing factors to changes in the state of marine ecosystems of these bays. The expert diagnostic models will be further refined to make the diagnosis more objective by analyzing the stress factors affecting ecosystem health. Customized decision support systems that include analytical tools catering to different users and use scenarios will also be developed, in support of coastal environment protection and management.

Monitoring changes in raft culture in China's coastal waters

Target: 14.2 By 2020, sustainably manage and protect marine and coastal ecosystems to avoid significant adverse impacts, including by strengthening their resilience, and take action for their restoration in order to achieve healthy and productive oceans.

Highlights

- *Dynamic monitoring datasets (at 30 m spatial resolution) of the distribution of raft culture in key coastal provinces of China in 2017, 2019 and 2020 are generated for the first time, aided by deep learning.*

- *Findings indicate that the area of marine raft culture in China is still in the growth phase, while the area of raft culture within the boundaries of the coastal ecological conservation red line has remained stable on the whole.*

Background

Marine raft culture is an important form of marine aquaculture. It has three subsets, namely, floating raft culture, cage culture and longline culture. Compared to nearshore pond and mudflat aquaculture, raft culture is more difficult to manage because it is further away from the coast. Because raft culture tends to be scattered around a large area, traditional monitoring methods, such as onsite measurement using navigation and positioning systems, is labor-intensive, time-consuming and unproductive when accurate results of a large area are required. As an important part of Big Earth Data, satellite imagery can help overcome the inadequacies of field survey and is a reliable, state-of-the-art technology for safe and effective multi-temporal dynamic monitoring of marine raft culture across large areas.

Data used

◎ Gaofen-3 and Sentinel-1/2 satellite imagery of China's coastal waters for 2017, 2019 and 2020, of which the 2017 and 2019 data were for the period April to September of each year and the 2020 data, from April to June.

◎ Validated field survey data of marine raft culture for 2018.

◎ Policy data, including data on red line planning for the protection of marine ecosystems.

Method

For the purposes of this study, an AI-enabled remote sensing approach that supports large-area, complex-scenario monitoring of marine raft culture farms was used. A large number of representative samples were selected along the south-north axis, to ensure the applicability of models obtained through machine learning to different scenarios. In view of the unique characteristics of remotely sensed imagery of raft culture farms, multi-core convolutional layers, additional texture features and other enhancements were used to improve the deep learning neural network.

Results and analysis

In this study, Jiangsu province and Fujian province were chosen to be monitored for changes in their raft culture farms (Fig. 6-6 and Fig. 6-7). It is found that most of raft culture farms are located close to shore. From 2017 to 2020, the total area of raft culture in the two provinces was in the growth phase, with a slowdown in the rate of growth.

（a）Distribution of offshore raft culture in Jiangsu province in 2017

（b）Distribution of offshore raft culture in Jiangsu province in 2019

（c）Distribution of offshore raft culture in Jiangsu province in 2020

（d）Variation of offshore raft culture in Jiangsu province in 2017-2019

（e）Variation of offshore raft culture in Jiangsu province in 2019-2020

（f）Statistics of the area of offshore raft culture in Jiangsu province

Offshore raft culture area   New raft culture area   Reduced raft culture area

0 20 40   80   120 km

↑ Figure 6-6. Observed distribution, and change thereto, of raft culture in Jiangsu province

Furthermore, a change analysis in the context of the ecological protection red line finds little change to most of the marine aquaculture within the boundaries of the red line after the red line came into force.

（a）Distribution of offshore raft culture in Fujian province in 2017

（b）Distribution of offshore raft culture in Fujian province in 2019

（c）Distribution of offshore raft culture in Fujian province in 2020

（d）Variation of offshore raft culture in Fujian province in 2017-2019

（e）Variation of offshore raft culture in Fujian province in 2019-2020

（f）Statistics of the area of offshore raft culture in Fujian province

Offshore raft culture area   New raft culture area   Reduced raft culture area

Figure 6-7. Observed distribution, and change thereto, of raft culture in Fujian province

Outlook

Marine aquaculture is not only an important means whereby marine resources are used for human purposes, but also an important factor that has a bearing on the health of marine ecosystems. While large-scale, whole-area monitoring using traditional methodology for aquaculture survey is very challenging, the increasing availability of satellite remote sensing data and other Big Earth Data provides a new way of overcoming this problem. Going forward, we shall extend the application of Big Earth Data to the relevant domains, determine the optimal remote sensing time slots for different raft culture farms in various marine areas, and improve the accuracy and timeliness of information obtained from marine aquaculture monitoring in terms of type, scale, period and any change in the aquaculture farm environment.

SDG 14

Summary

This chapter focuses on two SDG 14 targets pertaining to marine pollution reduction and marine ecosystem protection and presents three case studies, namely, distribution of marine debris and microplastics in China's coastal waters, the health of typical marine ecosystems and changes in nearshore raft culture, where dynamic and quantitative monitoring and assessment are enabled against the said targets at two levels, i.e. national (China) and local (typical areas), to provide effective support for evaluating the sustainable development of the marine environment against the relevant targets with data products, methodological models and support to policy-making.

Going forward, we shall further strengthen the application of spaceborne and airborne remote sensing data, AI and other technologies in the monitoring and analysis of SDG 14 indicators, in the hopes of extending the study of relevant indicators from China's coastal waters to distant waters on a larger scale and in greater depth, to develop a more complete system of data, techniques and methods for monitoring and evaluating the sustainable development of marine ecosystems.

SDG 14

SDG 15

SDG 15
Life on Land

Background

SDG 15 states, "Protect, restore and promote sustainable use of terrestrial ecosystems, sustainably manage forests, combat desertification, halt and reverse land degradation, halt biodiversity loss." Healthy ecosystems protect the planet and sustain livelihoods. Forests, wetlands, mountains and drylands, in particular, provide a wide range of environmental goods and services - clean air and water, biodiversity conservation and climate change mitigation. However, nature is under increasing stress and human activities have transformed nearly 75% of the Earth's surface, while biodiversity is being lost, with about 1 million species of fauna and flora on the brink of extinction and $1\,200\times10^4\,hm^2$ of land lost to drought and desertification each year, leading to the loss of valuable economic assets and livelihood opportunities (IPBES, 2019).

The Inter-Agency and Expert Group on SDG Indicators (IAEG-SDGs) has developed an SDG indicator tier classification system based on the maturity of monitoring methodologies and the availability of monitoring data at the global level. According to the IAEG-SDGs 2020 report, 10 of the 14 indicators under SDG 15 are classified as Tier I and four as Tier II ; with respect to the 10 Tier I indicators, about half of the countries are unable to provide data on a regular basis, an issue that is particularly pronounced in underdeveloped countries.

This report focuses on three aspects, namely ecological conservation, land degradation and biodiversity to monitor progress toward SDG 15 against four indicators: forest area as a proportion of total land area (SDG 15.1.1), proportion of biodiversity conservation sites (SDG 15.1.2), degraded land as a proportion of total land area (SDG 15.3.1) and the Red List Index (SDG 15.5.1), by fully leveraging Big Earth Data. The aim is to provide data products, methodological models and support to policy-making for UN agencies and other countries in the monitoring and implementation of SDG 15 indicators, thus contributing Chinese solutions to the attainment of SDG 15 targets.

Main Contributions

The dynamic, spatially disaggregated and quantitative monitoring and evaluation of multiple SDG 15 indicators at three levels—global, national (China) and local (typical areas) provide solid support for the sustainable development of life on land in the form of data products, methodological models and support to policy-making. For SDG 15.1.1, we achieved timely updating of global forest cover mapping products at 30 m spatial resolution (2019) and developed an integrated spatial-temporal-spectral feature extraction model for identifying forest types. For SDG 15.1.2, we localized the three global conditions for biodiversity conservation in China and made recommendations for biodiversity conservation and restoration. For SDG 15.3.1, we took a science-based approach to track and assess Land Degradation Neutrality (LDN) in China and analyzed its contribution to global LDN, along with an in-depth analysis of the dynamics and drivers of desertification and soil erosion in typical areas of China. For SDG 15.5.1, we analyzed in depth the risk factors facing flora diversity in China with recommendations for conservation strategies (Table 7-1).

		Table 7-1 Cases and Their Main Contributions	
Indicator	**Tier**	**Case**	**Contributions**
15.1.1 Forest area as a proportion of total land area	Tier I	Global/regional forest cover (2019)	**Data product:** global forest cover map at 30 m spatial resolution for 2019 **Method:** machine learning-enabled forest classification on global scale **Support to policy-making:** informing forest cover status at regional and global scales
		Spatiotemporal distribution of forest types in China's Yangtze River basin	**Data product:** datasets on distribution of forest types in the Yangtze River basin for 2018 (at 10 m resolution) **Method:** a method for time series remotely sensed image synthesis based on multi-rules and an integrated spatial-temporal-spectral framework for forest type feature extraction
15.1.2 Proportion of important sites for terrestrial and freshwater biodiversity that are covered by protected areas, by ecosystem type	Tier I	Applying three global conditions framework to the conservation and sustainable use of biodiversity in China	**Data product:** datasets on 3Cs for the conservation and sustainable use of biodiversity in China **Support to policy-making:** localizing the three global conditions and recommending strategies for ecosystem conservation and restoration in the context of the National Projects for the Conservation and Restoration of Major Ecosystems
15.3.1 Proportion of land that is degraded over total land area	Tier I	China's LDN progress tracking and its contribution to global LDN	**Data product:** datasets on global land degradation/improvement **Support to policy-making:** tracking and assessing China's LDN with an objective analysis of China's contribution to global LDN based on the IAEG-SDGs indicator system and globally shared data
		Dynamics between large-scale greening and soil and water conservation on the Loess Plateau and sedimentation of the Yellow River	**Method:** a model for quantifying the effect of vegetation cover on soil erosion control **Support to policy-making:** identifying spatial variations in the effectiveness of soil conservation on the Loess Plateau and informing policy-making on soil erosion control
		Processes of aeolian desertification in the semi-arid region and its peripheries in northern China and review of control outcomes	**Data product:** long time series data on the dynamics of aeolian desertification in semi-arid and surrounding areas of northern China (1975-2015) **Support to policy-making:** assessing the processes and drivers of aeolian desertification in semi-arid and surrounding areas of northern China over last four decades, to support desertification control
15.5.1 Red List Index	Tier I	China's plant diversity: risks and conservation strategies	**Data product:** datasets on risk distribution and conservation efforts of China's plant diversity **Method:** a method for identifying the threats and stressors to biodiversity, developed and refined **Support to policy-making:** identifying gaps in China's flora diversity conservation and recommending a combination of proactive conservation strategies and restoration solutions to protect the habitats of species

Case Study

Global/regional forest cover (2019)

Target: 15.1 By 2020, ensure the conservation, restoration and sustainable use of terrestrial and inland freshwater ecosystems and their services, in particular forests, wetlands, mountains and drylands, in line with obligations under international agreements.

Highlights

- *A remotely sensed global forest cover map for 2019 is independently produced at a spatial resolution of 30 m and an overall accuracy of 86.45%, providing valuable spatial data and effective decision-making support for the assessment of 2030 Agenda implementation progress.*

- *In 2019, there were 36.92x10^8 hm^2 of forests worldwide, covering approximately 24.78% of the Earth's total land area. Of all the continents, South America had the highest ratio of forest area to total land area (47.45%) and Oceania, the lowest (12.80%).*

Background

Forests are vital to human development. "Forests and trees make vital contributions to both people and the planet, bolstering livelihoods, providing clean air and water, conserving biodiversity and responding to climate change." (FAO, 2018a). In recent years, an increasing number of countries, organizations and companies have been involved in remote sensing surveys of global forest resources, such as the Global Forest Cover Change and Global Forest Watch. Since 2010, remote sensing data have been used extensively in the *Global Forest Resources Assessments* (FRAs), released by the Food

and Agriculture Organization of the United Nations (FAO) every five to ten years, to analyze the development of forests at regional and global levels and the possible impacts of changes in demographic, economic, institutional, technological and other external factors on forests (FAO, 2006, 2010, 2016). Rapid and accurate access to global forest cover information and accurate knowledge of the status and changes in forest resources are instrumental in enhancing forest management and utilization in response to global changes and achieving sustainable forest development.

Data used

◎ Global Landsat series imagery with 30 m spatial resolution acquired from 1 January 2019 to 31 December 2019.

Method

Forest referred to in this case is as defined in the *Global Forest Resources Assessment* (2020), namely, "land spanning more than 0.5 hectares with trees higher than 5 meters and a canopy cover of more than 10 percent, or trees able to reach these thresholds *in situ*. It does not include land that is predominantly under agricultural or urban land use" (FAO, 2018b). Enhanced by machine learning, big data analysis and other state-of-the-

art technologies, rapid monitoring of global forest cover with 30 m resolution was conducted based on long-time-series, multi-source satellite remote sensing data. Compared with similar maps that are currently available both in and outside of China, this product is more up to date, has higher temporal and spatial resolution and is more complete in its spatial coverage.
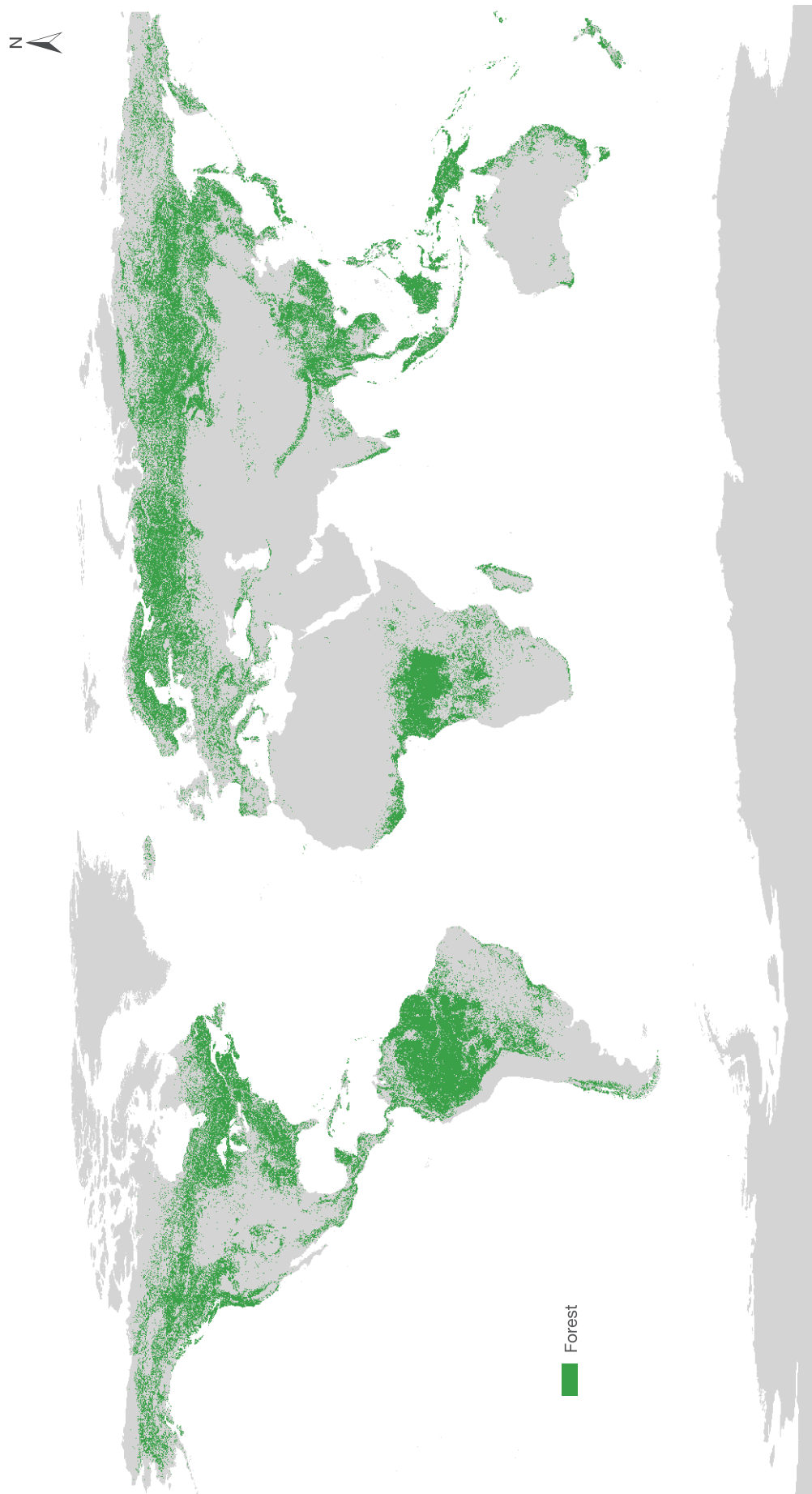
↑ Figure 7-1. Global forest distribution in 2019

Forest

Results and analysis

As at the end of 2019, the total area of global forests stood at 36.92×10^8 hm^2, covering approximately 24.78% of the world's total land area (149×10^8 hm^2). The spatial distribution of global forests is as shown in Figure 7-1. Forests are generally distributed in regions at specific latitudes, mostly in the tropical regions of South America, Central Africa and Southeast Asia, in the boreal regions of Russia and Canada, and along the Pacific coasts and Atlantic coasts.

The world is divided into four climate zones: tropical, subtropical, temperate and arctic. Forest distribution is not even across different zones (Table 7-2 and Fig. 7-2). The tropical zone has the largest forest area, accounting for nearly half of the world's total forest area, and 21.91% of the zone is covered by forests, ranking second in the world. This is mainly because the most important forest type, rainforest, is found in this zone. Although the forest area in the arctic zone accounts for approximately a quarter of the world's total only, it has the highest forest cover at 47.27%, largely because of the wide distribution of taiga along the intensely warming mid and high latitudes of the northern hemisphere and concentrated in northern Russia and Canada. Forest area and its percentage of land area in temperate and subtropical zones rank third and fourth respectively.

Table 7−2 Forest Cover by Climate Zone, 2019			
Climate zones	Forest area(10^3 hm^2)	% of global forest area	% of land area
Tropical	1 755 987.04	47.56	21.91
Subtropical	421 115.39	11.40	16.43
Temperate	602 494.36	16.32	20.49
Arctic	912 837.24	24.72	47.27
Total	3 692 434.03	100.00	24.78
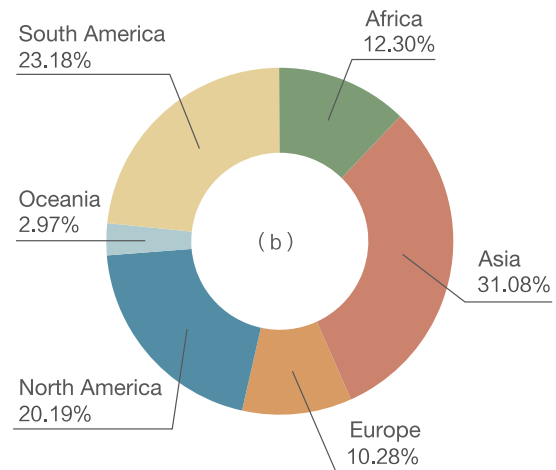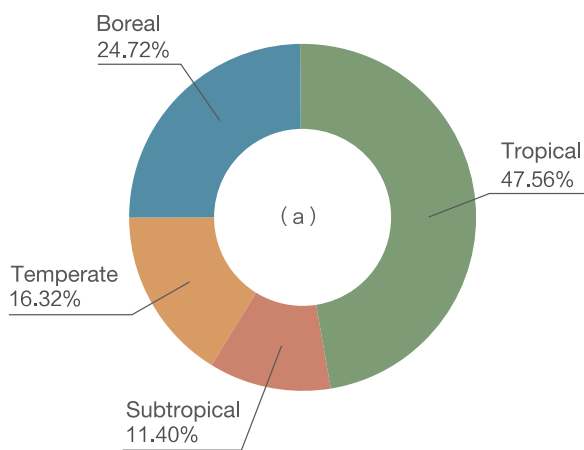
↑ Figure 7-2. Distribution of forests by climate zone and continent, 2019
  (a) By climate zone; (b) By continent

In terms of distribution by continent, forest cover varies significantly among the six continents (Antarctica excluded) (Table 7-3 and Fig. 7-2). Asia has the largest land area and the largest forest area, ranking fourth globally in forest cover. South America, although second in the world in terms of forest area, has the highest forest cover at 47.45% and its Amazon basin boasts the world's most extensive and contiguous tropical rainforests. Europe and North America have the second and third highest forest cover respectively. Oceania has the smallest land area, as well as the smallest forest area and forest cover among the six continents.

Table 7-3 Forest Cover by Continent, 2019			
Continent	Forest area (10^3 hm^2)	% of global forest area	% of land area
Africa	454 041.04	12.30	15.02
Asia	1 147 751.04	31.08	25.92
Europe	379 596.54	10.28	38.42
North America	745 487.64	20.19	31.78
Oceania	109 547.50	2.97	12.80
South America	856 010.27	23.18	47.45
Total	3 692 434.03	100.00	24.78

Outlook

Rapid development of global forest cover products is enabled on the basis of long-time-series, multi-source satellite remote sensing data by leveraging machine learning and big data analysis, to monitor implementation against SDG 15.1.1, "forest area as a proportion of total land area", and to compare and analyze the patterns of spatial distribution of forest cover by climate zone and by continent.

Using Big Earth Data, we will be able to release and update remotely sensed global forest cover products in real time. These products can help underresourced and underdeveloped countries and regions monitor changes in their forests, enhance conservation awareness and build greater forest management capacity, to make sustainable development of global forest resources a reality.

Spatiotemporal distribution of forest types in China's Yangtze River basin

Target: 15.1 By 2020, ensure the conservation, restoration and sustainable use of terrestrial and inland freshwater ecosystems and their services, in particular forests, wetlands, mountains and drylands, in line with obligations under international agreements.

Highlights

- *A remote sensing classification framework for identifying forest types is proposed, using multi-rule time-series imagery composition and combining spatial-temporal-spectral features with machine learning algorithm.*

- *A forest type distribution map in 2018 was produced covering Yangtze River basin in China with 10 m spatial resolution and an overall accuracy of 83.25%.*

Background

Accurate acquisition of data on forest area is a prerequisite for Indicator 15.1.1-related assessment. Globally, data used to measure forest cover mainly comes from specialized agencies such as the Food and Agriculture Organization of the United Nations. According to the *Global Forest Resources Assessment 2015*, forest loss is continuing worldwide (FAO, 2018a). Existing remote sensing data products for forest classification have some disadvantages, such as low spatiotemporal resolution and poor regional applicability. The Yangtze River basin spans three major economic zones in eastern, central and western China, and is the third largest river basin in the world, with a total area of 1.80×10^6 km^2 or 18.80% of China's total land area. The basin is primarily located in the subtropical evergreen broadleaved forest region, covering parts of the Qinghai–Tibet Plateau vegetation region. The Yangtze River basin has rich forest resources owing to its complex geological activities, climate change history and diverse topographic and environmental conditions. It is an important treasure-trove of forest resources for China. Socioeconomic development has brought into sharp relief the paradoxes between ecological needs and economic imperatives and between conservation and development along the Yangtze River economic belt. In this context, forest and other ecological resources in the Yangtze River basin are under threat. There is an urgent need to monitor forest type distribution in the Yangtze River basin and identify their spatiotemporal distribution patterns in the service of granular, sustainable management.

Data used

◎ Landsat time-series images at 30 m spatial resolution from 1985 to 2018.

◎ Sentinel-2 time-series images at 10 m spatial resolution from 2015 to 2019.

◎ A 30 m spatial resolution Digital Elevation Model of the Yangtze River basin.

◎ Yangtze River basin boundary data.

◎ Data from field surveys conducted in 2014, 2015 and 2018.

Method

In view of the demand that mapping of cloud cover and large-scale land cover has on high-quality remotely sensed images, a multi-rule multi-spectral time-series remote sensing image composition method was proposed in this case. Using the pixels of remotely sensed images covering the same area over the same time periods, high-quality cloudless remotely sensed images were composited for the area under study. Taking advantage of the high spatial resolution and higher spectral

resolution of Sentinel-2 images and the long-time series Landsat data, spectral-spatial-temporal feature datasets for forest type classification were established (Cheng *et al.,* 2019). Then, a forest type map at 10 m spatial resolution covering China's Yangtze River basin 2018 was acquired using machine learning algorithm based on cloud computing platform.

Results and analysis

The spatial distribution of forest types in the Yangtze River basin is shown in Figure 7-3. The survey by type indicates that forests in the Yangtze River basin are dominated by evergreen coniferous, mixed and evergreen broadleaved species. Evergreen conifers are concentrated around the upper reaches of the Yangtze and are common in such areas as Tongtian River, Yalong River and Jinsha River, accounting for approximately 15.76% of the total area; mixed forests are concentrated in the north–central part of the Yangtze River basin, found mainly in the eastern Hengduan Mountains and north of Qinling Mountains, accounting for 14.15% of the total area; evergreen broadleaved forests are concentrated around the Wu River, Liu River and Gan River along the middle to lower reaches of the Yangtze, accounting for approximately 7.29% of the total area. Deciduous broadleaved and deciduous conifers are a minority.

The results were validated against field survey data, and the validation indicated that the overall classification accuracy was 83.25%. The Producer's Accuracy (PA) ranged from 73.08% to 100%. The PA for deciduous needle-leaved forests was the highest, at 100%, with an omission error of 0. The User's Accuracy (UA) ranged from 56.59% to 94.50%. The UA for evergreen broadleaved forests was the highest, at 94.50%, indicating a minimal commission error.
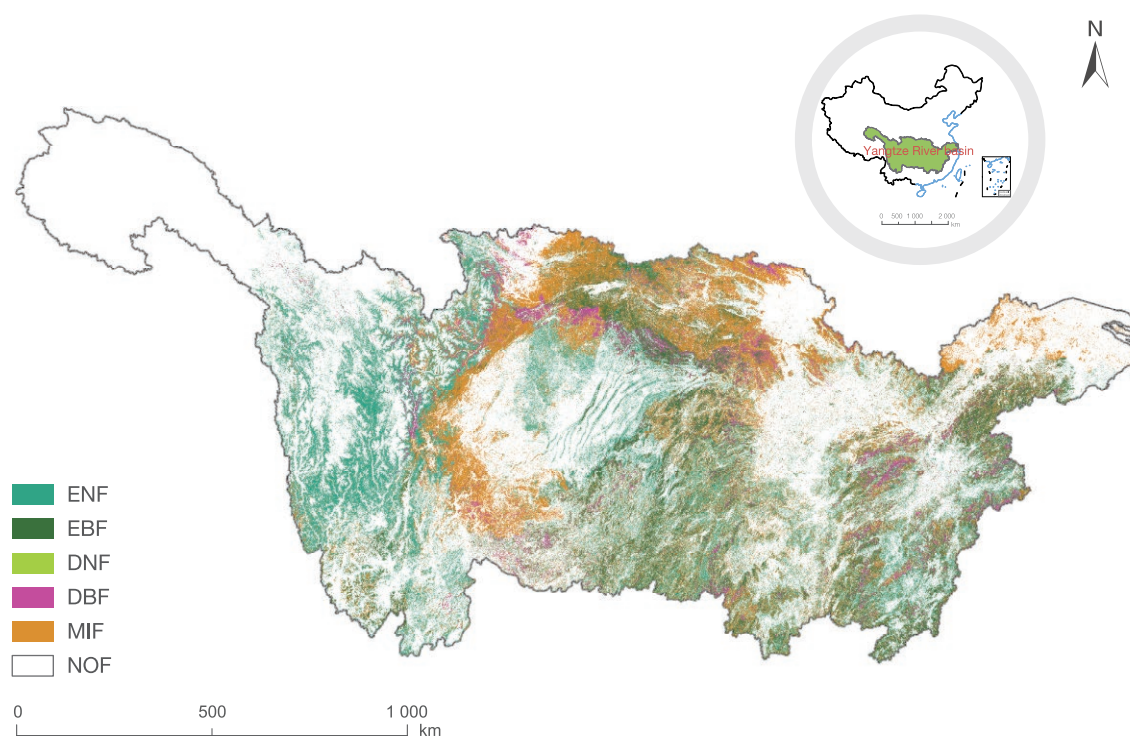
↑ Figure 7-3. Remotely sensed spatial distribution of forests by type in the Yangtze River basin
(NOF=Non-Forest area; EBF=Evergreen Broadleaved Forest; DBF=Deciduous Broadleaved Forest; ENF=Evergreen Needle-leaved Forest; DNF=Deciduous Needle-leaved Forest; MIF=Mixed Forest)

Outlook

To the best of our knowledge, this was the first study to create a remotely sensed forest type classification product at 10 m spatial resolution for the Yangtze River basin in 2018. Compared with previous data products, this product has a higher spatial resolution and more diverse and in-depth information on forest types, which can provide data support for the sustainable management of forest resources in the Yangtze River basin.

Going forward, it is our intention to extend the proposed method for mapping forest types with remote sensing data to the rest of China and generate a nationwide by-type forest map for 2018 at 10 m spatial resolution. Furthermore, we shall map forest subtypes within China against SDG 15.1.1, to inform the sustainable management of forest resources in China.

Applying three global conditions framework to the conservation and sustainable use of biodiversity in China

Target: 15.1 By 2020, ensure the conservation, restoration and sustainable use of terrestrial and inland freshwater ecosystems and their services, in particular forests, wetlands, mountains and drylands, in line with obligations under international agreements.

Highlights

- *Criteria and processes for the classification of the three conditions for the conservation and sustainable use of biodiversity in China are proposed.*

- *The pressure-state-response indicators of biodiversity vary across the three conditions. Condition 1 (Cities and Farms) is under great pressure; Condition 2 (Shared Landscapes) is highly biodiverse; and Condition 3 (Large Wild Areas) is under intensified conservation. Based on the results of this study, a proposal is made to optimize the spatial allocation of biodiversity conservation efforts in China.*

Background

SDG 15 emphasizes the importance of protecting, restoring and promoting the sustainable use of terrestrial ecosystems to the conservation of natural habitats and biodiversity (United Nations, 2015). Conservation actions are constrained by the socioeconomic status of different areas. Therefore, the development of tailored conservation policies is vital to more efficient biodiversity conservation efforts.

In the interest of conserving and sustainably using biodiversity, Locke *et al.* (2019) proposed that land be divided into three conditions for biodiversity conservation and management. In their proposal, Three Global Conditions (3Cs) are identified for

the world's land - Cities and Farms, Shared Landscapes, and Large Wild Areas - and different conservation and management strategies for each condition are proposed, thus creating a new framework for the differentiated conservation policies tailored to the realities of different regions. Based on the 3Cs framework, this study is to elaborate the criteria and processes of 3Cs classification in China and analyze the characteristics of 3Cs by using the "pressure-state-response" biodiversity model. Policy recommendations for the spatial optimization of China's biodiversity conservation and management are to emanate from the findings of the study.

Data used

◎ This study uses a range of data on demographics, land cover, net primary productivity, soil organic carbon, distribution of higher plants and terrestrial vertebrates, boundaries of protected areas and key biodiversity areas (Table 7-4).

Table 7-4 Data used in the case		
Item	**Data source**	**Spatial resolution**
Global population distribution (2015); Rates of global demographic change (1990-2015)	Socioeconomic Data and Applications Center	1 km
Global land use types (2015); Changes in global land cover (1993-2015)	European Space Agency	300 m

SDG 15

Table 7-4 Data used in the case		
Item	**Data source**	**Spatial resolution**
Net Primary Productivity (NPP) in China (2010)	Resource and Environment Science and Data Center, CAS	1 km
Global forest cover (2010)	Global Forest Watch	1 km
Global soil organic carbon stock	ISRIC	1 km
Global biomass carbon stock	CASEarth	3 km
Distribution of over 1 600 threatened endemic higher plant species in China	CASEarth	300 m
Distribution of over 600 terrestrial mammal species in China	CASEarth	10 km
Distribution of more than 1 200 bird species in China	CASEarth	10 km
Protected areas in China	CASEarth	Shapefile
Key Biodiversity Areas (KBAs)	World Database on KBAs	Shapefile

Method

China's land area is divided into 1 km × 1 km grid cells (excluding such water bodies as major inland lakes), each of which is assigned to one of the 3Cs against the following criteria. The distribution of indicators that reflect "pressure-state-response" of biodiversity in each condition is calculated separately. Population numbers are summed and other indicators averaged.

Condition 1 (C1): Cities and Farms

Population density≥1 000/km^2 OR percentage of agricultural and urban land > 50%

Condition 2 (C2): Shared Landscapes

Not C1 AND {percentage of agricultural and urban land > 0.5% OR Human Modification Index (Kennedy *et al.,* 2019) > 0.1}

Condition 3 (C3): Large Wild Areas

Identified as a wilderness patch larger than 10 km^2 according to Cao *et al.* (2019) AND percentage of agricultural and urban land ≤0.5% AND Human Modification Index≤0.1

Results and analysis

C1, C2 and C3 account for 25.0%, 48.1% and 26.9% of China's land area respectively. C1 and C3 are clearly separated by the Hu Line (Fig. 7-4).

The distribution of pressure-state-response indicators varies across the three conditions. Among the 3Cs, C1 is under the highest pressure, home to 73.5% of China's population, which saw the highest growth rate between 1990 and 2015. During the 1993-2015 period, 4.5% of natural habitats in C1 showed degradation, while some degree of restoration was observed in C2 and C3. Indicators of the state of biodiversity point to C2 as having the highest concentration of biodiversity, whereas more conservation efforts have been channeled into C3 than C1 and C2.
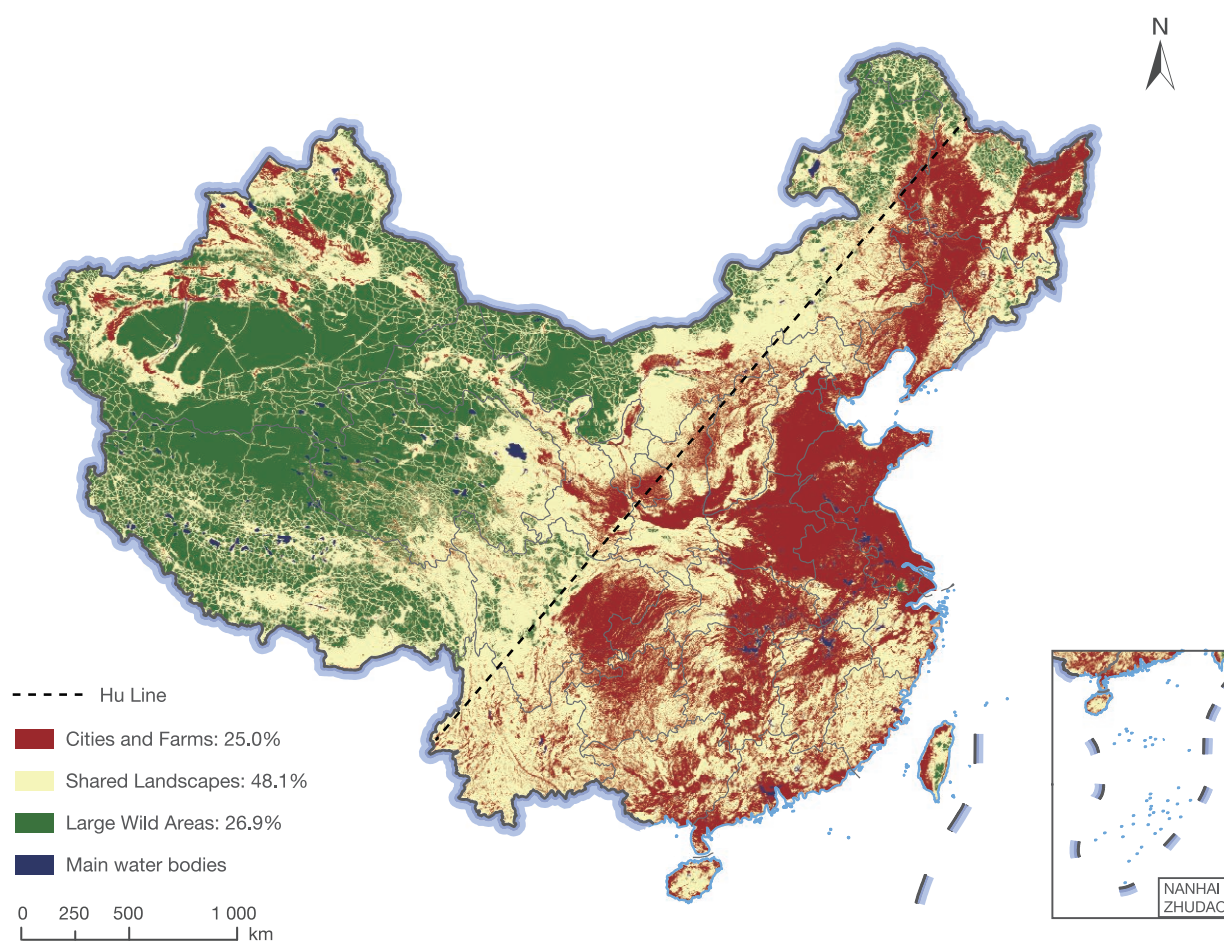
Figure 7-4. Distribution and proportions of 3Cs in China

Outlook

The findings of this study indicate that, of the three conditions, C2 (Shared Landscapes) has the highest concentration of biodiversity in China; the pressure on biodiversity is concentrated in C1 (Cities and Farms); and conservation efforts are concentrated in C3 (Large Wild Areas). The following considerations are recommended for China's future strategies to conserve and manage terrestrial biodiversity:

(1) Mitigating threats to biodiversity in C1, with a focus on reducing the emissions of pollutants, encouraging recycling and sustainable use of resources, promoting environmentally friendly agriculture, building green cities, and combating such illegal activities as overfishing and overhunting.

(2) Ramping up protection efforts in C2 to achieve conservation and sustainable use of natural resources and biodiversity through the establishment of new protected areas and other area-based conservation measures (such as community-based conservation actions), establishing corridors for connectivity between protected areas and reducing anthropogenic damage to natural habitats.

(3) Ensuring long-term conservation of biodiversity in C3 by tightening control on the exploitation and utilization of natural resources in C3, establishing large protected areas, and strengthening monitoring, scientific research and other conservation actions.

China's LDN progress tracking and its contribution to global LDN

Target: 15.3 By 2030, combat desertification, restore degraded land and soil, including land affected by desertification, drought and floods, and strive to achieve a land degradation-neutral world.

Highlights

- *This is one of the first studies to monitor and assess LDN baselines and progress at the globally consistent and spatially comparable national scale, on the basis of the UNCCD framework system and Big Earth Data.*

- *A trend of continuous improvement in China's LDN has been observed. Compared to the 2015 baseline, the net restored land area increased by 60.30% by 2018 and accounted for approximately 1/5 of the world's total, making it the number one contributor to global LDN.*

Background

The vision of SDG Target 15.3, "to achieve a land degradation-neutral world", is one of the key targets of the SDGs (United Nations, 2015). However, the definition of land degradation was a matter of considerable debate at one point, primarily as a result of divergence of opinion over the processes, causes, characteristics and effects of degradation. The lack of consensus is responsible for the huge discrepancies in the results of different land degradation assessments (4%-74% globally) and has seriously undermined the international community's ability to understand, at the scientific level, and accurately assess the real state of global/regional land degradation, thus hampering practical actions against, and effective management of, such degradation.

To tackle those challenges, the UN Inter-agency and Expert Group on SDGs (IAEG-SDGs) has defined a framework of indicators for Indicator 15.3.1 monitoring, including changes in land cover, land productivity and soil organic carbon, on the basis of which the United Nations Convention to Combat Desertification (UNCCD) and Group on Earth Observations Land Degradation Neutrality (GEO-LDN) Program have reviewed the methodologies for data selection and analysis and

developed a *Good Practice Guidance SDG Indicator 15.3.1* (Neil *et al.,* 2019). However, global-scale, spatially disaggregated baselines and progress data for SDG 15.3.1 remain absent as a direct consequence of the unavailability of relevant data, methodological uncertainties and political sensitivities. Nonetheless, globally comparable and spatially disaggregated SDG 15.3.1 baselines and assessment findings, consistent with the UN 15.3.1 monitoring indicator framework, remain important from the perspective of Science, Technology and Innovation (STI) for SDGs.

In 2019, the CASEarth Project conducted a global land degradation baseline assessment for the 2000-2015 timeframe and developed a national-scale LDN report. This assessment provides a reliable baseline for tracking the progress of SDG 15.3.1 and is an indispensable frame of reference for the assessment of the overall progress towards the realization of SDG 15.3. Taking advantage of these resources and guided by the UNCCD LDN monitoring framework, in 2020, CASEarth Project proceeded to monitor and assess global SDG 15.3.1 progress (against the 2015 baseline), focusing on China's LDN dynamics and its contribution to global LDN.

Data used

◎ Data from SDG 15.3.1 assessment for 2000-2015 (Guo *et al.,* 2019).

◎ Global land cover in 2015 and 2018 at 300 m spatial resolution from European Space Agency.

◎ 2000-2018 Enhanced Vegetation Index (EVI) data at 500 m spatial resolution.

◎ Global soil organic carbon, International Soil Reference and Information Centre (ISRIC) SoilGrid 250, at 250 m spatial resolution.

◎ RESOLVE Ecoregions 2017.

◎ Bulletins of Status Quo of Desertification and Sandification in China (2005, 2011 & 2015).
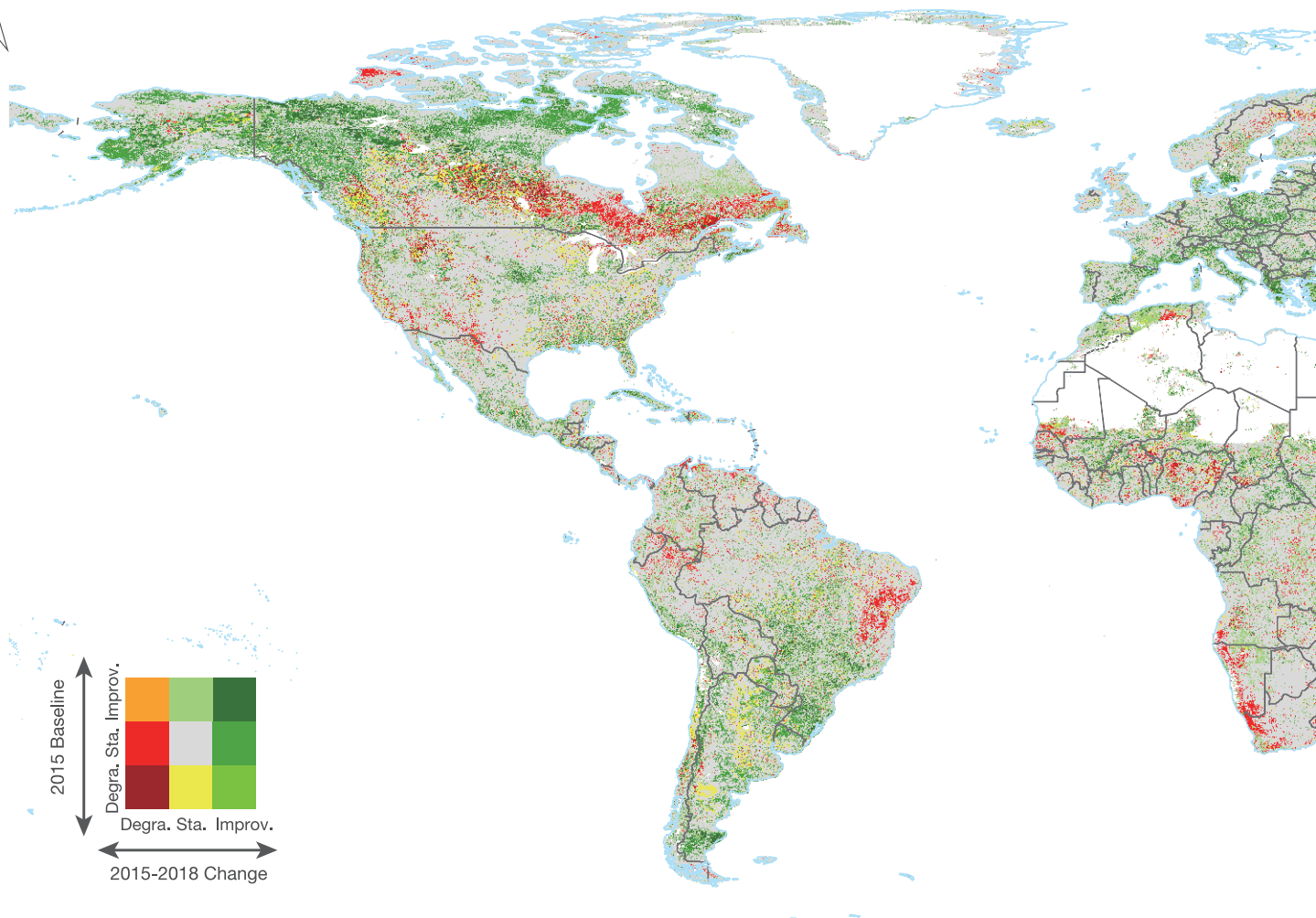
Figure 7-6.

◎ Statistical analysis of land degradation dynamics and status quo in China (2015-2018)

（a）

4.73%
1.21%
2.32%
0.33%
2.08%
28.05%
41.96%
19.32%

Legend:
- Degra.+Sta.
- Sta.+Degra.
- Degra.+Degra.
- Improv.+Degra.
- Degra.+Improv.
- Improv.+Sta.
- Sta.+Improv.
- Improv.+Improv.

（b）

Improvement   Degradation
Degradation/Improvement ratio

Woodland   Grassland   Cropland   Barren Land

2015 Baseline
Degra. Sta. Improv.
Degra. Sta. Improv.
2015-2018 Change

Figure 7-5.

Spatial distribution of global land degradation baselines and dynamics (2015-2018)

NANHAI
ZHUDAO

Method

Based on the assessed baselines for 2000-2015, a dynamic assessment for 2015-2018 was conducted against the three sub-indicators of the UN's IAEG-SDGs indicator system, i.e. land cover, land productivity and soil organic carbon. The land cover conversion matrix for 2015 and 2018 was used for land degradation and improvement assessment. Dynamic assessment of land productivity was made by analyzing the 2004-2018 trends, with significant increase, significant decrease and other changes defined as restored, degraded and stable respectively. Regarding soil organic carbon, assessment was don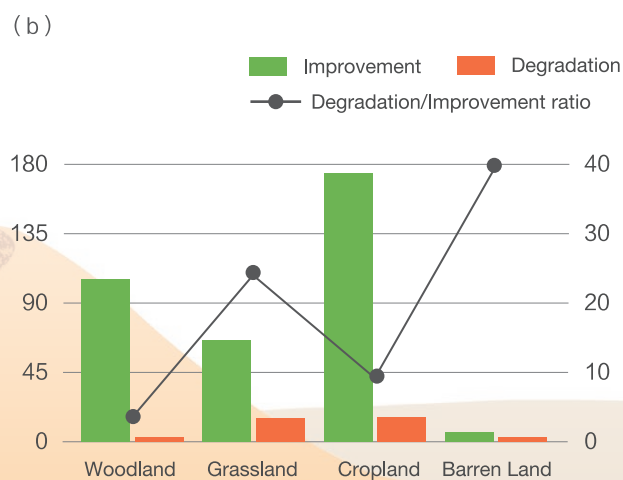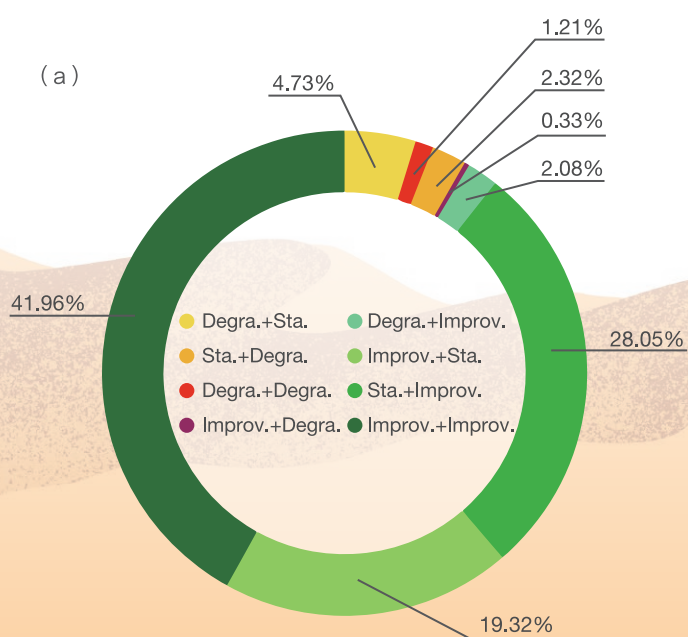e by correlating land cover changes with soil carbon changes as proposed by the Intergovernmental Panel on Climate Change (IPCC), thus identifying three levels of soil carbon: degraded, restored and stable. The 2015-2018 dynamics were assessed by combining the three sub-indicators of land cover, land productivity and soil carbon, on the principle that degradation under any of the sub-indicators constitutes degradation. The findings so arrived are then combined with 2015 baseline to get the progress of global land degradation.

Results and analysis

The dynamics of global land degradation from 2015 to 2018 are shown in Figure 7-5. Statistical analysis indicates that the overall trend of SDG 15.3.1 between 2015 and 2018 was positive, but there were certain spatial variations. China saw a steady improvement in LDN from 2015 to 2018 and its net restored area of degraded land increased by 60.30%, accounting for 17.76% of the global total in 2018 (the highest in the world), which is very similar to 18.24% in the base year of 2015, making China the largest contributor to global LDN.

According to the data on land degradation dynamics in China from 2015 to 2018 (Fig. 7-6), 29.16% of the land was restored, 1.56% degraded and 69.28% stable. Of the land whose status of degradation changed, compared to the 2015 baseline, 41.96% enjoyed continuous improvement, 28.05% went from stable to restored, 1.21% suffered continuous degradation and 2.32% went from stable to degraded. It is worth noting for the degraded land in 2015, 4.62×10^4 km^2 became more degraded, but 8.02×10^4 km^2 of land was reversed in 2018, pointing to China's success in land degradation recovery. The status of degradation also varied among different types of land cover. Current degradation was mainly observed in cropland and grassland. Judging by the ratios of degradation versus improvement, China's woodland was the best performer in ensuring the LDN target, followed by cropland, which had a lower degradation-to-improvement ratio despite some degradation and was therefore under no great pressure in ensuring the LDN target. However, grassland and barren land were at risk, with their current degradation-to-improvement ratios at 24.04% and 39.73% respectively. In view of the adverse effects of climate change, grassland and barren land warrant focused attention in the future.

Outlook

Guided by the UNCCD *Good Practice Guidance SDG Indicator 15.3.1* and using internationally shared datasets, this study established tracking and monitoring of Indicator 15.3.1, assessed China's LDN trend and identified the contribution of China's LDN to global LDN based on globally consistent and comparable data, thus providing important informational support for the attainment of Indicator 15.3.1.

The methodology used in the study is applicable on a global scale, emphasizing compliance with the IAEG-SDGs indicator system, and the findings are globally consistent and comparable. These findings, therefore, do not reflect country or region-specific SDG Target 15.3-related figures, as the degradation processes and indicator system considered at this scale are more complex. This does not mean, however, that the findings of this study have no significant referential value for understanding the progress toward Target 15.3 at national and regional levels. The state and trend of LDN in China examined through the lens of Big Earth Data are consistent with the conclusion of the National Forestry and Grassland Administration that "since 2004, the area of both desertification and sandification in China has declined for three consecutive monitoring periods and China has achieved zero growth in desertified land".

It is worth noting that the assessment of improvement and degradation strictly corresponds to the time periods under assessment (UNCCD-LDN scientific framework), so there are cases where the assessment findings indicate that improvement is under way but the land is actually in the status of degradation. Therefore, while we take note of the positive progress in LDN, we must be cognizant of the considerable challenges facing China in land degradation. In the future, science-informed conservation and management should be strengthened and the LDN monitoring methodology and capacity enhanced, with a view to achieving a higher level of LDN by 2030.

SDG 15

Dynamics between large-scale greening and soil and water conservation on the Loess Plateau and sedimentation of the Yellow River

Target: 15.3 By 2030, combat desertification, restore degraded land and soil, including land affected by desertification, drought and floods, and strive to achieve a land degradation-neutral world.

Highlights

- *Big Earth Data feeds into the calculation of the Soil Erosion Control Index (SECI) of different periods to quantify the effect of vegetation change on soil and water conservation .*

- *Since 2000, vegetation coverage on the Loess Plateau has been greatly improved, with an average increase of 17.06%, improving its effect on soil and water conservation by 22.00%.*

Background

Since 2000, thanks to the reversion of farmland to forest and grass as well as other soil erosion control measures, the ecological environment of China's Loess Plateau has undergone a profound transformation, with large-scale, significant improvements in its vegetation. As one of the few regions in the world where vegetation has markedly improved in recent years, it has attracted much international attention. With significant increases in vegetation comes a significant improvement in soil erosion on the Loess Plateau, as well as considerably reduced sedimentation in the Yellow River. Centering on SDG Target

15.3 of the UN 2030 Agenda, this study is designed to gauge the contribution of large-scale greening of the Loess Plateau over the past two decades to soil and water conservation by calculating the Soil Erosion Control Index (SECI) of chosen periods to track the effects of changed vegetation on erosion control, on the basis of remotely sensed data and Fraction of Vegetation Cover (FVC). The purpose is to explore and develop a new approach to investigate regional land degradation and monitor soil erosion control in the future.

Data used

◎ Fraction of Vegetation Cover (FVC) product from 2000 to 2019 at 1 000 m resolution, Global Land Service.

◎ Water Resources Bulletin, Yellow River Conservancy

Commission.

◎ Yellow River Sediment Bulletin, Yellow River Conservancy Commission.

Method

Using the FVC dynamic data of the Loess Plateau between 2000 and 2019, SECI is calculated as a measure of the ability of soil and water conservation strategies to control soil erosion (which may be construed as the effect of vegetation on erosion control if the measures taken are specific to vegetation only),

to work out the erosion control effect of large-scale vegetation restoration projects (including reforestation of farmland, grazing ban and afforestation) on the Loess Plateau in recent years, by investigating the effect of changed vegetation on erosion control using the Universal Soil Loss Equation (USLE).

Results and analysis

Over the past 20 years, the vegetation cover of the Loess Plateau has increased substantially (Fig. 7-7a), with an average increase of 17.06% across the region. Further studies indicate that the rate of vegetation increase varies among different areas and typical river basins: 16.06% in the Shaanxi part of the Loess Plateau, 21.58% in Yan'an City, 23.89% in north of Ganguyi along the Yanhe River, and 27.10% along the Dali River in northern Shaanxi.

The two-decade SECI increments for the Loess Plateau are shown in Figure 7-7b, indicating a correlation between the SECI and vegetation cover. The SECI registered an average increase of 22.00% for the entire Loess Plateau: 17.10% in the Shaanxi part of the Yellow River basin, 29.90% along the Dali River in northern Shaanxi, 12.30% in Yan'an City, and 18.10% in the upper reaches of the Yanhe River (north of Ganguyi).

→ Figure 7-7. Two-decade region-wide trends of vegetation (a) and increments in soil erosion control index (b) on Loess Plateau
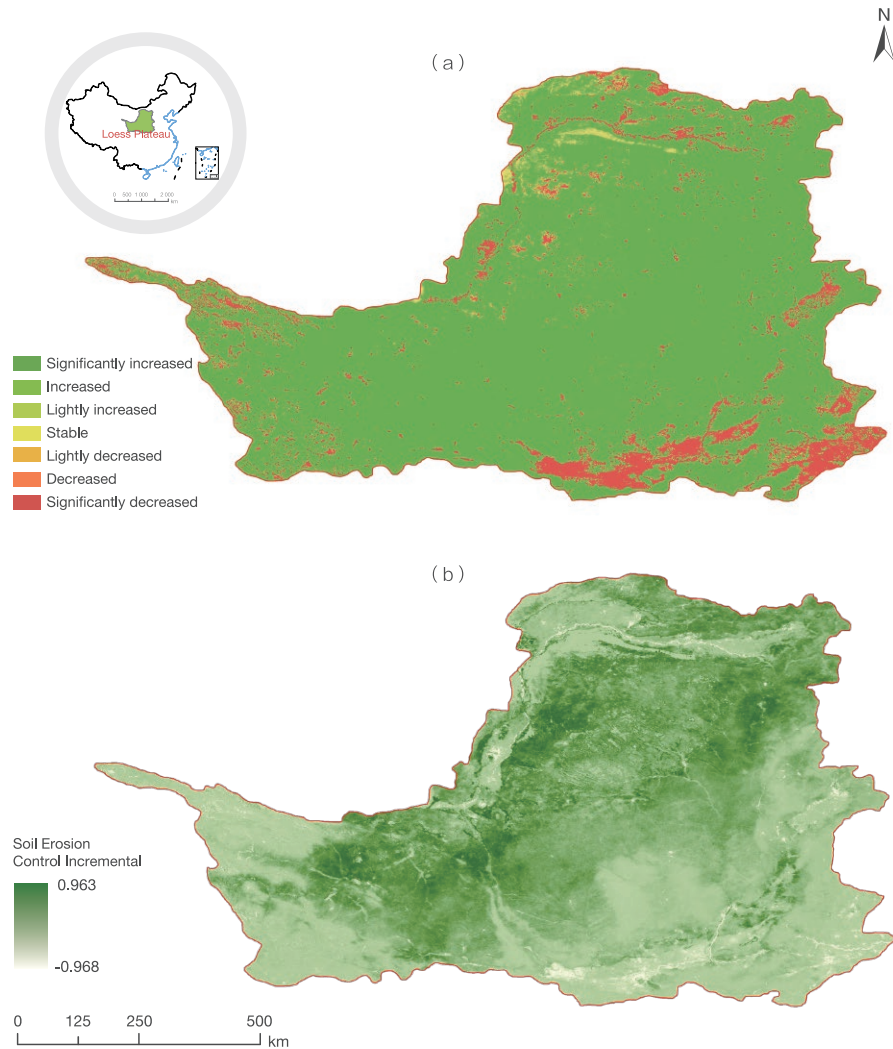
Outlook

For the purposes of this study, a Big Earth Data-based SECI was created to quantify the contribution of changed vegetation to soil erosion control. The findings indicate that the much improved vegetation cover of the Loess Plateau over the past 20 years has had a significant effect on soil and water conservation in the region, albeit to varying degrees from area to area.

Since the end of the 20th century, large-scale, intensive soil and water conservation projects for the Loess Plateau have been under way. During this period, the annual sediment discharge between Hekou and Longmen has been clearly responding to the human effort to reduce sedimentation, maintaining a low level of sediment discharge year after year. Since 2000, the annual sediment discharge at the Tongguan Hydrological Station of the Yellow River has been kept under 3.00×10^8 t, which is proof, at the receiving end, of the effectiveness of soil and water conservation on the Loess Plateau in recent years and that of the large-scale restoration of vegetation on the Plateau in stemming soil erosion.

SDG 15

Processes of aeolian desertification in the semi-arid region and its peripheries in northern China and review of control outcomes

Target: 15.3 By 2030, combat desertification, restore degraded land and soil, including land affected by desertification, drought and floods, and strive to achieve a land degradation-neutral world.

Highlights

- ◉ *Long-time-series datasets on the aeolian desertification in northern China from 1975 to 2015 are developed, providing important data support for accurately understanding the spatiotemporal processes of aeolian desertification in China.*

- ◉ *The year 2000 was a watershed in the aeolian desertification of China's semi-arid regions. Until 2000, there had been a degradation trend primarily because of irresponsible human activities such as overlogging, overcultivation and overgrazing. The aeolian desertification process began to reverse in 2000, largely thanks to the implementation of ecological protection policies.*

Background

Aeolian desertification is a type of desertification induced by the actions of wind-blown sand (Wang *et al.,* 2015). It occurs and develops mainly in the semi-arid agro-pastoral ecotones and pastoral zones of northern China, which are also the main areas where the reversal of aeolian desertification has taken place in recent years. To monitor the trends of aeolian desertification in those areas and analyze how spatiotemporal changes in the aeolian desertified land respond to climate variation and anthropogenic factors is of vital importance, because the findings can help identify how aeolian desertification occurs and evolves and predict its future trajectory, so that policy-makers can develop appropriate control measures informed by science.

Data used

◎ US Landsat time series data from 1975 to 2015.

◎ 1:100 000 scale topographic maps.

◎ 1:1 000 000 topographic maps, Ministry of Natural Resources.

Method

Aeolian desertification information was extracted in compliance with the aeolian desertification classification system and interpretation keys. The classification system used in this study comes from *the Classification System for Remote Sensing Monitoring of Aeolian Desertification in Northern China*. The latter classifies aeolian desertification into four types: shifting, semi-shifting, semi-fixed and fixed sands. They correspond to four levels of severity of aeolian desertification: extremely severe, severe, moderate and light (Wang *et al.,* 2004).

Results and analysis

Figure 7-8 shows the distribution of aeolian desertified areas in the semi-arid areas and their peripheries in northern China. Aeolian desertification within the monitored region is most prominent in five sandy lands, where aeolian desertification accelerated between 1975 and 2000 with an average growth rate of approximately 2 486.57 km^2 per annum. From 2000 onward,

Slight　Moderate　Severe　Extremely severe

0　200　400 km
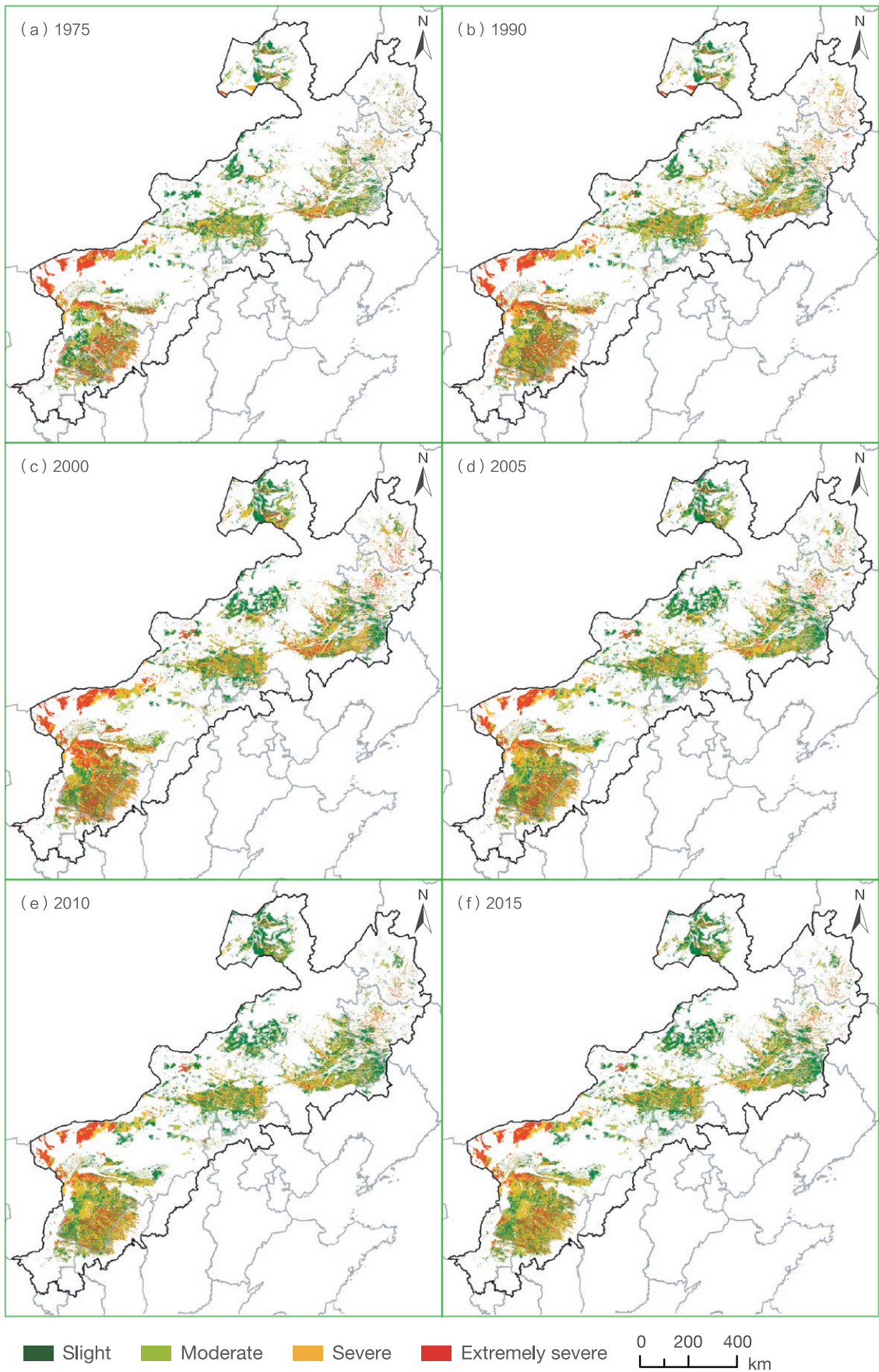
↑ Figure 7-8. Spatiotemporal distribution of aeolian desertification in semi-arid region and its peripheries in northern China

the aeolian desertification process began to slow down and the area of aeolian desertified land began to shrink gradually, with an average reduction of 578.35 km^2 per annum, much slower than the expansion prior to 2000. The rate of reversal since 2000 has varied between different periods: The reversal was quite fast between 2000 and 2005, at an average reduction rate of 1 129.05 km^2 per annum. It went down to 604.81 km^2 per annum between 2005 and 2010. Then, from 2010 to 2015, the area of aeolian desertified land remained practically unchanged, down by a mere 5.96 km^2 in a space of five years.

Spatiotemporal changes varied among different types of aeolian desertified land (Fig. 7-9). Slightly and moderately aeolian desertified areas accounted for approximately 62% of the total area, while severely and extremely severely aeolian desertified areas accounted for approximately 38% of the total. The area of slightly aeolian desertified land increased in all periods except 1975-1990 when it decreased, and the increase was particularly significant in the post-2000 period, indicating that the intensity of aeolian desertification in the monitored region was easing. The trends of moderately and severely aeolian desertified areas were rather similar: They increased significantly between 1975 and 1990, before easing off and then stabilizing gradually after 2000. The area of extremely severe desertification changed drastically over time: a sharp increase prior to 2000, followed by a swift drop. This pattern is further proof of a general trend of reversal, i.e. a lessening in the intensity of aeolian desertification in tandem with the decreasing area of aeolian desertification in the semi-arid areas of northern China after 2000.
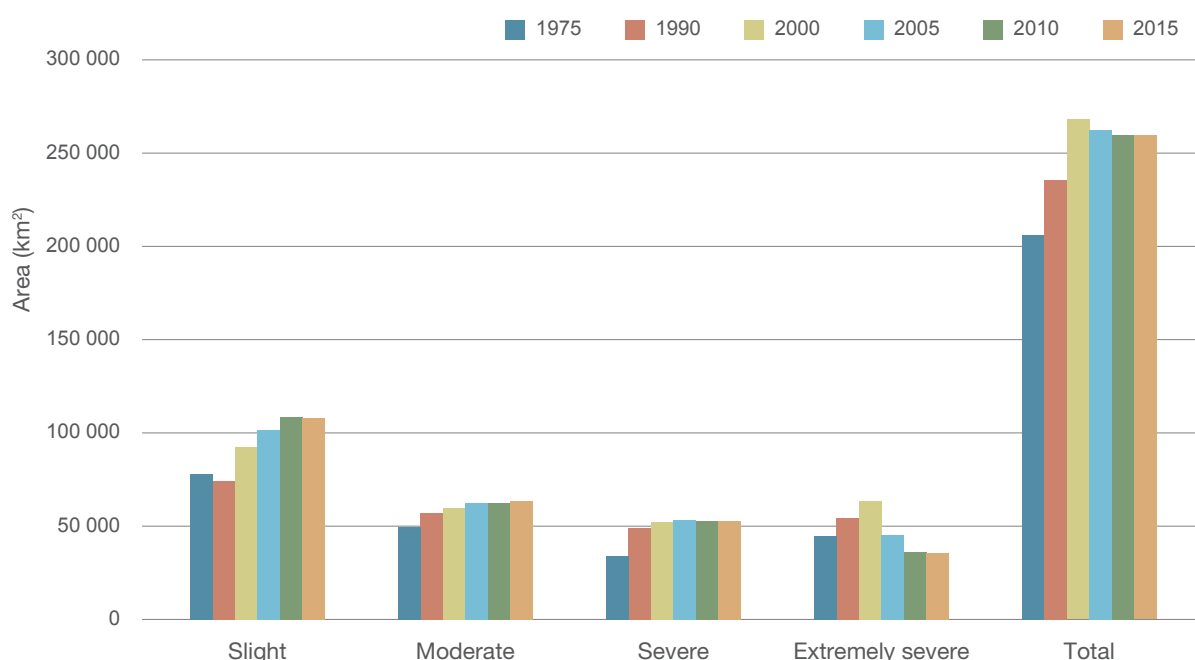
↑ Figure 7-9. Changes in the area of aeolian desertified land in northern China over time

Outlook

Aeolian desertification in the semi-arid areas and their peripheries in northern China is a result of the fragilities and volatilities of the local ecosystems and, to a larger extent, of anthropogenic causes. In the past 40 years, the natural environment context has not changed significantly. During the same period, however, there have been significant changes in climate and human activities. For a start, in the context of precipitation unchanged in the region as a whole and reduced precipitation in isolated areas, the main sign of climate change is a higher incidence of heavy rainfall coupled with a lower frequency of precipitation in general. This pattern has been particularly pronounced since 2010. Secondly, human activities have gradually transitioned from overcultivation, overgrazing

and overlogging prior to 2000 to reforestation and regrassing of farmland, grazing ban by fencing off pastures and rotation grazing with rest periods, which are more sustainable ways of using land with environmental protection in mind. The variations of climatic and human behavior in different periods subjected aeolian desertification to the action of different drivers in those periods. Studies indicate that the occurrence and expansion of aeolian desertification from 1975 to 2000 was largely a result of irrational human activities. The reversal of desertification from 2000 to 2010 is primarily attributable to the implementation of environmental protection policies. This reversal process slowed down from 2010 to 2015, largely because of droughts.

China's plant diversity: risks and conservation strategies

Target: 15.5 Take urgent and significant action to reduce the degradation of natural habitats, halt the loss of biodiversity and, by 2020, protect and prevent the extinction of threatened species.

Highlights

- *The Biodiversity Risk Index (BRI) that describes the risk of extinction is more widely applicable than the Red List Index, which is based on multiple dynamic assessments.*

- *In areas facing high risks and high pressures from the compounding effect of biodiversity risks and anthropogenic pressures, protected areas only cover 4%. Developing conservation and restoration strategies tailored to the local realities to address conservation gaps will help improve the efficiency of conservation and halt species loss.*

Background

Human activities and land use have brought about unprecedented pressures and stresses on the natural environment, leading to the extinction of species in their thousands. In order to achieve the ambitious SDG Target 15.5 (i.e. to take urgent and significant action to reduce the degradation of natural habitats, halt the loss of biodiversity and protect and prevent the extinction of threatened species), countries and the international community as a whole must, as the first order of business, identify ways and means to achieve these objectives at the spatial level and determine which areas should be given priority in management and conservation, to achieve the greatest synergy between the conservation and use of biodiversity.

In the past, when prioritizing conservation areas on the principle of minimum area and wider protection of species, attention was focused on the hotspots of species distribution rather than the risks of species extinction, to the neglect of the intensity of anthropogenic threats to species, thus greatly undermining the effectiveness of efforts to mitigate species loss. This study uses China's protected plants as an example and provides an analysis of key areas where protected plants are at risk and the sanctuaries where they seek refuge, by taking into account a range of factors, including species distribution, habitats, elevation and human activities, with the help of Big Earth Data. These sanctuaries are critical to the survival of many threatened species, but most of such high-value habitats remain unprotected. Conservation and restoration actions are imperative to halt the extinction of species.

Data used

◎ Distribution of species, Global Biodiversity Information Facility, National Specimen Information Infrastructure, Chinese Field Herbarium, China flora of plant, provincial flora, and local records.

◎ Digital Elevation Model, Big Earth Data sharing portal.

◎ Land Cover product in 2018 at 300 m, European Space Agency.

◎ Vector of Protected Areas, Big Earth Data sharing portal, Resource and Environment Data Cloud Platform, World Database on Protected Areas.

◎ Human footprint map (McGowan, 2016).

Method

Integrating distribution data from multiple sources; factoring in habitat preferences of species and elevation limits; and filtering out areas unsuitable for species distribution by referring to land cover and elevation maps to bring the distribution range closer to actual distribution (Brooks *et al.,* 2019). Optimizing the BRI based on the distribution of species and the risk categories of more than 30 000 plant species on the *Red List of Chinese Species* published by the Ministry of Ecology and Environment in 2016, using the following formula:

$$\mathrm{BRI} = \sum_{i=1}^{N} \frac{\mathrm{WS}_i}{\log_{10}(\mathrm{Area}_i)}$$

where N is the number of species in the grid cell; WS_i is a linear weighted score based on the International Union for Conservation of Nature (IUCN) conservation status of the ith species (i.e. Least Concern = 0, Near Threatened = 0.2, Vulnerable = 0.4, Endangered = 0.6, Critically Endangered = 0.8 and Extinct = 1.0); and $Area_i$ is the total area of geographic distribution (km^2) of ith species in the cell. Based on the bivariate distribution map of BRI and Human Footprint (HFP) at a resolution of 3 km, identifying key areas of where species are threatened and sanctuaries where species are unthreatened, with a view to providing important information for effectively mitigating and halting species loss.

Results and analysis

Areas with high risk of species extinction but low threat from human activities are concentrated in the high-altitude mountainous areas in northern Yunnan marked by an abundance of endemic species (Fig. 7-10b), whereas the top 25% priority areas with high risk of species extinction and high threat from human activities are located in the more developed southern regions of China marked by a high concentration of human activities (Fig. 7-10c). Western China has large swathes of relatively intact wilderness providing better habitats where species are in better shape and less threatened by human activities (Fig. 7-10d). Although Inner Mongolia and northern Xinjiang face high-intensity grazing, habitat fragmentation and other anthropogenic threats, northwest China as a whole is home to an abundance of ubiquitous species and the risk of species extinction there is relatively low (Fig. 7-10e).
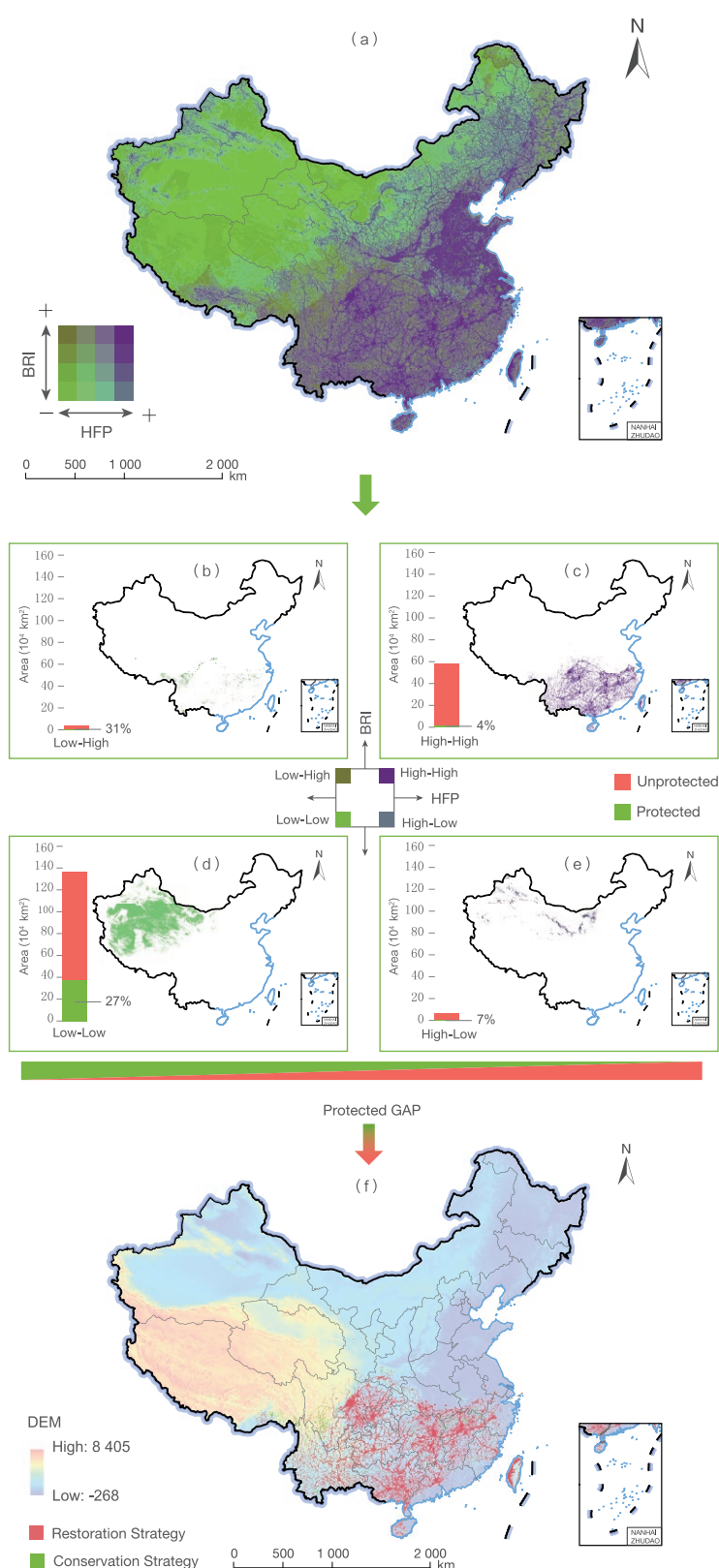

Figure 7-10. Bivariate maps of Biodiversity Risk Index (BRI) vs Human Footprint (HFP), and plant diversity protection gaps in China

It is worth noting that only 4% of protected areas are found in high-risk, high-threat areas (Fig. 7-10c) and 31% of protected areas are in high-risk, low-threat areas. Species in these areas generally are in the high threat categories and live in severely fragmented habitats, where the risk of biodiversity loss and conservation value are high. For the former, strategies should be in place to restore the fragmented habitats; for the latter, conservation strategies are required to expand the area under conservation as a priority, to protect the sanctuaries on which the survival of species depends. In low-risk and low-threat regions, protected areas cover 27%, most of which are wilderness with uninterrupted landscapes and minimum human modification. They boast the largest area of protected land and a relatively low biodiversity risk. In general, the coverage of protected areas is low in regions under high anthropogenic pressures, which were overlooked in the past. It is difficult to set up protected areas in fragmented and degraded habitats with high BRI. In those regions, the main strategy should be the restoration of habitats and strong legislation be put in place to limit the threat to habitats and mitigate the loss of biodiversity. Since extinction is irreversible, it is all the more important to be proactive in providing protection for the currently unprotected areas and the habitats of unique biodiversity, to improve human well-being and encourage economic development in non-high-risk regions.

Outlook

As a holistic measure of anthropogenic pressures, the Human Footprint (HFP) has become a powerful tool for predicting species extinction risk (Allan *et al.,* 2019; Mokany *et al.,* 2020). By collating HFP data, this study has identified hotspots where plant diversity is under threat, as well as sanctuaries of plant diversity in China. Drawing on the distribution of current protected areas, the study has mapped the gaps in the conservation of China's plant diversity and recommended tailored area-based conservation and management measures. The recommendations include the following: combining the creation of more protected areas to provide proactive protection with restoration management strategies that focus on management and mitigation of threats to protect habitats on which species depend for their survival; identifying areas for future protected areas expansion and important areas for enhanced habitat restoration management in China in order to achieve the SDGs; providing information on conservation gaps and useful methodologies for the implementation of national conservation action plans to halt biodiversity loss; and improving protected areas planning and the development of action plans.

Summary

By focusing on forests, land degradation and biodiversity, this chapter has discussed the development of Big Earth Data-enabled SDG indicator evaluation modeling and methodology at three levels, i.e. global, national (China) and local (typical areas), against four SDG indicators, namely, forest area as a proportion of total land area (SDG 15.1.1), proportion of biodiversity conservation sites (SDG 15.1.2), degraded land as a proportion of total land area (SDG 15.3.1) and the Red List Index (SDG 15.5.1). We have achieved dynamic, spatially disaggregated and quantitative multi-indicator monitoring and mapping under SDG 15; acquired key datasets on global forest cover (at 30 m resolution) and the state and scope of threat to, and cumulative stress on, China's protected flora and fauna; developed some key methodologies, such as integrated spatial-temporal-spectral forest feature extraction and quantification of the effects of changed vegetation on soil loss control; and proffered policy recommendations regarding the dynamics of China's land degradation neutrality and its contribution to global effort, aeolian desertification and mechanisms of change in soil erosion in northern China, and the conservation of China's biodiversity in the framework of the three global conditions and conservation strategies.

Volcanic crater, Wudalianchi National Park

Summary and Prospects

The year 2020 marks the start of the Decade of Action for achieving the United Nations Sustainable Development Goals. What has transpired over the past five years points to some gaps and shortfalls in the implementation of the 2030 Agenda, including data deficit, lack of research on the indicator system, and imbalance in development. The onus is on the STI community to deliver more. Of all the needs that must be met, data and methodology take precedence, both in utility and in urgency.

Focusing on 18 targets under six SDGs, this report presents studies on the application of Big Earth Data to the implementation of SDGs, with a view to contributing methodologies and datasets to global efforts to achieve these SDG targets.

(1) SDG Indicators 2.2.1 and 2.4.1 (Zero hunger): Between 2002 and 2017, the prevalence of stunting among children under five years of age in China declined from 18.8% to 4.8%, fulfilling the 5.9% target prescribed in SDG 2.2. Through more extensive multiple cropping, China will be able to harvest crops from an additional area of $1.35 \times 10^5 \, \text{km}^2$ to $3.63 \times 10^5 \, \text{km}^2$, and the yield of rice and wheat in regions with the largest area sown to these crops can potentially increase by 13.3% and 12.5%, respectively, over the 2015 levels, which means the total production of both crops nationwide will be able to meet the forecasted consumption for 2030. On the other hand, there is room for a 17-19% reduction in the application of nitrogen and phosphorus fertilizers for China's three major staple food crops, without impacting their production.

(2) SDG Indicators 6.3.2 and 6.6.1 (Clean water and sanitation): Between 2000 and 2019 in China, water transparency (Secchi Disk Depth, SDD) in lakes was generally good and a trend of continuous improvement was observed. Between 2015 and 2018, the area of mangrove forests in China registered a net growth of 22.11%, evidence of marked success in the restoration effort, alongside a net reduction of 2.59% in the area of *S. alterniflora*, whose invasion was brought under effective control. Significant changes have been observed in 50% of the water area of Ramsar sites in Asia, Europe, and Africa between 2000 and 2018, of which 58% were on a growth trajectory.

(3) SDG Indicators 11.1.1 and 11.2.1 (Sustainable cities and communities): Since 1990, the ratio of land consumption rate to population growth rate has grown in 434 cities in China. Then, in 2015, the expansion of urban built-up areas began to slow down. There were significant spatial disparities in 2019 between North and South China and between East and West China in the shantytown demographics of the main urban districts in 27 Chinese cities, with the shantytown population exceeding 3% of the total urban population in four cities. Compared to the 2015 level, open public space as a proportion of built-up areas in 342 prefectural cities increased by 1.5% on average. Among them, close to 50 cities had an open public space ratio of over 20%. In 2018, an average 80.56% of the urban population in China had easy access to public transportation and that ratio increased by varying margins over 2015 in approximately 80% of cities. The 2018 SDG 11 integrated index in 28 provincial-level administrative regions showed varying degrees of improvement over 2015.

(4) SDG Targets 13.1 and 13.2 (Climate action): Since the late 1990s, the frequency and intensity of extreme high-temperature events and heatwaves have markedly increased, and relatively defined extreme high-temperature events and heatwaves in high-latitude and high-altitude regions warrant close attention. A high-probability forecast for a forward shift in the anthesis and maturation of China's main crops through the 2030s points to a risk of yield reduction for wheat and maize, which calls for adjustments and improvements in such areas as crop management and breeding of improved varieties.

(5) SDG Targets 14.1 and 14.2 (Life below water): The average abundance of floating debris in China's coastal waters in 2018 was down by approximately 25% compared to the 2010-2014 average. Most of the microplastics found in China's coastal waters in 2019 were fibers, threads, pellets/granules, and fragments. Between 2015 and 2019, the ecosystems of Jiaozhou Bay, Sishili Bay, and Daya Bay were in good health on the whole. Between 2017 and 2020, the area of raft culture in China's seas was growing on the whole, but the area of raft culture within the boundaries of the coastal ecological conservation red line remained more or less stable.

(6) SDG Indicators 15.1.1 and 15.1.2 (Life on land): Between 2000 and 2019, vegetation cover on China's Loess Plateau improved significantly, with the overall effect of vegetation on soil loss control up by 22%. Between 2015 and 2018, China's LDN showed a positive trend as evidenced by a 60.30% growth in the net area of land restored, representing approximately one fifth of the net area of land restored globally and making China the number one contributor to global LDN. Conserving and sustainably using biodiversity under the 3Cs framework was implemented in China and findings indicate that the coverage of protected areas in regions under high risk and high stress from the compounding effects of biodiversity risks and anthropogenic pressures is on the low side, prompting recommendations for tailored solutions to protect and restore unprotected or underprotected areas.

The scourge of COVID-19 that began in early 2020 has posed a serious challenge to public health and is hitting the world economy hard on all fronts, making the implementation of the 2030 Agenda at the global level an uphill struggle. Given this context, it is incumbent upon the global community to consider, in greater depth, how to accelerate the implementation of this agenda and explore ways and means of using STI, Big Earth Data in particular, to overcome the constraints that are holding back sustainable development.

(1) Globally, the lack of data on indicators remains a major obstacle to the achievement of SDGs. Many countries, especially developing countries, have not been able to monitor and map their progress in meeting SDG indicators through the effective use of sophisticated technology. The dearth or absence of SDG-related data is a yawning gap in the toolkit.

(2) Keeping close tabs on the progress in the implementation of the 2030 Agenda at the global level calls for a well-developed system of evaluation methodology and criteria. Therefore, improving the SDG indicator system and its evaluation methodology supported by Big Earth Data is now an important project that demands the immediate attention of the global scientific and technological community.

(3) Big Earth Data, as a powerful tool for dynamic and objective macroscale monitoring, has the potential to provide an abundance of large-scale, cyclic information for policy-making support in relation to SDGs (Guo, 2018). However, such potential of Big Earth Data in support of SDG implementation at the global level has yet to be fully understood by policy-makers, scientists and practitioners in different disciplines, hence the urgent need to ramp up scientific and technical cooperation on Big Earth Data whereby methodologies and data can be shared and the implementation of SDGs accelerated.

To date, Chinese scientists have undertaken a range of projects using Big Earth Data in the service of sustainable development. Their efforts should continue and focus on the following priorities to study a host of major scientific issues standing in the way of SDGs with a systematic and holistic approach.

(1) How Big Earth Data can support the SDGs deserves closer study. Implementing the SDGs requires an approach that integrates economic, social, and environmental dimensions, leading to the creation of a new, more participatory discipline, namely, sustainability science, the objective of which is to generate useful scientific knowledge for sustainable development. The dynamic macroscale monitoring capabilities associated with Big Earth Data provide an important tool with which to evaluate economic, social, and environmental sustainability, and make it possible to integrate data from multiple sources to generate more relevant and richer information for support to policy-making. Going forward, it is necessary to apply Big Earth Data to the analysis of the dynamics among economic, social, and environmental factors subsumed in the SDGs, with a view to refining the SDG indicator system.

(2) SDG data sharing services based on Big Earth Data should be upgraded. Further research will be conducted on a range of technologies for, inter alia, real-time access, on-demand aggregation, multi-source integration, open sharing, and analysis of SDG-related data. The Chinese Academy of Sciences has produced 8 PB of data, to which more data in the order of petabytes are being added annually.

These resources should be put to good use, to develop a methodological system for Big Earth Data-enabled SDG assessment and measurement; to collect, process, and produce SDG-related data; and to deliver complete lines of data products for SDG assessment, which are then shared with the UN family, including agencies and Member States, as a substantive solution to overcome data deficit in the implementation of SDGs.

(3) Capacity building for the use of Big Earth Data to monitor and map SDG progress should be stepped up. An important objective of sustainable development is to address unbalanced development and underdevelopment at the global level and make sure no one is left behind. Only through proactive sharing of the STI deliverables to benefit technologically disadvantaged countries by way of international cooperation can the 2030 vision be realized globally to the greatest extent possible (Guo, 2017). The next step is to build SDG data infrastructure that integrates high-performance computing, big data analysis, and artificial intelligence to create a data visualization and comprehensive analysis platform for SDG research, and to provide human resources training for developing countries in the Big Earth Data-enabled monitoring and evaluation of SDG progress.

(4) Knowledge support for SDGs with Big Earth Data should be strengthened. STI is instrumental in achieving sustainable development. Given the ever tighter resources and environmental constraints on our planet, there is an urgent need to effectively observe and understand the changing patterns of environmental resources in the Earth system and to investigate the relationship between humanity and the planet and the interplay between this relationship and sustainable development, so as to achieve common development through more effective science-informed solutions. Going forward, science and technology will be fully leveraged to provide critical support in the form of knowledge, expertise, and technical means for balanced development across economic, social, and environmental pillars and the achievement of the 2030 Agenda.

Acronyms & Abbreviations

BP Ratio	Bacillariophyta Pyrrophyta Ratio
BRI	Biodiversity Risk Index
CAS	Chinese Academy of Sciences
CASEarth	CAS Big Earth Data Science Engineering Program
CCMP	Cross-Calibrated Multi-Platform
Chl a	Chlorophyll a
COVID-19	Corona Virus Disease 2019
DEM	Digital Elevation Model
DSSAT	Decision Support System for Agrotechnology Transfer
EGR	Economic Growth Rate
EGRLCR	Ratio of Economic Growth Rate to Land Consumption Rate
EVI	Enhanced Vegetation Index
FAO	Food and Agriculture Organization of the United Nations
FVC	Fraction of Vegetation Cover
GDP	Gross Domestic Product
GEO	Group on Earth Observations
GEO-LDN	Group on Earth Observations Land Degradation Neutrality
GEV	Generalized Extreme Values
GF-2	Gaofen-2
GPP	Gross Primary Productivity
HFP	Human Footprint
IAEG-SDGs	Inter-Agency and Expert Group on SDG indicators
IPCC	Intergovernmental Panel on Climate Change
ISRIC	International Soil Reference and Information Centre
IUCN	International Union for Conservation of Nature
JRC	Joint Research Centre of the European Commission
KBAs	Key Biodiversity Areas
LCR	Land Consumption Rate
LCRPGR	Ratio of Land Consumption Rate to Population Growth Rate
LDN	Land Degradation Neutrality
LWS	Level of Water Stress

MODIS	Moderate Resolution Imaging Spectroradiometer
NDVI	Normalized Difference Vegetation Index
OECD	Organisation for Economic Co-operation and Development
OLI	Operational Land Imager
PE	Polyethylene
PET	Polyethylene Terephthalate
PGR	Population Growth Rate
PMUD	Population in Main Urban Districts
PPST	Proportion of Population in Shantytowns
PS	Polystyrene
PST	Population in Shantytowns
RCP	Representative Concentration Pathway
RS-CYM	Remote Sensing-Crop Yield Model
SDD	Secchi Disk Depth
SDG	Sustainable Development Goal
SDSN	Sustainable Development Solutions Network
SECI	Soil Erosion Control Index
STI	Science, Technology and Innovation
TFM	Technology Facilitation Mechanism
TRMM	Tropical Rainfall Measuring Mission
UN	United Nations
UNCCD	United Nations Convention to Combat Desertification
UNDRR	United Nations Office for Disaster Risk Reduction
UN-Water	United Nations Water
VIIRS/DNB	Visible Infrared Imaging Radiometer Suite Day/Night Band
WHO	World Health Organization
WWF	World Wide Fund for Nature

References

Allan, J. R., Watson, J. E. M., Di Marco, M., *et al.* (2019). Hotspots of human impact on threatened terrestrial vertebrates[J]. *PLoS Biology* 17: e3000158. DOI:10.1371/journal.pbio. 3000158.

Black, R. E., Victora, C. G., Walker, S. P., *et al.* (2013). Maternal and child undernutrition and overweight in low-income and middle-income countries[J]. *Lancet* 382: 427–451. DOI: 10.1016/S0140-6736(13)60937-X.

Brooks, T. M., Pimm, S. L., Akçakaya, H. R., *et al.* (2019). Measuring terrestrial area of habitat (AOH) and its utility for the IUCN Red List[J]. *Trends in Ecology & Evolution* 34: 977–986. DOI: 10.1016/j.tree.2019.06.009.

Cao, Y., Carver, S., Yang, R. (2019). Mapping wilderness in China: Comparing and integrating Boolean and WLC approaches[J]. *Landscape and Urban Planning* 192: UNSP 103636. DOI: 10.1016/j.landurbplan. 2019.103636.

Chang, N. N., Luo, L., Wang, X. C., *et al.* (2020). A novel index for assessing the water quality of urban landscape lakes based on water transparency[J]. *Science of the Total Environment* 735: 139351. DOI:10.1016/j.scitotenv.2020.139351.

Chen, Y. H., Zhang, R. J., Ge, Y., *et al*. (2019). Downscaling census data for gridded population mapping with geographically weighted area-to-point regression kriging[J]. *IEEE Access* 7: 149132–149141. DOI: 10.1109/ACCESS.2019. 2945000.

Cheng, K., Wang, J. L.(2019). Forest type classification based on integrated spectral- spatial-temporal features and random forest algorithm—A case study in the Qinling mountains[J]. *Forests* 10: 559. DOI: 10.3390/f10070559.

Deville, P., Linard, C., Martin, S., *et al.* (2014). Dynamic population mapping using mobile phone data[J]. *Proceedings of the National Academy of Sciences of the United States of America* 111: 15888–15893. DOI: 10.1073/pnas.1408439111.

FAO. (2006). Global Forest Resources Assessment 2005: Progress towards Sustainable Forest Management. Rome. www.fao.org/docrep/008/a0400e /a0400e00.htm.

FAO. (2010) . Global Forest Resources Assessment 2010. Rome. http://www.fao.org/forestry/fra2010.

FAO. (2016).Global Forest Resources Assessment 2015: How are the World's Forests Changing? Rome. http://www.fao.org/3/a-i4808e.pdf.

FAO. (2018a). The State of the World's Forests 2018-Forest Pathways to Sustainable Development. Rome. http://www.fao.org/3/I9535EN/i9535en.pdf.

FAO. (2018b). Terms and Definitions: FRA2020. Rome.http://www.fao.org/forest-resources -assessment/en/.

FAO, IFAD, UNICEF, *et al*. (2019). The State of Food Security and Nutrition in the World 2019. Safeguarding against Economic Slowdowns and Downturns. Rome. http://www.fao.org/3/ca5162en/ca5162en.pdf.

FAO. (2020). FAOStat: FAOSTAT Online Statistical Service. https://crops.extension. iastate.edu/faostat.

Gong, P., Chen, B., Li X. C., *et al*. (2019). Mapping essential urban land use categories in China (EULUC-China): Preliminary results for 2018[J]. *Science Bulletin* 65: 182–187. DOI: 10.1016/j.scib.2019.12.007.

Guo, H. D., Wang, L. Z., and Liang, D. (2016). Big Earth Data from space: A new engine for Earth Science[J]. *Science Bulletin* 61 (7): 505–513.DOI: 10.1007/s11434-016-1041-y.

Guo, H. D. (2017). Big Earth Data: A new frontier in Earth and Information Sciences[J]. *Big Earth Data* 1 (1–2): 4–20. DOI:1 0.1080/20964471.2017.1403062.

Guo, H. D. (2018). Steps to the Digital Silk Road[J]. *Nature* 554: 25–27.DOI: 10.1038/d41586-018-01303-.

Guo, H. D., Liu, J., Qiu, Y. B., *et al*. (2018). The Digital Belt and Road program in support of regional sustainability[J]. *International Journal of Digital Earth* 11:7, 657-669. DOI: 10.1080/17538947.2018.1471790.

Guo, H. D., *et al*. (2019). Big Earth Data in Support of the Sustainable Development Goals (2019). Beijing: Science Press and EDP Sciences.

Guo, H. D., Goodchild, F. M., and Annoni, A. (2020a). Manual of Digital Earth. Singapore: Springer.

Guo, H. D., Nativi, S., Liang, D., *et al*. (2020b). Big Earth Data science: an information framework for a sustainable planet[J]. *International Journal of Digital Earth* 13:7, 743-767.

DOI: 10.1080/17538947.2020.1743785.

Han, Q., and Niu, Z. (2020). Construction of the Long-Term Global Surface Water Extent Dataset Based on Water-NDVI Spatio-Temporal Parameter Sets. *Remote Sens*., 12(17), 2675. doi:https://doi.org/10.3390/rs12172675.

Henry, R. C., Engström, K., Olin, S., *et al*. (2018). Food supply and bioenergy production within the global cropland planetary boundary[J]. *PLOS ONE* 13: e0194695. DOI: 10.1371/journal. pone. 0194695.

Hu, S. J., Niu, Z. G., Chen, Y. F. (2017). Global Wetland Datasets: a Review. *Wetlands* 37:807-817.DOI: 10.1007/s13157-017-0927-z.

Immerzeel, W. W., Lutz, A. F., Andrade, M., *et al*. (2019). Importance and vulnerability of the world's water towers[J]. *Nature* 577: 364–369. DOI: 10.1038/s41586-019-1822-y.

IPBES. (2019). Global assessment report on biodiversity and ecosystem services of the Intergovernmental Science-Policy Platform on Biodiversity and Ecosystem Services. In: Brondizio,E. S., Settele, J., Díaz,S. , *et al*., Eds. IPBES secretariat, Bonn, Germany. DOI: 10.5281/zenodo.3553579.

Jia, M. M., Wang, Z. M., Zhang, Y. Z., *et al*. (2018). Monitoring loss and recovery of mangrove forests during 42 years: The achievements of mangrove conservation in China[J]. *International journal of applied earth observation and geoinformation* 73: 535–545. DOI: 10.1016/j.jag.2018.07.025.

Kennedy, C. M., Oakleaf, J. R., Theobald, D. M., *et al*. (2019). Managing the middle: A shift in conservation priorities based on the global human modification gradient[J]. *Global Change Biology* 25: 811–826. DOI: 10.1111/gcb.14549.

Lafortune, G., Fuller, G., Moreno, J., *et al*. (2018). Global SDG Index and Dashboards Methodology. New York: Bertelsmann Stiftung and Sustainable Development Solutions Network (SDSN). http://sustainabledevelopment.report.

Lee, L. H., Lee, Y. D. (2015). The impact of water quality on the visual and olfactory satisfaction of tourists[J]. *Ocean & Coastal Management* 105: 92–99. DOI: 10.1016/j.ocecoaman.2014.12.020.

Lehner, B., Doll, P. (2004). Development and validation of a global database of lakes, reservoirs and wetlands[J]. *Journal of Hydrology* 296: 1–22. DOI: 10.1016/j. jhydrol. 2004.03.028.

Li, Z., Yan, Z. W., Wu, H. Y. (2015). Updated homogenized China temperature series with physical consistency[J]. *Atmospheric and Oceanic Science Letters* 8: 17–22.

DOI:10.3878/ AOSL20140062.

Liu, Y. J., Chen, Q. M., Ge, Q. S., *et al*. (2018a). Spatiotemporal differentiation of changes in wheat phenology in China under climate change from 1981 to 2010[J]. *Science China Earth Sciences* 61: 1088–1097. DOI: 10.1007/s11430-017-9149 -0.

Liu, Y. J., Chen, Q. M., Ge, Q. S., *et al*. (2018b). Modelling the impacts of climate change and crop management on phenological trends of spring and winter wheat in China[J]. *Agricultural and Forest Meteorology* 248: 518–526. DOI: 10.1016/j. agrformet.2017.09.008.

Locke, H., Ellis, E. C., Venter, O. *et al*. (2019). Three global conditions for biodiversity conservation and sustainable use: An implementation framework[J]. *National Science Review* 6: 1080–1082. DOI: 10.1093/nsr/nwz136.

Mao, D. H., Liu, M. Y., Wang, Z. M., *et al*. (2019). Rapid invasion of spartina alterniflora in the coastal zone of mainland China: Spatiotemporal patterns and human prevention[J]. *Sensors* 19: 2308. DOI: 10.3390/s19102308.

Mao, D.H., Wang, Z. M., Du, B. J., *et al*. (2020). National wetland mapping in China: A new product resulting from object-based and hierarchical classification of Landsat 8 OLI images[J]. *ISPRS Journal of Photogrammetry and Remote Sensing* 164: 11–25. DOI: 10.1016/j.isprsjprs. 2020.03.020.

McGowan, P. J. K. (2016). Mapping the terrestrial human footprint[J]. *Nature* 537, 172–173. DOI:10.1038/537172a.

Mokany, K., Ferrier, S., Harwood, T., *et al*. (2020). Reconciling global priorities for conserving biodiversity habitat[J]. *Proceedings of the National Academy of Sciences* 117: 9906–9911. DOI: 10.1073/pnas.1918373117.

Mueller, N. D., Gerber, J. S., Johnston, M., *et al*. (2012). Closing yield gap through nutrient and water management[J]. *Nature* 490: 254–257. DOI: 10.1038/nature 11420.

Neil, C. S., Jacqueline, R. E., Glenn, J. N., *et al*. (2019). Developing good practice guidance for estimating land degradation in the context of the United Nations Sustainable Development Goals[J]. *Environmental Science & Policy* 92: 349–355. DOI: 10.1016/j.envsci.2018.10.014.

Pekel, J. F., Cottam, A., Gorelick, N., *et al*. (2016). High-resolution mapping of global surface water and its long-term changes[J]. *Nature* 540: 418–422. DOI: 10.1038/nature20584.

Pojani, D.,Stead, D. (2015). Sustainable urban transport in the developing world: Beyond megacities[J]. *Sustainability* 7: 7784–7805. DOI: 10.3390/su7067784.

Pollard, P., Huxham, M.(1998). The european water framework directive: A new era in the management of aquatic ecosystem health?[J]. *Aquatic Conservation: Marine and Freshwater Ecosystems* 8: 773–792. DOI:10.1002/(SICI)1099-0755(1998110)8:6<773::AID-AQC313> 3.0.CO;2-R.

Rapport, D. J. (1995). Ecosystem health: Exploring the territory[J]. *Ecosystem Health* 1: 5–13. DOI: 10.11821/dlyj201502010.

Ray, D. K., Ramankutty, N., Mueller, N. D., *et al*. (2012). Recent patterns of crop yield growth and stagnation. *Nature Communications* 3:1293. DOI: 10.1038/ncomms2296.

Sachs, J., Schmidt-Traub, G., Kroll, C., *et al*. (2019). Sustainable Development Report 2019. New York: Bertelsmann Stiftung and Sustainable Development Solutions Network (SDSN). http://sustainabledevelopment.report.

Sachs, J., Schmidt-Traub, G., Kroll, C., *et al*. (2020). The Sustainable Development Goals and COVID-19. Sustainable Development Report 2020. Cambridge: Cambridge University Press.

United Nations. (2015). Transforming our world: The 2030 Agenda for Sustainable Development. Division for Sustainable Development Goals: New York, NY, USA . https://sustainabledevelopment.un.org/post2015/transformingourworld.

United Nations. (2018). World Urbanization Prospects: The 2018 Revision, Online Edition.http://www.indiaenvironmentportal.org.in/content/455130/world-urbanization-prospects-the-2018-revision/.

United Nations. (2019). The Sustainable Development Goals Report 2019. New York: United Nations.

UN-Water. (2018). Progress on water use efficiency 2018: Piloting the monitoring methodology and initial findings for SDG indicator 6.4.1. https://www.unwater.org/ publications/progress-on-water-use-efficiency-641/.

Wang, T., Wu, W., Xue, X., *et al*. (2004). Spatial-temporal changes of sandy desertified land during last 5 decades in northern China[J]. *Acta Geographica Sinica(Chinese Edition)* 59: 203–212. DOI: 10.1007/BF02873097.

Wang, T., Xue, X., Zhou, L. H., *et al*. (2015). Combating aeolian desertification in Northern China[J]. *Land Degradation and Development* 26: 118–132. DOI: 10.1002/ldr.2190.

Wang, J. W., Zhang, J. H., Bai, Y., *et al*. (2020). Integrating remote sensing-based process model with environmental zonation scheme to estimate rice yield gap in Northeast China[J]. *Field Crops Research* 246: 107682. https://doi.org/10.1016/j.fcr.2019.107682.

West, P. C., Gerber, J. S., Engstrom, P. M., *et al*. (2014). Leverage points for improving global food security and the environment[J]. *Science* 345: 325–328. DOI: 10.1126/science.1246067.

Wurm, M., Stark, T., Zhu, X. X., *et al*. (2019). Semantic segmentation of slums in satellite images using transfer learning on fully convolutional neural networks[J]. *ISPRS Journal of Photogrammetry and Remote Sensing* 150: 59–69. https://doi.org/10.1016/j.isprsjprs. 2019.02.006.

Xu, Z., Chau, S. N., Chen, X., *et al*. (2020). Assessing progress towards sustainable development over space and time[J]. *Nature* 577: 74–78. Doi: 10.1038/s41586-019-1846-3.

Zhang, Z. H., Deng, S. F., Zhao, Q. D. *et al*. (2019). Projected glacier meltwater and river run-off changes in the Upper Reach of the Shule River Basin, north-eastern edge of the Tibetan Plateau[J]. *Hydrological Processes* 33: 1059–1074. DOI: 10.1002/hyp.13384.

Zheng, Y. M., Zhang, H. Y., Niu, Z. G., *et al*. (2012). Protection efficacy of national wetland reserves in China[J]. *Chinese Science Bulletin* 57: 1116–1134. DOI: 10.1007/s11434-011-4942-9.

Zheng, Y. M, Niu, Z.G., Gong, P., *et al*. (2015). A database of global wetland validation samples for wetland mapping[J]. *Science Bulletin* 60: 428–434. DOI: 10.1007/s11434-014 -0717-4.

Zhou, C. C., Liu, X., Wang, Z. W., *et al*. (2016). Assessment of marine debris in beaches or seawaters around the China Seas and coastal provinces[J]. *Waste Management* 48: 652–660. DOI: 10.1016/j.wasman.2015.11.010.

Zuo, L. J., Zhang, Z. X., Carlson, K. M., *et al*. (2018). Progress towards sustainable intensification in China challenged by land-use change[J]. *Nature Sustainability* 1: 304–313. DOI: 10.1038/s41893-018-0076-2.

Core Team of Authors

Leading author

Guo Huadong   Aerospace Information Research Institute, Chinese Academy of Sciences

Authors (Alphabetically arranged)

Bai Yun   Qingdao University

Bian Zhen   University of Jinan

Cao Yue   Tsinghua University

Chen Fang   Aerospace Information Research Institute, Chinese Academy of Sciences

Chen Yu   Aerospace Information Research Institute, Chinese Academy of Sciences

Chen Jingbo   Aerospace Information Research Institute, Chinese Academy of Sciences

Chen Yaxi   Aerospace Information Research Institute, Chinese Academy of Sciences

Cheng Kai   Institute of Geographic Sciences and Natural Resources Research, Chinese Academy of Sciences

Cheng Zhifeng   Institute of Geographic Sciences and Natural Resources Research, Chinese Academy of Sciences

Cui Yuran   Aerospace Information Research Institute, Chinese Academy of Sciences

Ding Gangqiang   National Institute for Nutrition and Health, Chinese Center for Disease Control and Prevention

Dong Yingying   Aerospace Information Research Institute, Chinese Academy of Sciences

Dou Changyong   Aerospace Information Research Institute, Chinese Academy of Sciences

Du Shiqiang   Shanghai Normal University

Du Wenjie   Aerospace Information Research Institute, Chinese Academy of Sciences

Du Wenwen   National Institute for Nutrition and Health, Chinese Center for Disease Control and Prevention

Duan Hongtao   Nanjing Institute of Geography and Limnology, Chinese Academy of Sciences

Fan Lijun   Institute of Atmospheric Physics, Chinese Academy of Sciences

Fan XinYue   Research Center for Eco-Environmental Sciences, Chinese Academy of Sciences

Fang Hongyun   National Institute for Nutrition and Health, Chinese Center for Disease Control and Prevention

Fang Shibo   Chinese Academy of Meteorological Sciences

Feng Yaya   Northwest Institute of Eco-Environment and Resources, Chinese Academy of Sciences

Gao Fenglei   First Institute of Oceanography, Ministry of Natural Resources

Gao Yunfei   Yellow River Basin Monitoring Center of Water-Soil Conservation and Eco-Environment

Gu Haifeng   First Institute of Oceanography, Ministry of Natural Resources

Han Qianqian   Aerospace Information Research Institute, Chinese Academy of Sciences

Han Qunli   Aerospace Information Research Institute, Chinese Academy of Sciences

He Guojin   Aerospace Information Research Institute, Chinese Academy of Sciences

Hou Yanfang	Aerospace Information Research Institute, Chinese Academy of Sciences
Hu Ziyuan	Institute of Oceanology, Chinese Academy of Sciences
Huang Lei	Aerospace Information Research Institute, Chinese Academy of Sciences
Huang Chunlin	Northwest Institute of Eco-Environment and Resources, Chinese Academy of Sciences
Huang Wenjiang	Aerospace Information Research Institute, Chinese Academy of Sciences
Jia Li	Aerospace Information Research Institute, Chinese Academy of Sciences
Jia Gensuo	Institute of Atmospheric Physics, Chinese Academy of Sciences
Jia Mingming	Northeast Institute of Geography and Agroecology, Chinese Academy of Sciences
Jiang Huiping	Aerospace Information Research Institute, Chinese Academy of Sciences
Li Li	National Institute for Nutrition and Health, Chinese Center for Disease Control and Prevention
Li Sheng	Peking University
Li Zhen	Institute of Atmospheric Physics, Chinese Academy of Sciences
Li Jiabao	China University of Geosciences (Wuhan)
Li Jingxi	First Institute of Oceanography, Ministry of Natural Resources
Li Liping	Aerospace Information Research Institute, Chinese Academy of Sciences
Li Xiaosong	Aerospace Information Research Institute, Chinese Academy of Sciences
Li Xiaoyu	Institute of Oceanology, Chinese Academy of Sciences
Liang Dong	Aerospace Information Research Institute, Chinese Academy of Sciences
Liao Jie	Northwest Institute of Eco-Environment and Resources, Chinese Academy of Sciences
Liu Dong	Nanjing Institute of Geography and Limnology, Chinese Academy of Sciences
Liu Jie	Aerospace Information Research Institute, Chinese Academy of Sciences
Liu Mingzhang	Peking University
Liu Shulin	Northwest Institute of Eco-Environment and Resources, Chinese Academy of Sciences
Liu Yujie	Institute of Geographic Sciences and Natural Resources Research, Chinese Academy of Sciences
Long Tengfei	Aerospace Information Research Institute, Chinese Academy of Sciences
Lu Qi	Institute of Desertification Studies, Chinese Academy of Forestry
Lu Shanlong	Aerospace Information Research Institute, Chinese Academy of Sciences
Ma Keping	Institute of Botany, Chinese Academy of Sciences
Mao Dehua	Northeast Institute of Geography and Agroecology, Chinese Academy of Sciences
Mi Xiangcheng	Institute of Botany, Chinese Academy of Sciences
Mu Haowei	Lanzhou Jiaotong University
Niu Zhenguo	Aerospace Information Research Institute, Chinese Academy of Sciences
Ouyang Zhiyun	Research Center for Eco-Environmental Sciences, Chinese Academy of Sciences
Peng Yan	Aerospace Information Research Institute, Chinese Academy of Sciences
Qu Yi	Institute of Natural Resources and Ecology, Heilongjiang Academy of Sciences
Shangguan Donghui	Northwest Institute of Eco-Environment and Resources, Chinese Academy of Sciences

Shen Xiaoli	Institute of Botany, Chinese Academy of Sciences
Shen Ming	Nanjing Institute of Geography and Limnology, Chinese Academy of Sciences
Shi Jinlian	Beijing Technology and Business University
Song Xiang	Northwest Institute of Eco-Environment and Resources, Chinese Academy of Sciences
Song Xiaoyu	Northwest Institute of Eco-Environment and Resources, Chinese Academy of Sciences
Su Chang	National Institute for Nutrition and Health, Chinese Center for Disease Control and Prevention
Sun Chengjun	First Institute of Oceanography, Ministry of Natural Resources
Sun Xiaoxia	Institute of Oceanology, Chinese Academy of Sciences
Sun Zhongchang	Aerospace Information Research Institute, Chinese Academy of Sciences
Tang Chao	Aerospace Information Research Institute, Chinese Academy of Sciences
Tu Kai	Institute of Atmospheric Physics, Chinese Academy of Sciences
Wang Xiao	Aerospace Information Research Institute, Chinese Academy of Sciences
Wang Chengyi	Aerospace Information Research Institute, Chinese Academy of Sciences
Wang Zujia	Aerospace Information Research Institute, Chinese Academy of Sciences
Wang Bao	Northwest Institute of Eco-Environment and Resources, Chinese Academy of Sciences
Wang Meng	Aerospace Information Research Institute, Chinese Academy of Sciences
Wang Rui	Aerospace Information Research Institute, Chinese Academy of Sciences
Wang Futao	Aerospace Information Research Institute, Chinese Academy of Sciences
Wang Huijun	National Institute for Nutrition and Health, Chinese Center for Disease Control and Prevention
Wang Jianghao	Institute of Geographic Sciences and Natural Resources Research, Chinese Academy of Sciences
Wang Jingwen	University of Chinese Academy of Sciences
Wang Juanle	Institute of Geographic Sciences and Natural Resources Research, Chinese Academy of Sciences
Wang Lizhe	China University of Geosciences (Wuhan)
Wang Penglong	Northwest Institute of Eco-Environment and Resources, Chinese Academy of Sciences
Wang Shijin	Northwest Institute of Eco-Environment and Resources, Chinese Academy of Sciences
Wang Shixin	Aerospace Information Research Institute, Chinese Academy of Sciences
Wang Shudong	Aerospace Information Research Institute, Chinese Academy of Sciences
Wang Xinyuan	Aerospace Information Research Institute, Chinese Academy of Sciences
Wang Yuewei	China University of Geosciences (Wuhan)
Wang Yunchen	Northwest Institute of Eco-Environment and Resources, Chinese Academy of Sciences
Wang Zongming	Northeast Institute of Geography and Agroecology, Chinese Academy of Sciences
Wei Mingyue	Aerospace Information Research Institute, Chinese Academy of Sciences
Wu Bingfang	Aerospace Information Research Institute, Chinese Academy of Sciences
Wu Taixia	Hohai University
Wu Wenbin	Institute of Agricultural Resources and Regional Planning, Chinese Academy of Agricultural Sciences
Xing Qiang	Aerospace Information Research Institute, Chinese Academy of Sciences

Xu Weihua	Research Center for Eco-Environmental Sciences, Chinese Academy of Sciences
Xu Shiwei	Agricultural Information Institute, Chinese Academy of Agricultural Sciences
Xue Xian	Northwest Institute of Eco-Environment and Resources, Chinese Academy of Sciences
Yan Xin	Aerospace Information Research Institute, Chinese Academy of Sciences
Yan Dongmei	Aerospace Information Research Institute, Chinese Academy of Sciences
Yan Shijie	Aerospace Information Research Institute, Chinese Academy of Sciences
Yang Rui	Tsinghua University
Yao Fengmei	University of Chinese Academy of Sciences
Yu Rencheng	Institute of Oceanology, Chinese Academy of Sciences
Yu Qiangyi	Institute of Agricultural Resources and Regional Planning, Chinese Academy of Agricultural Sciences
Yu Wen	Agricultural Information Institute, Chinese Academy of Agricultural Sciences
Yuan Bo	Lanzhou Jiaotong University
Zhang Bing	National Institute for Nutrition and Health, Chinese Center for Disease Control and Prevention
Zhang Li	Aerospace Information Research Institute, Chinese Academy of Sciences
Zhang Miao	Aerospace Information Research Institute, Chinese Academy of Sciences
Zhang Sha	Qingdao University
Zhang Yi	Aerospace Information Research Institute, Chinese Academy of Sciences
Zhang Jiahua	Aerospace Information Research Institute, Chinese Academy of Sciences
Zhang Kebin	Beijing Forestry University
Zhang Xiaomei	Aerospace Information Research Institute, Chinese Academy of Sciences
Zhang Zengxiang	Aerospace Information Research Institute, Chinese Academy of Sciences
Zhang Zhaoming	Aerospace Information Research Institute, Chinese Academy of Sciences
Zhao Chang	First Institute of Oceanography, Ministry of Natural Resources
Zhao Xiaoli	Aerospace Information Research Institute, Chinese Academy of Sciences
Zhao Xiaoqian	Institute of Botany, Chinese Academy of Sciences
Zheng Yaomin	Aerospace Information Research Institute, Chinese Academy of Sciences
Zhou Liang	Lanzhou Jiaotong University
Zhou Yi	Aerospace Information Research Institute, Chinese Academy of Sciences
Zhou Zhengxi	Institute of Oceanology, Chinese Academy of Sciences
Zhu Li	Institute of Botany, Chinese Academy of Sciences
Zuo Lijun	Aerospace Information Research Institute, Chinese Academy of Sciences